REPORT DOCUMENTATION PAGE

Form Approved OMB No. 0704-0188

1. REPORT DATE *(DD-MM-YYYY)*	2. REPORT TYPE	3. DATES COVERED *(From – To)*
14-09-2006	Final Report	07-Jan-02 - 14-Sep-06

4. TITLE AND SUBTITLE

Studies of Plasma Instabilities Excited by Ground-based High Power HF (("Heating") Facilities and of X and Gamma Ray Emission in Runaway Breakdown Processes

5a. CONTRACT NUMBER
ISTC Registration No: 2236p

5b. GRANT NUMBER

5c. PROGRAM ELEMENT NUMBER

6. AUTHOR(S)

Dr. Aleksander Viktorovich Gurevich

5d. PROJECT NUMBER

5d. TASK NUMBER

5e. WORK UNIT NUMBER

7. PERFORMING ORGANIZATION NAME(S) AND ADDRESS(ES)
P. N. Lebedev Physical Institute
Leninsky pr.,53
Moscow 117924
Russia

8. PERFORMING ORGANIZATION REPORT NUMBER

N/A

9. SPONSORING/MONITORING AGENCY NAME(S) AND ADDRESS(ES)

EOARD
PSC 821 BOX 14
FPO AE 09421-0014

10. SPONSOR/MONITOR'S ACRONYM(S)

11. SPONSOR/MONITOR'S REPORT NUMBER(S)
ISTC 01-7033

12. DISTRIBUTION/AVAILABILITY STATEMENT

Approved for public release; distribution is unlimited.

13. SUPPLEMENTARY NOTES

14. ABSTRACT

This report results from a contract tasking P. N. Lebedev Physical Institute as follows: The investigation will focus on how high power HF radio waves and quasistationary electric field interact with collisional plasmas, such as the earth's ionosphere or thunderstorm atmosphere.

The aim of this proposal to investigate:

1. The interaction of Langmuir turbulence with surrounding ionospheric plasma determining kinetics of thermal and suprathermal electrons;
2. The optic emission of suprathermal electrons;
3. The effect of ionospheric drifts on the generation of field aligned small scale striations;
4. The runaway breakdown process in inhomogeneous thunderstorm electric field;
5. X-ray emission in different gases due to runaway breakdown phenomena in a laboratory cyclotron installation;
6. An influence of combined effects of runaway breakdown and cosmic rays on lightning processes in thunderstorm atmosphere.

15. SUBJECT TERMS
EOARD, Physics, Radiofrequency Wave Propagation

16. SECURITY CLASSIFICATION OF:			17. LIMITATION OF ABSTRACT	18, NUMBER OF PAGES	19a. NAME OF RESPONSIBLE PERSON
a. REPORT	**b. ABSTRACT**	**c. THIS PAGE**	UL		GEORGE W YORK, Lt Col, USAF
UNCLAS	UNCLAS	UNCLAS		66	**19b. TELEPHONE NUMBER** *(Include area code)* +44 (0)20 7514 3154

Standard Form 298 (Rev. 8/98)
Prescribed by ANSI Std. Z39-18

**Final
Project Technical Report
of ISTC 2236p**

**Studies of Plasma Instabilities Excited by Ground-based
High Power HF ("Heating") Facilities and of X and
Gamma Ray Emission in Runaway Breakdown Processes**

(January 1, 2002 – June 30, 2006)

**Alexandr Viktorovich Gurevich
(Project Manager)**

P.N. Lebedev Physical Institute of RAS

_____ A.V. Gurevich
Project Manager

_____M.A. Vasiliev
Director
the I.E. Tamm Theoretical Physics Division,
P.N. Lebedev Physical Institute of RAS

August, 2006

Title of the Project	Studies of Plasma Instabilities Excited by Ground-based High Power HF ("Heating") Facilities and of X and Gamma Ray Emission in Runaway Breakdown Processes
Contracting Institute	P.N. Lebedev Physical Institute, Russian Academy of Sciences (RAS)
Participating Institutes	
Project Manager,	Gurevich Alexander Viktorovich, Academician, RAS
Phone number, Fax number	Phone: +7(495)1326414, Fax: +7(495)1358533
E-mail address	alex@lpi.ru
Commencement Date,	01/01/2002
Duration	4.5 years
Keywords	Ionosphere Exciting, powerful radio waves, Langmuir turbulence, gas breakdown, runaway electrons, X-ray, gamma emission, electron-cyclotron discharge, FM radio-wave radiation, storm discharge, extensive atmospheric shower.

LIST of CONTENTS

Introduction

Project goals:

1. Elaborate the kinetic theory of the suprathermal electron generation by the Langmuir turbulence;
2. Theoretically investigate the pump excitation of the molecular optic lines by the suprathermal electrons in the ionosphere, compare calculation results s with observational data;
3. Elaborate the theory of the radio wave self-focusing on the striations in F-region of the ionosphere; explain the developing of striation bunches taking into account the theory results, in particular, the ionosphere drifts;
4. Measure the X-ray and Gamma-ray emissions in different gases in the runaway breakdown processes; obtain the dependence of the X-ray emission characteristics on the charge number;
5. Measure simultaneously the electric field jumps and the Gamma-ray and X-ray flashes in thunderstorm atmosphere; search for the correlations between these phenomena;
6. Find short-time flashes of the UHF radio emission during thunderstorm

Technical Approach

The theoretical part of the project is devoted to the development of the theory of interaction of the powerful radio wave with ionosphere plasma. It is planned to investigate the process of the Langmuir turbulence exciting in the real conditions of non-uniform ionosphere. Preliminary investigations show that such turbulence is excited in a thin layer at the height corresponding to the pump-wave reflection point. This turbulence, in particular, accelerates electrons. Electrons leave the accelerating layer and excite the molecules. It leads to the observed ionosphere luminosity.

To provide a correct description of the processes the kinetic theory and the corresponding numerical model will be developed. . The optic emission of the ionosphere will be calculated and compared with experimental data as well.

Another theoretical problem to be solved during the project performance is the structuring of the ionosphere under the action of powerful radio wave. It is known (Kelly et al., 1995, Gurevich et al., 1995) that striations arise nearby the upper hyroresonance space. The nonlinear process of the interaction of the pump wave with the striations will be investigated. It is supposed that such a theory will explain the observed large-scale irregularities – bunches of striations.

We plan further researches of electron cyclotron resonance breakdown initiated by injected electron beam and also studies of the nature of self-sustained electrical breakdown and discharge governed by runaway electrons. There will be obtained characteristics of breakdown governed by runaway electrons (REs) versus the discharge parameters such as the air and other gases pressure, power of the electric field generator and the fast electrons flux initiating the discharge. There will be studied a balance between the energy absorbed by plasma and various channels of plasma energy losses such as the energy spent for production and heating of the plasma, radiation energy losses and losses due to the generation of the fast electrons. . Characteristics of a newly discovered phenomenon, namely, the self-sustained breakdown governed by REs, depending on the parameters of the experimental configuration will be studied both experimentally and theoretically. Optical, X-ray and UHF-cyclotron spectra will be studied.

The experimental investigations of X and γ emissions stimulated by runaway breakdown effect will be carried out at the Lebedev Institute facility situated at the heights of 3300 – 4000 m in the Tien Shan mountains. The facility has a well-developed complex of special installations to detect EAS (Abrashikov et al, 1986). It is being modernized now by an installation of the set of scintillator detectors to detect γ and X - ray emission in atmosphere. In 1999 the first results demonstrating a significant enhancement of 100 – 500 keV emission in atmosphere during thunderstorms were obtained. The most difficult experimental problem is to separate γ and X emissions generated due to runaway breakdown effect from radon background emission. It is possible to separate these two different sources of X emission studying time evolution of the signals. Runaway breakdown effect gives short pulses of emission while the typical time of radon decay is approximately 30 minutes. To analyze a rapid evolution of X-ray emission we suppose to use in addition to existing detection facilities NaJ scintillator detectors.

Another phenomena accompanying the runaway breakdown process is time correlated jumps of the electric field. We propose to study these correlations, measuring time evolution of the electric field and correlated fast changes of the field with X and γ ray bursts.

It is planned to conduct permanent monitoring of EAS and search of their correlations with X-ray bursts to test the theoretical predictions of lightnings triggering by combined action of runaway breakdown and high energy ($\varepsilon \geq 10^{15}$–10^{16} eV) cosmic ray particle (Gurevich et al., 1999).

Work Performed and Results

Task 1.   Study of the interaction of Langmuir turbulence with surrounding ionosphere plasma

The specialty of the Langmuir turbulence (LT) in the ionosphere plasma is that it occupy a thin-altitude layer about $100 \div 200$ m compared to about decades kilometers characteristic altitude gradients of plasma concentration and temperature. The electron free path length is usually larger than LT layer. So, LT develops practically in non-collision plasma. The nonlinear stage of LT is determined in the case by the modulation instability and is described by the Zakharov hydrodynamic equations. Their theoretical analysis and numerical investigations held in number of papers allowed to determine the intensity and the spectrum of the plasma and ion-sound stabilized oscillations, the number and the structure of cavitons. It also allowed investigating the process of caviton nonlinear compression (caviton collapse). However, there is no electron acceleration in the hydrodynamic theory. It doesn't allow to determine the number of accelerated electrons as well as their back feedback influence on the plasma stable oscillations.

The kinetic theory should be used to describe the electron behavior. Qualitatively the process looks in the following way. The acceleration takes place when the moving electrons cross the cavitons, and has a local character. At that only fast electrons appurtenant to the distribution function tail are accelerated. As for slow (thermal) electrons, they adiabatic oscillate in caviton and do not absorb the energy from the field. However, the formation of electron distribution function in its high energy part has a following specific character under ionosphere conditions. The thickness of the accelerating plasma layer, as in was mentioned above, is less then the electron free path length. That's why the electron accelerated in the layer can turn back colliding with the air molecules outside the layer and pass the accelerating layer once more gaining the energy. Then the process repeats. The fast electron energy will increase until the energy they lost in collisions will not match with the gained in the accelerating layer. The acceleration effect is multiple increased due to the multiple electron passing through the LT layer; the accelerated electron region extent increases scores of times and reaches hundreds kilometers.

Earlier we have developed such theory of multiple acceleration taking into account in the strong way only the processes outside the accelerating layer. In the layer itself a phenomenological solution was used. In particular, the caviton dimension and their number were set as phenomenological parameters. In this year work we aspire to avoid the mentioned defect and to develop the strict kinetic solution of the problem not only inside but also outside the accelerating layer.

The model includes the kinetic equation for the non-collision electrons inside the LT acceleration layer and the kinetic equation for the electrons outside the layer. The late takes into account the dispersion and energy looses of accelerated electrons, the elastic and non-elastic collisions both with the charged and neutral components of ionosphere plasma. The boundary conditions for the electron distribution function inside the accelerating layer were formulated on the base of the analytic solution of the kinetic equation for the outside region. These boundary conditions take into account the probabilistic character of both the energy looses by accelerated electrons and their backwards reflection.

The model obtained could be solved only by using the effective numerical method. Calulations were done by the standard particle-in-cell method, developed for the collisionless plasma. Since the strong electric oscillations are excited in the layer the energy absorption becomes significant even for the rare collisions. These collisions are taken into account in the calculations by specially designed numerical method were model particles move under the action of external and self-consistent electrical fields. The last one is calculated from Poisson's equation for every time step. The particles are used for the description of both ion and electron components of a plasma. Some test programs were developed to check the algorithm including the study of particles dynamics, the conservation laws control and the numerical diagnostic methods for the model. These subprograms include outputs of spatial distributions of plasma parameters and a number of temporary dependences. Taking into account the available computers, base computing parameters appropriated to the problems considered were determined. The modern numeral methods used in the algorithm allowed, in particular, to reach the allowable size of space range up to 2000 Debay lengths, the number of model particles – up to 8

mln. (number of particles of each type can reach 4 mln.) and the ratio of masses of model electrons and ions – up to 300000. It corresponds to the real ratio in ionosphere case.

The method designed to include collisions is based on the method particle in cells. We found the analytic dependency connecting the physical collision frequency v with the total number of model collisions N_c. It has the form: $N_c = N \cdot \Delta t \cdot v$, were N is the total number of model particles, Δt – time step. The numerical experiments to determine the similar dependency were done. At that the problem of relaxation of initial plasma perturbation was solved. In Fig.1 the analytical and numerical results are compared. The solid line presents the analytic formula and the symbols correspond to the numerical results. The main result of the investigation is that the model relaxation goes in such way that the exciting energy is uniformly distributed between three degrees of freedom — axes x, y and z.
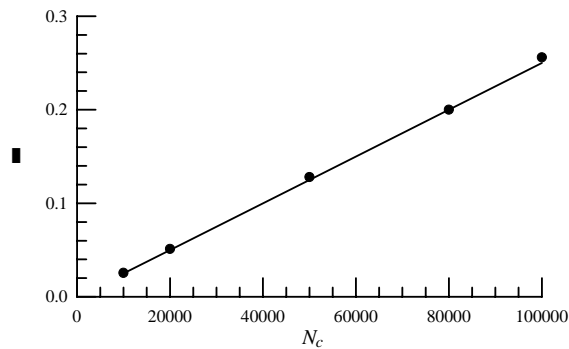

Fig.1.1.

The developed algorithm was tested. According to the theory the intrinsic noise in the model particle system is significantly larger than in the similar system of real particles. The investigation of the intrinsic noise (in the external field-free system) was done for different time step Δt, space step Δx and total particle number N. For example, while the total particle number grew from $2 \cdot 10^6$ to $4 \cdot 10^6$ the intrinsic noise decrease from 1.2 to 0.6. Here the intrinsic noise is measured (in normalized units) an integral of the squared electric field over the total system length (2000 Debye lengths).

The influence of the boundary conditions, collisions and the adiabatic switch of external electric field was studied. These factors don't determine the noise level but they do determine the electric field growth rate. The influence of the local external field distribution in the range is about $100 \div 400$ Debye lengths. Strong density gradients occur at the field boundaries. In the case of the rare collisions the cavitons appear in the electric field range. In the case of the frequent collision cavitons are not observed.

The numerical simulation of the process of the Langmuir turbulence exciting and it's coming out to the stationary regime was done. The simulation was done for the real ionosphere conditions. It required a large number of computer experiments with different parameters and regimes. Finally the conditions of coming up to the stationary regime were found. After the pump wave was switched on the sharp growth of field oscillations take place, and only after 300 – 1000 electron periods the quasi-stationary regime was reached. An example of such solution is presented in Fig.1.2. The electron distribution function was studied in the thermal region. It was shown that it Maxwell like. It's temperature depending on the energy of the pump wave.
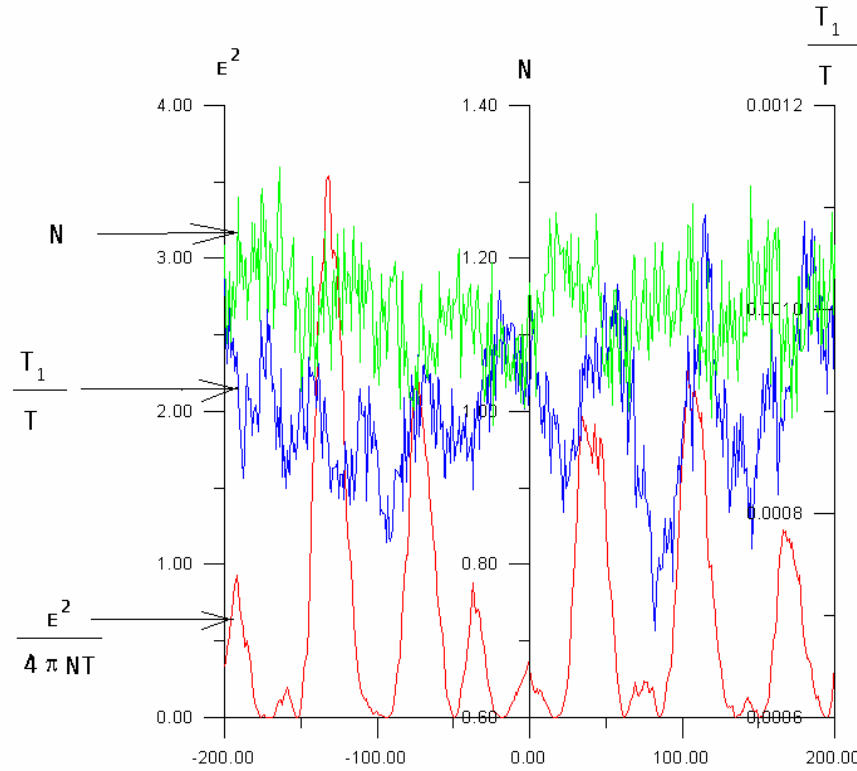
Fig.1.2.

The simulations of LT development show that as far as electric field amplitude of the pump wave exceeds the critical value electric field oscillations concentrated in the density depletions (cavitons) sharply increase. Due to the parametric instability the plasma oscillations arise. As it is seen in Fig.1.2 the oscillations lead to the oscillations field energy increasing. The electrons oscillation energy increase simultaneously. In Fig.1.2 example the electron oscillation energy reaches the significant portion of their thermal energy (up to 50% and even more) as early as $t \approx 200 \div 300$ (in inverse plasma frequency units). At that, the electric field energy and the electron kinetic energy oscillate with doubled electron plasma frequency. The oscillations are in antiphase.
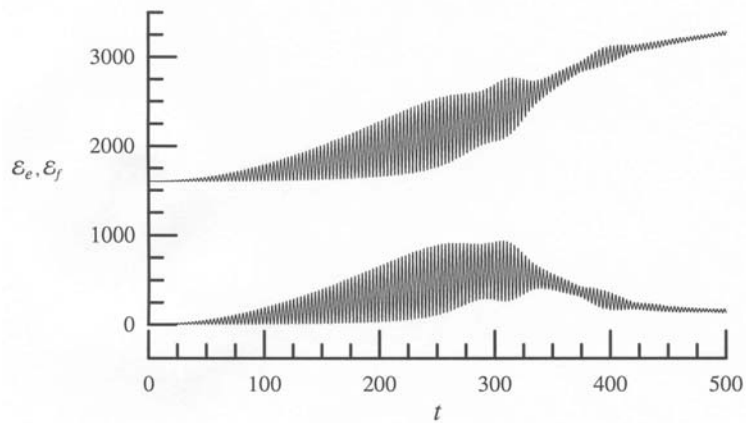

Fig.1.3. Time dependence of the electron energy density ε_e and the electric field ε_f .

Starting from $t_m \approx 250 - 300$ the monotonous energy grow stops due to exciting strong non-linear processes determined by the development of the modulation instability. Time t_m for the case of ion-electron mass ratio about 100 corresponds exactly to the ion oscillation characteristic time and, correspondingly, to the modulation instability increment in strong field. It is seen that the instability suppress the sharp growth of the field and electron energy. Simultaneously the combined oscillations of electrons and ions arise. The plasma density depletions – cavitons appear. They are shown in Fig.3 for time $t=350$. The developed density depletions with the depth up to $0.2 \div 0.3$ of the non-perturbed electron density are seen. At that the electron and ion density perturbations are similar – cavitons are semi-neutral. The cavi-

ton width is about 15÷20 Debye radius, the characteristic distance between them is approximately 50 Debye radius. Naturally, the regions of strong excited cavitons coincide with the regions of pump-wave field amplitude maximum. The density depletions are well correlated with with the average density of plasma oscillations captured in cavitons (Fig.1.3).

The captured wave is stationary as it is seen in Fig.1.4 At that the oscillation phases vastly differ even in two neighboring cavitons. In the fist time interval up to $t = 400 \div 500$ the caviton depth strongly increases. Then the growth become weaker and at $t > (1 \div 2) \, 10^3$ the ion-sound wave with the amplitude $0.2 \div 0.3$ is established. It is filled with relatively weak electron oscillations (Fig.1.5). So, the cavitons in the case do not collapse but stabilize. *The stabilization takes place due to the plasma oscillations (excited in the density depletions by the pump wave) absorption by the accelerated electrons.*

The further turbulence develops leads to the caviton pulsation stabilization. The obtained fast particle distribution function is shown in Fig.1.6.

The theory is presented in [4], see the list of publications.
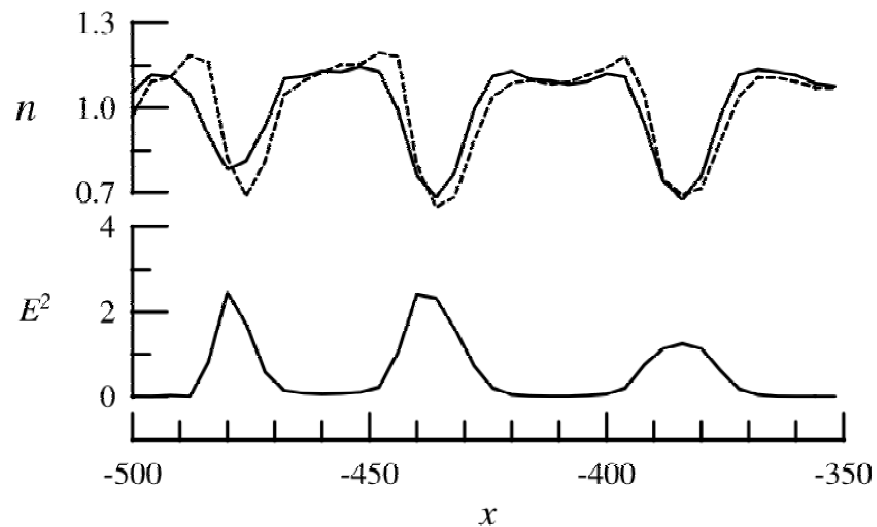
Fig.1.3. Dependency of the ion density (solid line)and electron density (dashed line) - up, and the electric field squared (here and below normalized by the thermal energy of plasma) - down, on the coordinates for time t=350. Here and below x - the distance in Debye lengths count off from the pamp-wave maximum position.
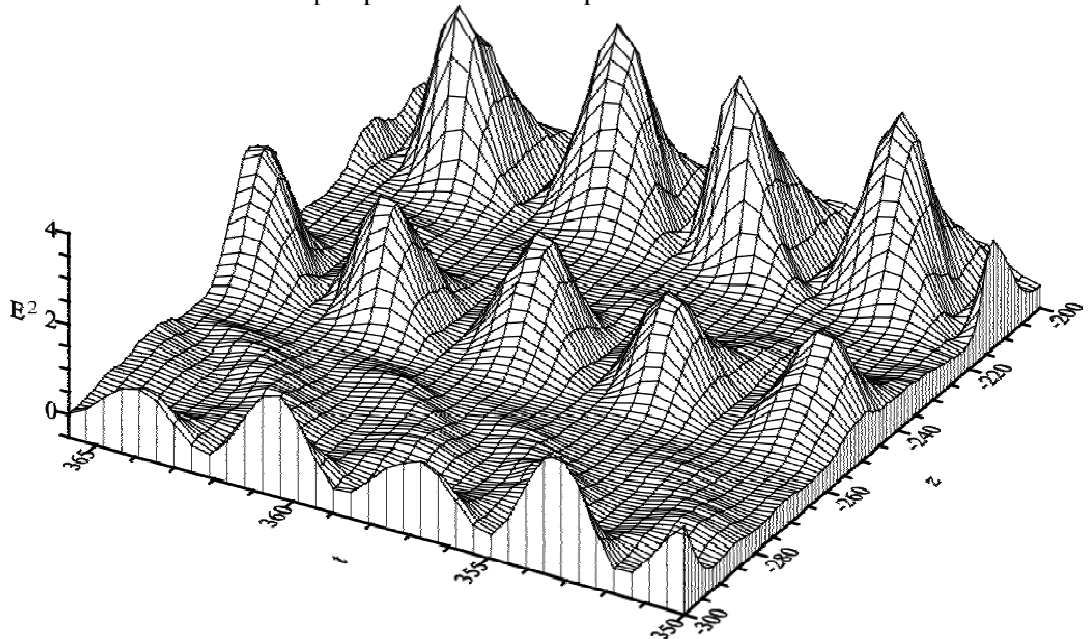
Fig.1.4. Space-time distribution of the electric field squared in the range from -300 to -200 Debye lengths and in the time range from 350 to 366. See capture to Fig.3.

Fig.1.5. Space-time distribution of the electric field squared (up) and level lines of plasma density (down) in the range from -300 to -200 Debye lengths and in the time range from 1500 to 1520. See capture to Fig.1.3.

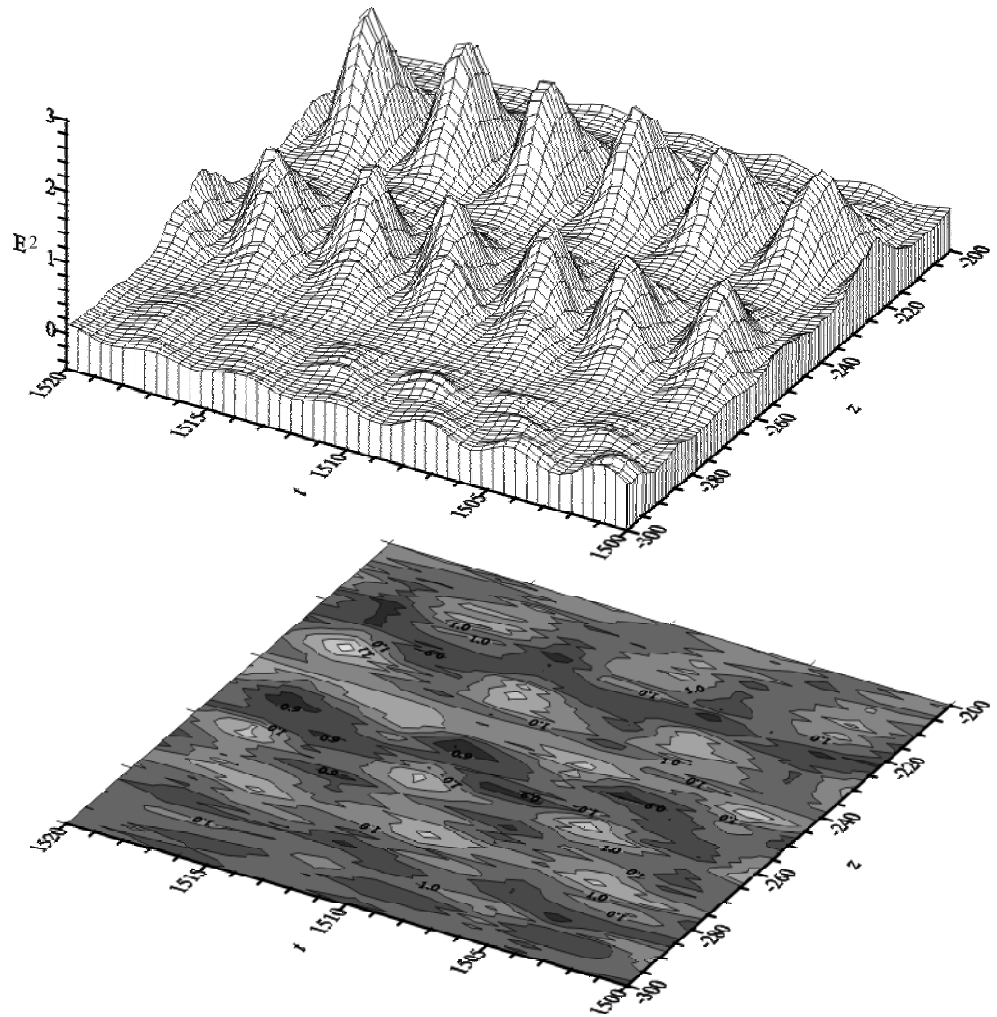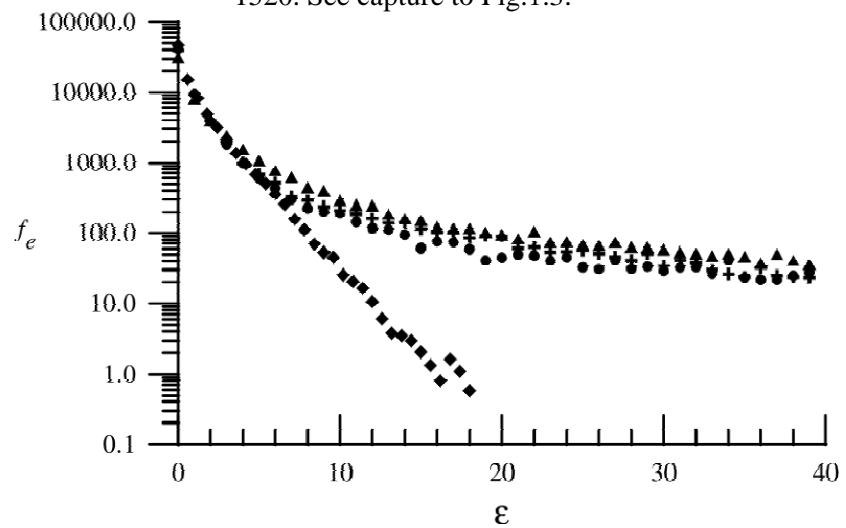Fig.1.6. The electron distribution function for different times: rhombuses — t=0, circles — 300, crosses — t=1000 и triangles — t=3000

Task 2.   Theoretical study of the optic emission excited by the suprathermal electrons

Tasks 2 and 3 are strong connected with each other. That's why we place the joint report on these Tasks in the next Section.

Task 3.   Developing of the theory of Ionosphere structuring under the action of powerful radio wave

A new effect in ionospheric modification by powerful radio waves was found during last year experiments at high latitude (HAARP, TROMSO) and mid latitude (SURA) facilities [1]. The very strong and fully reproducible plasma perturbations in ionosphere are observed exactly in *magnetic zenith direction}* – the point in the sky where the line of sight from the powerful transmitter is directed parallel to the field line. The magnetic zenith effect comes as a result of strong nonlinear process of plasma structuring anomalous heating and acceleration of electrons determined both by the developing of striations and by the exciting of upper hybrid turbulence.

1. Basic relations

The strong interaction of the powerful heater wave with ionospheric plasma in F layer is determined by two instabilities excited in the reflection region of pump O-wave: resonance instability and parametric instability.

The *resonance instability* take place in the vicinity of the upper hybrid resonance point z_{uh}, where ionospheric plasma density N(z):

$$N(z_{uh}) = \frac{\pi m}{e^2}(f_0^2 - f_c^2) \tag{1}$$

Here f_0 is a frequency of a pump wave and f_c – electron gyrofrequency. The resonance instability results in simultaneous excitation of upper hybrid plasma waves and small scale density depletions, aligned magnetic field – *striations*. Just these processes treated together are called upper hybrid turbulence. Generation of striations is one of the most important physical phenomena discovered during ionospheric modifications. A theory describing stationary state of isolated striations has been developed by Gurevich, Lukyanov and Zybin [3]. According to this theory there are two main features of stationary striations: the strong enhancement of electron temperature inside striations (($T_e \approx (2 \div 4) \, T_e$)) and a permanent small deficit of plasma density $N_1 = N - N_0 \approx -(002 \div 0.1)N_0$. The negative density perturbations inside striations N_1<0, have an important physical consequence. Because of this, the average electron density is reduced during the excitation of a large number of striations. This fact results in a new nonlinear process –*self-focusing on striations* of the pump wave E_0 [4].

The enhancement of the field E_0 in the focusing region leads in turn to an increase of the striations. Thus, there is a close nonlinear connection between striation generation and focusing of a pump wave, which results in formation of {\it nonlinear structures} in the disturbed region of ionosphere [5]. A significant peculiarity of self-focusing on striations is connected with the fact that this process *is strongly anisotropic* – the focusing take place in the plane perpendicular to the magnetic field only. Thus the direction parallel to the Earth magnetic field is singled out – all nonlinear structures selforganized due to self-focusing on striations are aligned the magnetic field. One of such structures – a *soliton - type* solution describing "bunches" of striations and soliton - like pump wave field distribution was described in [4].

During *in situ* rocket measurements at Arecibo Kelley et al [6] observed striations directly. The nonlinear structuring – bunches of striations (solitons) and large scale structures ("patches") are manifested in the observations as well [6],[7]. It was shown by the theory that in northern or midlatitude ionosphere self-focusing lead to formation of the large nonlinear structures aligned magnetic field, which consists of a number of closely packed solitons – bunches of striations [5]. Pump wave trapped and focused inside this structure propagates along magnetic field [8].

The anomalous absorption of a pump wave on striations lead to the strong ohmic heating of electrons in the focused region due to collisional damping of effectively excited inside striations upper hybrid waves [8] what results in production of red line emission [9] in upper hybrid turbulence region.

The *parametric instability* take place in the Langmuir resonance z_L close to reflection point of the pump wave $N(z)=N(z_L)$:

$$N(z_L) = \frac{\pi m}{e^2} f_0^2 \tag{2}$$

The parametric instability results in the effective excitation of Langmuir electron and ion plasma waves and generation of Langmuir turbulence region. Nonlinear processes in Langmuir turbulence lead to creation of Langmuir *cavitons* – density depletions filled by the Langmuir plasma oscillations [10],[11]. The theory of the corresponding processes is described in Task 1.

The fast electrons, passing through the turbulent region filled with cavitons obtain the energy from the trapped in caviton plasma oscillations. The main feature of this mechanism is that the energy is gained only by fast electrons whose velocity is high enough $v > a/(\pi f_0)$, where a is a scale of a caviton [12]. Low energy electrons oscillate in the caviton adiabatically and do not get any additional energy.

The relative role of these two main turbulent processes in ionospheric modifications is determined by the conditions of their excitation. The striations exists when amplitude of pump wave field E_0 exceeds E_{th}^s [3]:

$$E_{th}^s = 35.3(\cos\alpha)^{-1}(T_0 N)^{1/2}\sqrt{\frac{L_T^2}{L_0 L_N}\sqrt{\frac{\delta V_{T_e}}{c}}}F_s\left(\frac{F_s}{f_0}\right) \tag{3}$$

Here α – magnetic field inclination angle, N and T_0 non disturbed density and temperature of plasma electrons. L_T, L_N and L_0 are characteristic scales in ionosphere determined below (6), (8). At the F-layer heights $z \approx 300$ km parameter $L_T/\sqrt{L_0 L_N} \approx 1$. Small parameter δ describes mean part of electron energy lost in one collision, in F layer for thermal electrons $\delta \approx 10^{-4}$, $V_{T_e} = \sqrt{T_e/m}$ – thermal velocity of electrons, c – speed of light. Factor $F_s(f_c/f_0) \approx 1$.

The threshold electric field for parametric instability (Silin [16], DuBois and Goldman [17]) is:

$$E_{th}^p = 4(N T_0)^{1/2}\sqrt{\frac{\nu}{f_0}}F_p(T_i/T_0) \tag{4}$$

Here T_i is ion temperature, ν_e – collision frequency of electrons, factor $F_p \approx 1$. Taking into account relations (3), (4), one can rewrite the excitation parameters $e_s = E_0/E_{th}^s$ и $e_p = E_0/E_{th}^p$ in a form:

$$\backslash e_s = \frac{E_0}{E_{th}^s} = 5\sqrt{\frac{(EPR)_{MW}}{(f_{0MHz})^2}}\left(\frac{300\,km}{z_L}\right)\left(\frac{T_0}{10^3 K^\circ}\right)^{-3/4}\left(\frac{\delta}{10^{-4}}\right)^{-1/2}q_s\kappa_s \tag{5}$$

$$e_p = \frac{E_0}{E_{th}^p} = 1.2\sqrt{\frac{(EPR)_{MW}}{(f_{0MHz})^3}}\left(\frac{300\,km}{z_L}\right)\left(\frac{T_0}{10^3 K^\circ}\right)^{1/4}q_p \cdot 10^{-K_{as}/2}\kappa_s \tag{6}$$

$$q_{p\max} = 1.90\left(\frac{2\pi f_0}{c L_0}\right)^{1/6}, \quad q_s = \sqrt{\frac{f_0}{f_c}}, \quad L_0 = \left(\frac{N}{\frac{dN}{dz}}\right)_{z_L}$$

In numerical expressions *ERP* – effective radiated power in MW, f_0 – pump wave frequency in MHz, z_L – reflection point height for vertical propagation of O-wave in km. Factors q_s and q_p describe the growth of the pump O-wave amplitude in the vicinity of reflection point, $q_{p\,max}$ given in (6) is the main Airy maximum [18], K_{as} is anomalous absorption on striations. Factor $\kappa_s(z,\theta)$ describes the diminishing of pump wave amplitude due to its scattering on striations (field aligned scattering). We consider here the beam propagating along magnetic field ($\theta = 0$), in this case factor $\kappa_s \approx 1$.

As an a example we will consider now the HAARP facility. The *ERP* for HAARP as a function of frequency f_0 is presented in the Table 1.

Table 1
ERP as function of wave frequency for HAARP (2001)

f_0 (MHz)	ERP (MW)	ERP/f_0^2	ERP/f_0^3
3.0	14.2	1.58	0.53
3.2	20.0	1.98	0.61
4.0	37.5	2.34	0.58
5.0	67.3	2.68	0.54
6.0	93.6	2.6	0.44
7.0	131	2.67	0.38
8.0	179	2.8	0.35

One can see from (5) and Table 1, that stationary striations condition $e_s > 1$ is well fulfilled at any frequency not only for full HAARP power, but at 10% of ERP or even less.

Quite different situation is for parametric instability (6). Here the amplitude growth factor q_p near reflection point plays a decisive role. At the first Airy maximum q_p\approx 5 and excitation conditions $q_p > 1$ are well fulfilled. But that is correct only at the first moments after transmitter is put on [19], [20]. As soon as striations are excited (it takes *1* sec or more) anomalous absorption on striations K_{as} becomes important. The absorption takes place below z_L and diminishes pump wave amplitude in Langmuir resonance z_L. The dependence of K_{as} on pump wave frequency f_0 is a very important factor – both the upper hybrid waves energy absorption $\sim f_0^{-2}$) and dimension of anomalous absorption region $\Delta_{uh} \propto f_0^{-2}$ (see (9)) are growing effectively with diminishing of pump frequency f_0. Due to this fact, for low values f_0\approx 3 - 4 MHz factor K_{as} can reach 6 – 8 dB and even more [18], [21]. It means, that for HAARP conditions (see Table 1.) at {\it low pump frequency} $f_0 \approx 3 \div 4$ MHz we have strongly excited striations and strong anomalous heating in striations. At the same time parametric instability is very weak or not excited at all. For *high pump frequencies* $f_0 \approx 6 \div 9$ MHz absorption and heating in striations is not so strong and parametric instability could be well excited. Analogous situation is for TROMSO and SURA facilities

That is why , discussing magnetic zenith effect in modified F layer of ionosphere one has to consider two different limits. For low frequency (or *heating*) limit optic emission from the disturbed ionospheric region is determined by anomalous heating of electrons in striations. For high frequency (or *multiple acceleration*}) limit Langmuir turbulence plays the main role. It should be noted, that for the beam directed to magnetic zenith the role of magnetic field inclination angle α is significant. It would be considered in the section 5.

\subsection{Heating}.

Let us consider the effect of ohmic heating due to anomalous absorption of the pump wave. Heating and transport processes determine the significant changes of electron temperature and plasma density in ionospheric F-region. It is important that the transport processes in the upper ionosphere are strongly anisotropic. It means that considering the large scale plasma structures one can take into account the transport along magnetic field only. The transport equations for plasma density N and electron temperature T_e take the form [18]

$$\frac{\partial N}{\partial t} = -\gamma N + \frac{\partial}{\partial s}\left(D_e \frac{\partial N}{\partial s} + D_{T_e} \frac{N}{T_e} \frac{\partial T}{\partial s} \right) \tag{7}$$

$$\frac{\partial T_e}{\partial t} = \frac{Q}{N} - \delta\nu(T_e - T_0) + \frac{\partial}{\partial s}\left(\kappa_e \frac{\partial T_e}{\partial s} \right)$$

Here γ^{-1} is recombination time, D_e – diffusion and D_{Te} thermodiffusion coefficients. The first term Q in right side of second equation determines the heating of electrons. It describes the power density dissipation due to anomalous absorption of the pump wave. Term $\delta\nu$ determines energy loss due to elastic and inelastic collisions of electrons with ions and neutrals, κ_e – electron thermal conductivity along magnetic field.

The characteristic scales of plasma density L_N and electron temperature L_T as follows from (7) are:

$$L_N = \sqrt{\frac{D_e}{\gamma}}, \qquad L_T = \sqrt{\frac{\kappa_e}{\delta\nu}} \qquad (8)$$

In conditions of ionospheric F layer (see [18], § 5.3, Table 16)

$$L_N \approx L_T \approx 30\,\text{km}$$

The ohmic heating of electrons due to anomalous absorption of the pump wave on striations take place in the vicinity of the upper hybrid resonance z_{uh} (1). The width of absorption region Δ_{uh}:

$$\Delta_{uh} \le z_L - z_{uh} \approx \frac{f_c^2}{2f_0^2} L_0 \qquad (9)$$

The gardient scale L_0 determined by (6) usually is *50 – 100* km. For ionospheric F-layer the conditions $\Delta_{uh} \ll L_N, L_T$ are always fulfilled. It means that the heating in (7) is local and could be presented in a form

$$Q = \left(\int Q(s_1)ds_1\right)\delta(s), \qquad \int Q(s_1)ds_1 = 3\delta_0 \nu_{e0} N_0 T_0 q$$

Here $\delta(s)$ is Dirac delta - function, and q is dimensionless parameter which define the disturbances of plasma density and temperature due to anomalous absorption:

$$q = \frac{8\pi P(r_\perp)e^2}{\omega_0^2 \sqrt{m\delta} T_0^{3/2}} F_b \approx 8.0p\frac{(ERP)_{MW}}{(f_{0MHz})^2}\left(\frac{1000^\circ}{T_0}\right)^{3/2}\left(\frac{10^{-4}}{\delta}\right)P_1(\theta)F_b \qquad (10)$$

$$P = 1 - \exp(-2K_{as}(f_0))$$

Here we supposed that the pump wave frequency f_0 is below the critical frequency of F layer, $P(r_\perp)$ is absorbed energy flux, T_0 – non disturbed electron temperature. In numerical expressions $P = p \cdot (ERP)$, where absorption coefficient $p \approx 0.7 \div 0.9$, and factor $P_1(\theta)$ normalized on the unity $P_1(0){=}1$ describes the angular power distribution in the beam. δ is the mean part of electron energy dissipated in collisions, F_b is the beam focusing factor, determined below.

Following [18] §5.3 let us now find a stationary solution of (7-10). It is shown at Fig.1. We see that due to anomalous absorption the electron temperature T increases with q, but quite slowly. The plasma density is always diminishing $N_1 < 0$ but the depletion value is rather small. At $q{=}20$ depletion $|N_1/N|$ reaches maximum value $|N_{1m}/N| = 0.16\,L_N/L_T$ (see Fig.1) At $q \ll 1$ | $N_1/N| = q\,L_N/(2L_T)$.

Thus we see, that density depletions initially are growing with q, but at $q \ge 0.1$ nonlinear processes began to play a decisive role, leading to saturation N_1/N.

3. Beam focusing.

The density depletion region in ionosphere is determined by anomalous absorption of pump wave on striations. Due to transport processes it begins from the heights of the order of $L \approx 30 - 50$ km below the reflection point of O - wave. The numerical analysis performed in [5] demonstrates that in northern or midlatitude ionosphere the significant part of beam should be trapped in the depletion region. If the beam is initially directed along magnetic field $\theta = 0$, this effect is especially strong. Main part of the beam propagates along the magnetic field lines **B** and focused in the plane $r_\perp$ perpendicular to **B**. The focusing is described by nonlinear parabolic equation [4], [8]

$$2ik\frac{\partial E}{\partial s} + \frac{\partial^2 E}{\partial x^2} + \frac{\omega^2}{c^2} <\varepsilon_2(E)> E = 0, \qquad E = E_{th}^s \sqrt{\eta} e^{i\phi} \qquad (11)$$

Here we supposed for simplicity that the beam is one-dimensional. Nonlinear term in the case of focusing on striations has a specific form:

$$\langle\varepsilon_2(\eta)\rangle = 0.04\left(1 - \frac{1}{\eta^2}\right) \quad \text{для} \qquad \eta \ge 1 \qquad (12)$$

$$\langle\varepsilon_2(\eta)\rangle = 0 \qquad \text{для} \qquad \eta < 1$$

The natural initial conditions for the beam in ionosphere at $s = 0$ are:

$$\eta_0(x) = e_s^2 \left[1 - \left(\frac{x}{a} \right)^2 \right] \tag{13}$$

Here $a = \theta_0 z_0 \cos\alpha$ is the effective width of a beam at the beginning of nonlinear region z_0 and θ_0 is launch beam angle width.

The solution of equation (11)–(12) is shown at the Fig.2. One can see from equation (11), that integral $\int \eta(x)dx$ is conserved. It means that with the growth of intensity the width of the beam is diminishing, as is shown at the Fig.2a,b .

Thus we see that during propagation along magnetic field **B** the initial width of trapped beam due to self focusing on striations could become significantly less. It is determined by the focusing factor $F_b = 2 - 3$ or even higher

4. Shift of reflection point}

Near the reflection point the pump wave amplitude is increased [34]. The amplitude increasing leads to the plasma heating. Owing to this the plasma perturbations become amplified. The relation between increasing temperature, density depletion, and its dependence on absorbed HF power one can see in Fig.1. The change in electron density results in distribution of the wave field. Let us consider the effect of these changes for a not too strong field, $E_0^2 < E_p^2$, where $E_0^2 = 3T \frac{m}{e^2} \delta(\omega^2 + v_e^2)$. The last condition is equivalent $q < 1$ or $log(q) < 0$ in Fig.1.

Equation (7) for the electron temperature takes the form [18]:

$$L_T^2 \cos^2\alpha \frac{d^2 \Delta T}{dz^2} - \Delta T = -\frac{2\phi\phi_H E_0^2 T_{e0}}{E_p^2 \sqrt{\varepsilon}}, \qquad z < z_0 \tag{14}$$

Here α is the angle of magnetic field to vertical direction, ε – dielectric constant, φ and φ_H polarization factors (see [18], §5.2.2). When the concentration perturbation is taken into account, the dielectric constant in the reflection region has a form

$$\varepsilon = \frac{z_0 - z}{L_0} - \frac{\Delta N}{N_0}, \quad \frac{\Delta N}{N_0} = -k_T \frac{\Delta T}{T_0}$$

Here z_0 is the reflection point of the wave in unperturbed medium, a linear plasma density gradient was supposed, and the changes of dielectric constant caused by density decreasing shown in Fig.1 is taken into account. It is possible to introduce a new reflection point z_1 at which $\varepsilon(z_1)=0$: $z_0 - z_1 = L_0 \frac{\Delta N(z_1)}{N_0}$

The difference $z_0 - z_1$ is the shift of reflection point determined by heating of plasma by pump wave. To calculate this shift it is necessary to solve the equation (14). The solution of this equation and the shift of the reflection point was obtained previously in [18]. This shift depends on parameter $\xi = \left((\phi\phi_H k_T)^{1/2} E_0/E_p \right)^{-4/3} \frac{L_T}{L_0 \cos\alpha}$.

For $\xi << 1$ $\qquad z_1 - z_0 = \frac{3}{2^{2/3}} \left((\phi\phi_H k_T)^{1/2} E_0/E_p \right)^{4/3} L_0 \tag{15}$

For $\xi >> 1$ $\qquad z_1 - z_0 = \phi\phi_H k_T E_0^2/E_p^2 \left(\frac{\pi L_0}{L_T \cos\alpha} \right)^{1/2} L_0 \tag{16}$

Let us estimate the shift of reflection point. One can see that for typical ionospheric condition in F-layer at the effective radiated power $P > 10$ MW parameter $E_0^2 / E_p^2 \geq 0.05$ and the shift of reflection point is: $z_1 - z_0 \geq 2 \div 5$ km. The shift is growing with the power of heating facility and can reach $20 - 30$ km.

\subsection{Beam inclination}

Let us discuss the beam propagation when the magnetic field is inclined at the angle α to the vertically inhomogeneous ionosphere. According to the linear theory [34] the reflection of the plane ordinary wave

inclined initially in the magnetic meridian plane at small angle χ to vertical take place in Langmuir resonance z_L (2) if $\chi < \chi_s$, where

$$\chi_s \approx \sqrt{\frac{f_c}{f_0 + f_c}}\alpha, \quad \alpha << 1,$$

and $f_c = eH/2\pi mc$ is the cyclotron frequency. In ionospheric conditions $f_c \approx 1.3 - 1.4$ MHz The reflection at heights higher than the upper hybrid resonance point z_{uh} take place if $\chi \leq \chi_t$, where

$$\chi_t = \chi_s + \Delta, \qquad \Delta \approx \frac{f_c}{f_0}\sqrt{\frac{L_0}{z_L}} \tag{17}$$

Thus the excitation of striations leading to the complex of nonlinear process considered previously is significant for the ray beams with $\chi \leq \chi_t$. We note that nonlinear effects in the reflection region for the rays with $\chi \approx \chi_t$ are strongly amplified due to the growth of the pump O -wave amplitude in the vicinity of reflection point z_{duh} [34]. For all rays which have the inclination angle bigger than χ_t the reflection point according linear theory is located below the upper hybrid resonance. The upper hybrid turbulence could not be excited in this case if we consider linear processes only. But if nonlinear effects are taken into account, according to the results of the previous section (15), (16) the location of the reflection point is shifted due to plasma heating. This shift is big enough and in real heating experiments at $P \geq 10$ MW it allows to penetrate HF power above upper hybrid resonance point and excite upper hybrid turbulence in the magnetic zenith direction.

Thus the excitation of striations leading to the complex of nonlinear processes considered previously is significant not only for the rays of beam with $\chi \leq \chi_t$ but for the rays with $\chi \geq \chi_t$ as well due to the nonlinear shift of reflection point [34]. Considering HAARP facility we see that in the frame of linear theory at high frequency range $f_0 \geq 5$ MHz the condition (17) is fulfilled only for a part of the beam, as is shown at Fig.3. According to nonlinear theory due to the strong field amplification the shift of reflection point in the vicinity of double upper hybrid resonance z_{duh} is large (15), (16) (see Fig.3). Parameter e_s (5) is large ($e_s >> 1$) and effective excitation of striations can take place at any frequency $f_0 \leq 8 - 10$ MHz (see Table 1). Striations are extended along magnetic field from this point up and downwards, as is shown at Fig.3b. Thus nonlinear cavitons and nonlinear cavity are formed up to 20 – 30 km below point z_{duh}. The pump wave effectively trapped inside the cavity as was already shown by the detailed ray tracing calculations in [5] (see Fig.1 [5]). It leads to additional heating in the cavity. Due to this significant part of the beam energy at high pump frequencies ($f_0 \sim 5 - 10$ MHz) will reach the Langmuir resonance region and serve for the effective excitation of Langmuir turbulence (see [5] Fig.1 and section 1.1 of this paper). For HAARP conditions angle $\chi_{duh} \approx \alpha$ is close enough to magnetic zenith angle (see Fig. 3b). Thus we see that at high pump power at the northern HAARP ($\alpha \approx 14°$) and Tromso ($\alpha \approx 12°$), facilities the excitation of high frequency Langmuir resonance due to nonlinear shift of reflection point and developing of striation mechanism is effective.

For midlatitude conditions (SURA) the structure of disturbed region for the given beam inclination angle χ is shown in the Fig.3c. The maximal heating effect take place near the beam reflection point z_0. The heated region during some time spreads along magnetic field up to the upper hybrid resonance point in accordance with the relations (15), (16). Then the resonance instability is developing what results in the effective growth of striations. In the region filled with striations due to self focusing on striations soliton-like structures are developing. As a result beam is trapped. Due to anomalous absorption of trapped pump wave on striations a strong heating of electrons take place. That lead to the creation of a large nonlinear structure with high electron temperature and average density depletion up to 10 % (dashed region in Fig.3c.).

This structure is growing along magnetic field in both directions from the upper hybrid resonance point at the significant distance an order of L_T. In that way the nonlinear channel along magnetic field is formed. The channel is directed into magnetic zenith; inside this channel a part of pump wave is trapped. Approximate condition for beam inclination angle χ which determines the most strong magnetic zenith effect for mid and low latitude ionosphere has the form:

$$\chi \approx \alpha - \frac{L_0}{z_L} \tag{18}$$

As follows from (18) magnetic zenith effect depends significantly on magnetic field inclination, pump wave power P and frequency f, and the width of the beam θ_b, ($\theta_b < L_0/z_L$).

The detailed measurements and further development of the theory can throw additional light on the magnetic zenith effect physics.

For the low frequency pump wave $f_0 \approx 3 - 4$ MHz the situation is quite analogous to the one considered in the section 1. Condition (17) could be fulfilled for the beam maximum up to $\alpha \approx 30°$ and the whole beam power determine the pure heating nonlinear processes at magnetic zenith. Additionally it should be taken into account that the averaged plasma depletion in the UH cavity is less or equal 10 %, what means that for beam frequency $f \leq 4$ MHz the trapped beam became weak in Langmuir resonance region.

Really:

$$\frac{N(z_L) - N(z_{uh})}{N(z_L)} \approx \frac{f_c^2}{f_0^2} > 0.1, \quad \text{for} \quad f_0 \leq 4\,\text{MHz}$$

We note, that in early Arecibo experiments growth of plasma electron temperature up to $T_e/T_0 \approx 2 - 3$ was observed after a long time heating (30 min) simultaneously with large plasma density reductions – up to 40 % [29-31]. The magnetic field aligned structures were not established in these works. Recently large scale plasma density depletion elongated magnetic field was observed in a long time heating experiments at TROMSO, HAARP and SURA [33].

6. Multiple acceleration

Multiple acceleration is effective when strong Langmuir turbulence is excited. It determines the structure of a high energy tail of electron distribution function and a wide spread of fast electrons around the Langmuir turbulence layer. Multiple acceleration process is described by kinetic equation for energetic electrons in ionospheric plasma. Solution of kinetic equation obtained in [13] has a form:

$$f(\varepsilon, s) = C K_0 \left(\varepsilon \big/ T_{ef} \right) \exp\left[-\left| \int_{z_L}^{s} \frac{ds'}{L_e(s')} \right| \right]$$

Here $K_0(x)$ is modified Bessel function, T_{ef} – effective temperature, determined by acceleration of electrons in cavitons excited in Langmuir turbulence layer. $L_\varepsilon(s) = (\sqrt{3\delta} N_m(s)\sigma_t)^{-1}$ – characteristic scale of the region filled with fast electrons, N_m – density of neutrals in ionospheric plasma, σ_t transport cross section of electron collisions, δ – mean part of electron energy lost in one collision. We note, that electrons, having energy $\varepsilon \leq 2$ eV in F- layer collide with neutral molecules mainly, inelastic collisions are not significant; parameter δ grew up with ε taking values $\delta \approx 10^{-2} - 0.1$ [13], [14]. Parameter C is directly connected with the number density of fast electrons N_f or the full dissipated power P_a of the pump wave which goes to the acceleration of electrons in cavitons:

$$C = \frac{N_f}{8\pi} \left(\frac{m}{T_{ef}} \right)^{3/2} = \frac{m^2}{4\pi^3 \left(\delta \big/ 3 \right)^{1/3} T_{ef}^3} P_a \tag{20}$$

Parameters T_{ef} and P_a are determined by the characteristic width and the number of cavitons in the Langmuir acceleration layer. To find these parameters or to match the distribution function in the tail (19) with its main thermal part, a numerical solution of kinetic equations in conditions of the strong Langmuir turbulence was recently performed in 2[15]. An example of this solution is presented at Fig.4. One can see from the figure that in the high energy tail distribution function is close to maxwellian with very high effective electron temperature $T_{ef} \gg T_0$ just as it follows from (19). For the considered conditions $ERP = 180$ MW, $f_0 = 8$ MHz effective temperature $T_{ef} = 10.5$ eV, power $P_a = 120$ kW and number density of fast electrons $N_f = 2.2 \times 10^{-4} N_e$. In dependence of conditions at high frequency limit HAARP power dissipated to electron acceleration P_a, is 7 – 15 % of the full power P_0 radiated by the transmitter.

We note that the pump wave propagating along magnetic field can reach the Langmuir resonance z_L only inside the focusing region due to diminishing of plasma density.

7. Discussion and the comparison with the observations

As an example, we will compare now the theory with the results of experiments [1]. Optic emission of red and green lines is determined by excitation and quenching of $O(^1D_2)$ and $O(^1S_0)$ electronic levels. Emission intensity I can be presented in the form:

$$I_{630} = 10^{-6} A_{12} \int \tau_q K_e^{(1)} N_e N_O dz, \qquad I_{557.7} = 10^{-6} \int K_e^{(2)} N_e N_O dz \tag{21}$$

Here I is expressed in Rayleighs, $K_e^{(1)}$ and $K_e^{(2)}$ are the excitation rates

$$K_e^{(n)} = 4\pi \int \sigma_e^{(n)} v^3 f_0(v) dv$$

where $\sigma_e^{(n)}$ is excitation cross section, $f_0(v)$ – distribution function of electrons normalized on the unity, N_e and N_O – density of electrons and oxygen atoms, \tau_q – quenching factor

$$\tau_q = \frac{1}{1 + \left(k_q^{N_2} N_{N_2} + k_q^{O_2} N_{O_2} + k_q^e N\right) t_1},$$

where quenching rates are $=2.3 \times 10^{-11}$ cm^3 s^{-1}, $k_q^O{}_2 = 5 \times 10^{-11}$ cm^3 s^{-1}, $k_q^e = 8.6 \times 10^{-10}$ cm^3 s^{-1}, N_{N2}, N_{O2} – number density of nitrogen and oxygen molecules, $t_1 = 150$ sec – life time of O(^{1}D$_2$) electronic level [22], [23]. Note that in F-layer the factor τ_q is determined mainly by N$_2$ molecules and could be approximated at $z = 300$ km (see [18] Table 1) as

$$\tau_q = \frac{1}{1 + 0.8 \left(N_{N_2} \Big/ 1.8 \times 10^8 \text{ cm}^{-3}\right)}. \tag{22}$$

Factor A_{12} appears here because the pumping of O(^{1}D$_2$) level is followed by two transitions O(^{1}D$_2 \to {}^3$P$_2$) and O(^{1}D$_2 \to {}^3$P$_1$) having 630 nm and 636.4 nm correspondingly. In observations 630 nm line is seen what means that only fraction of optical energy

$$A_{12} = \frac{A_{630}}{A_{630} + A_{630.4}} \approx 0.76 \tag{23}$$

goes to excitation of the observed line. Here $A_{630} = 5.1 \times 10^{-3}$ s^{-1} and $A_{636.4} = 1.6 \times 10^{-3}$ s^{-1} are the Einstein coefficients, O(^{1}D$_2$) lifetime is $t_1 = (A_{630} + A_{636.4})^{-1} = 150$ s. Electron impact cross sections for exciting O(^{1}D) and O(^{1}S) levels could be interpolated according [24] as:

$$\sigma(\varepsilon) = C_1(\varepsilon - \varepsilon_{th}) \exp\left\{-\frac{\varepsilon - \varepsilon_{th}}{\varepsilon_m - \varepsilon_{th}} k(\varepsilon)\right\} \tag{24}$$

For O(^{1}D) parameters are:
$\varepsilon_{th} = 1.96$ eV, $\varepsilon_m = 6$ eV, $C_1 = 2.1 \times 10^{-17}$ cm^2 eV^{-1}, $\sigma_m = 3 \times 10^{-17}$ cm^{-2} $\tag{25}$
and $k(\varepsilon)$ is a correction factor. For O(^{1}D)
$\varepsilon_{th} = 4.17$ eV, $\varepsilon_m = 14$ eV, $C_1 = 0.7 \times 10^{-18}$ cm^2 eV^{-1}, $\sigma_m = 2.5 \times 10^{-18}$ cm^{-2} $\tag{26}$
and correction factor $k(\varepsilon) \approx 1$. Interpolation (24) – (25) is correct from ε_{th} up to $\varepsilon \approx 30$ eV with the accuracy 10 %.

Low frequency limit
At the pump frequencies 3 – 4 MHz the decisive role is played by the heating of electrons in modified ionosphere. For HAARP as follows from Table 1 and Fig.1. electron temperature in this case can reach 3000° – 4000°. Supposing distribution function maxwellian we determine for full HAARP *ERP* and (21) – (25) in a focused region (see [1] $\Delta\theta = 6°$, $\Delta z = 30$ km) red line intensity $I_{630} = 210 – 300$ R in full agreement with observations [1].

Power dependence of I_{630} at low pump frequency according to the theory is shown at Fig.5. One can see a reasonable agreement between the theory and observations. At high electron temperatures $T_e > 3000°$ strong energy dissipation due to excitation of N$_2$ vibration levels lead to saturation of observed I_{630} emission. In some of the power ramp saturation effect is even clearer pronounced (see [1], Fig.5). Note, that kinetic effects in the tail of electron distribution function could be significant also [25].

High frequency limit
At high pump frequencies $f_0 \approx 6 – 9$ MHz according to the theory optic emission is determined by multiple acceleration process. Using distribution function (19) for full HAARP ERP (Table 1), we obtain from (19), (24), (25) green line intensity $I_{577.7} \approx 30 – 60$ R in agreement with experimental data (see [1] Fig.4). Green to red line maximal intensities relation as follows from the theory (19) – (25) in these conditions is 0.20 – 0.30, what is close enough to observational results ([1] Fig.4).

According to the theory the emission is growing effectively with the number density of oxygen atoms N_O. On the other hand the red line intensity declines with N_{N2}. Thus we see that the height distribution of ionospheric neutral components in the O - wave reflection region affect the emission significantly.

Note that for full HAARP *ERP* the theory predicts, that the red line emission both in low frequency and a high frequency limits is of the order *200 – 300* R. Green line in the same time is effectively growing with

the frequency, being close to zero at $f_0 < 4$ MHz. A good agreement between observations and theory is seen.

Time dependence of the red line thermal emission was already discussed in [25]. The main part here is played by $O^1(D)$ level long lifetime. The roles of the heating and focusing processes taking additional time of the order $20 - 40$ s are seen in observations [1] as well. Mostly interesting is the significant time delay of the green line (observed in [1]) which is of the order $\Delta t \approx 20$ s. Green line emission life time is about 1 sec. The effective acceleration and energy loss time $\tau_\varepsilon = (v N_m \sigma)^{-1}$ at $\varepsilon \approx 10$ eV, according to the theory is of the order of 1 sec also. It means that the focusing effects, which are determined by the diffusion and thermodiffusion processes should play the main role. At the heights $z \approx 300$ km diffusion coefficient along magnetic field $D_{//} \approx 2.4 \times 10^{10}$ cm^2 s^{-1} ([18] Table 16). Then the characteristic scale of the initial focusing effect is $R_f \propto \sqrt{2 D_{||} \Delta t} \approx 10$ km. The fully established focusing length could be $2 - 3$ times higher, what agrees with our discussion at section 1.4. So it looks that namely the striation formation and focusing process determine the temporal dependence of the spot emission. Much more detailed experimental and theoretical study of this problem is needed.

Fine structure

The disturbed region of ionosphere is strongly inhomogeneous due to existence of striations and bunches of striations. A special space filling factor η, which takes into account the influence of inhomogeniety of the optic emission was introduced in [9]. The inhomogeniety lead to a specific fine structure of optic emission both in electron heating (low frequency limit) and multiple acceleration cases. The emission consists of a strongly elongated magnetic field structures. Their characteristic scales along magnetic field lines can reach several kilometers. Across magnetic field they are of two types: a few meters $(2 - 5$ m$)$ and hundred meters. These structures can move all together due to general ionospheric drift determined by the external electric field. Analogous drift of the optic emission region as a whole was observed in [26], [28]. But a complex mutual motion of excited regions determined by drifts in the fluctuating internal electric fields also should exist. These internal drifts could be amplified by a specific drift instability [6], [7], [4].

So the theory predicts that the detailed study of optic emission in modified ionosphere can show a complicated fluctuating structure of emission region of aurora type. We emphasize that this "artificial aurora" is produced at the heights 300 km, much higher than the main region of natural aurora.

{\bf Flux of energetic electrons into magnetosphere}

The theory of multiple acceleration allows finding the tail of distribution function – its energy ε and height z dependence if the composition of neutral components in ionosphere is known. It follows that for a high frequency heater wave not only red 630 and green 557.7 but intensities of other oxygen and nitrogen lines: $\lambda = 777.4$ $(\varepsilon = 10.99$ eV$); \lambda = 844.6$ $(\varepsilon = 10.74$ eV$); \lambda = 391.4$ $(\varepsilon = 18.74$ eV$)$ could be predicted. More than that, the flux of suprathermal electrons flowing into magnetosphere could be found as well [13]. The estimates show that in our experimental conditions flux of electrons with characteristic energies $5 - 20$ eV and full power $P_f \approx 5 - 10$ kW is flowing into magnetosphere. This result agrees with the one obtained in [32] from direct observations of suprathermal electrons in Arecibo using ISR technique [14].

Much more detailed studies of optic emissions at different lines in magnetic zenith experiments at $f_0 = 6 - 9$ MHz are needed. These studies are to be combined with the theory and numerical calculations. Such approach could allow developing a new method of active studies in magnetosphere / plasmosphere using reproducible and controllable beam of energetic electrons generated in ionospheric modifications.

8. Conclusions

According to presented theory the ionospheric modification effects are strongly amplified when powerful beam of radio emission is trapped in the cavity due to nonlinear process and directed along magnetic field lines. This {\it magnetic zenith effect} is determined by self-focusing on striations and anomalous heating which leads to the formation of a cavity elongated for hundred kilometers. The theory predicts the dependence of magnetic zenith effect on the main parameters: pump wave power and frequency, inclination angle of magnetic field, pump beam width and inclination. A good agreement between the theory and recent observations is demonstrated.

The possibilities of further experimental and theoretical studies of magnetic zenith effect are indicated. Such studies could allow to develop new method of active investigation of magnetosphere / plasmasphere using reproducible and controllable beam of energetic electrons, generated in ionospheric modifications.

References

[1] T.Pedersen, M. McCarrick, E.Gerken, C.Selcher, D.Sentman, H.Carlson, A.Gurevich, Geophys.Res.Lett. 30 (4), 1169, 2003.
     M.T.Rietveld, J.M.Kosch, N.F.Blagoveshchenskaya, V.A.Kornienko, T.B.Leyser and T.K.Yeoman, J. Geophys. Res. 108, A4, 1141, 2003.
     E.Gerken, RF Ionospheric Interaction Workshop, 389, 18-21 April, Santa Fe 2004
     M.Kosch, RF Ionospheric Interaction Workshop, 117, 18-21 April, Santa Fe 2004
     E.D.Tereshchenko, B.Z.Khudukon, A.V.Gurevich, K.P.Zybin, V.L.Frolov, E.N.Myasnikov, N.V.Muravieva, H.C.Carlson, Phys.Lett.A 325, 381, 2004.
[2] A.V.Gurevich, K.P.Zybin, H.Carlson, T.Pedersen, Phys.Lett.A 305, 264, 2002
[3] Gurevich A.V. K.P.Zybin and A.V.Lukyanov, Phys.Rev.Lett. 75, 2622, 1995.
[4] Gurevich A., T.Hagfors, H.Carlson, A.Karashtin and K.Zybin Phys.Lett.A. 239, 385, 1998
[5] Gurevich A., H.Carlson, M.Kelley, T.Hagfors, A.Karashtin and K.Zybin, Phys.Lett.A. 251, 311, 1999
[6] Kelley M.C., T.L.Arce, J.Salowey, H.Sulzer, W.T.Armstrong, M.Carter, L.Duncan, J. Geophys.Res. 100, 17.367, 1995
[7] Franz T.L., M.C.Kelley and A.V.Gurevich, Radio Sci. 34, N2, 465 - 475, 1999
[8] Gurevich A.V., H.C.Carlson and K.P.Zybin Phys.Lett.A 288, 231 - 239, 2001.
[9] Gurevich A.V., G.M.Milikh, J.Geophys. Res. 102, 389 - 394, 1997
[10] DuBois D.F., A.Hanssen, H.A.Rose, D Russel. J.Geophys. Res. 98, 17, 543, 1993.
[11] P.Stubbe J.Atmosph.Terr.Phys., 58, 349, 1996
[12] Wang J.G., D.L.Newman, M.V.Goldman J.Atmos. Sol.Terr.Phys. 59, 2461 -2474, 1997
[13] Gurevich A.V., Ya.S.Dimant, G.M.Milikh, V.V.Vaskov, J.Atmosph. Terr. Phys. 47, 1057, 1985
[14] Carlson H.C., V.B.Wickvar, G.P.Mantas J. Atmosph. Terr. Phys., 44, 1089 - 1098, 1982
[15] A.V.Gurevich, H.C.Carlson, Yu.V.Medvedev and K.P.Zybin, Plas. Phys. Rep. (Fizika Plazmy) v.30, N 12, 995, 2004
[16] Silin V.P., Sov.Phys. JETP 21, 1127 - 1135, 1965
[17] DuBois D.F., M.V.Goldman. Phys.Rev.Lett. 14, 544 - 547, 1965
[18] Gurevich A.V., Nonlinear phenomena in the ionosphere, Springer -Veralag, New York, 1978
[19] Cheung P.Y., M.D.Sulzer, D. DuBois and D.A.Russell. Phys.of Plasmas, 8, 3, 802-812 2001
[20] DuBois D.F., D.A.Russell P.Y.Cheung and M.P.Sulzer Phys. of Plasmas, 8, 3, 791 - 801, 2001
[21] Gurevich A.V., A.V.Lukyanov and K.P.Zybin. Phys.Lett.A., 211, 363, 1996
[22] Torr M.R., and D.G.TorrRev. Geophys., 20, 91, 1982
[23] Berrington K.A. and P.G.Burke, Planet. Space. Sci., 29, 377, 1981
[24] Mantas G.P., Carlson H.C., Geophys. Res. Lett., 18, 159, 1991
[25] Mishin E., H.C.Carlson, T.Hagfors Geophys. Res. Lett., 27, 2857 - 2860, 2000
[26] Pedersen T.R., H.C.Carlson Radio Sci. v.36, 609 , 2001
[27] Bernhardt P.A., L.M.Duncan, C.A.Tepley, R.A.Bhenke and J.P. Sheerin Adv. Space Res. 8, 271 - 278, 1988
[28] Bernhardt P.A., M.Wong, J.D.Huba, B.G.Fejer, L.S.Wagner, J.A.Goldstein, C.A.Selcher, V.L.Frolov and E.N.Sergeev J. Geophys. Res., 105, A5 10,657 - 10,671, 2000
[29] Djuth F.T., B.Thide, H.M.Ierkic and M.P.Sulzer Geophys.Res.Lett., 14,9, 953, 1987
[30] Duncan L.M., J.P.Sheerin, R.A.Bhenke Phys.Rev.Lett. 61, 239 - 242, 1988
[31] Bernhardt P.A., C.A.Tepley, and L.M.Duncan J.Geophys.Res., 94, A7, 9071 - 9092, 1989a.
[32] Gurevich A.V., H.C.Carlson, G.M.Milikh, K.P.Zybin, F.T.Djuth, K.M.Groves Geophys. Res. Lett., 27, 2462, 2000.
[33] Gurevich A.V., E.Fremouw, J.Secan and K.Zybin, Phys.Lett.A. 301, 307 (2002).
[34] Ginzburg V.L., "Propagation of electromagnetic waves in plasma", Moscow, Nauka (1967)
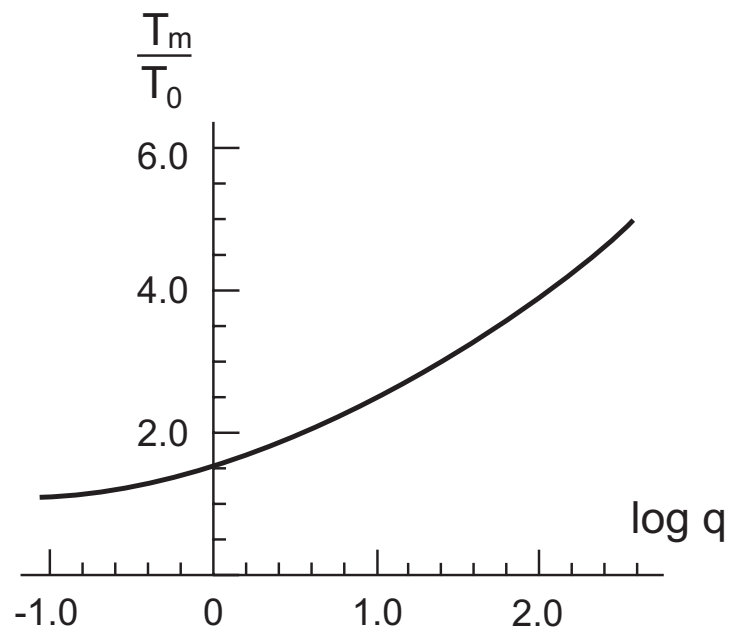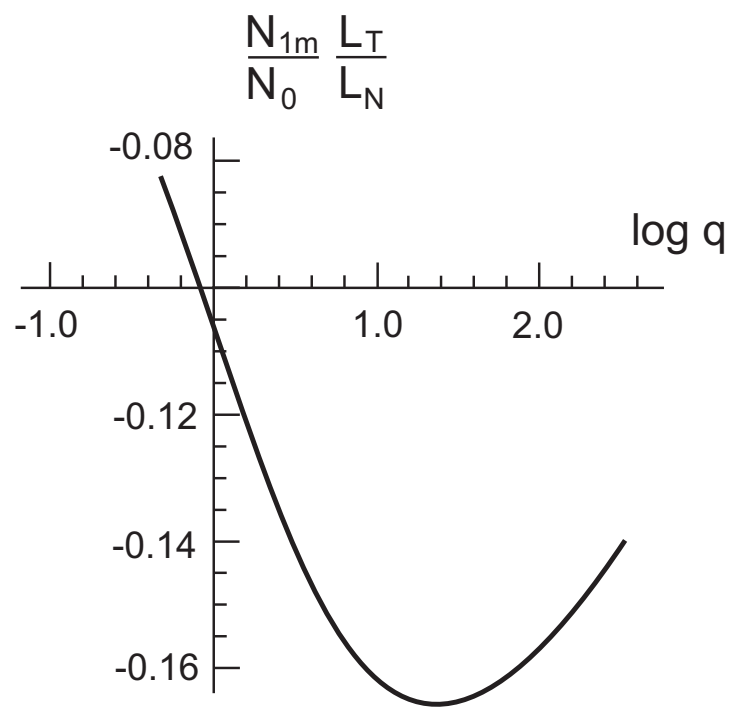
Fig.1a

Fig.1b

Fig.1. Established electron temperature (1a) and density disturbances N_{1m} (1b) as function of logarithm of dimensionless pump wave power absorption q. Temperature T_m and density depletion N_{1m} are normalized on non disturbed values T_0 and N_0. Parameter q is determined by formulae (10).
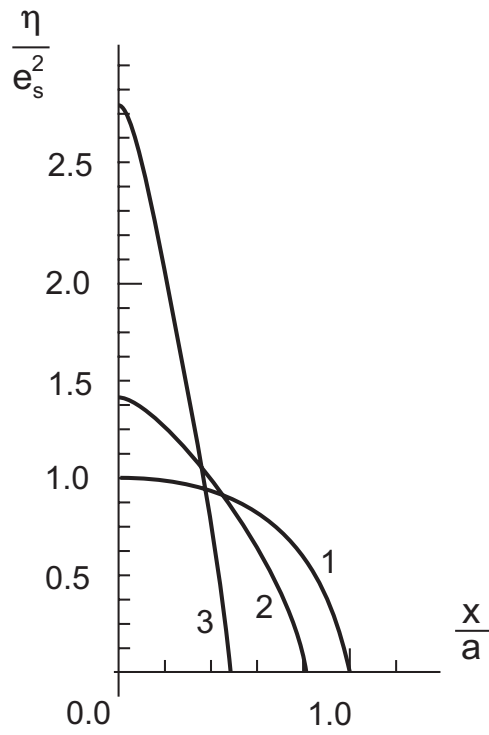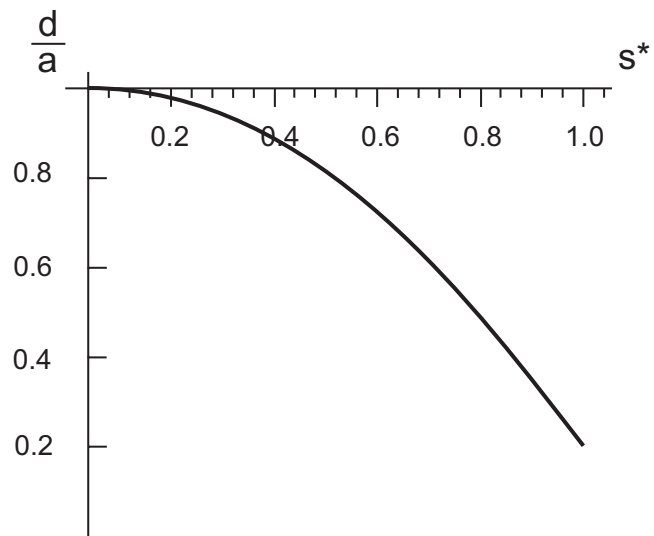
Fig.2a

Fig.2b

Fig.2. Beam focusing.
a. Normalized beam intensity η/e_s^2 distribution at different distances s^*;

1. $s^* = 0$, 2. $s^* = 0.5$, 3. $s^* = 0.8$, $s^* = 0.28$ were $s^* = s/a$ is the normalized on a distance along magnetic field. $s^* = 0$ – the beginning of striation region.
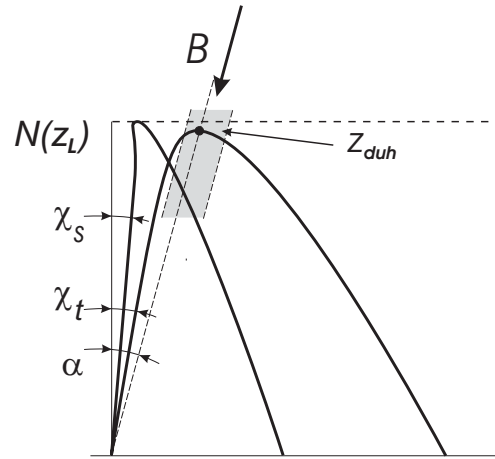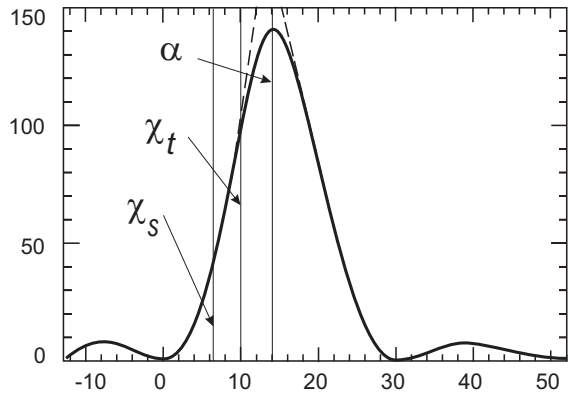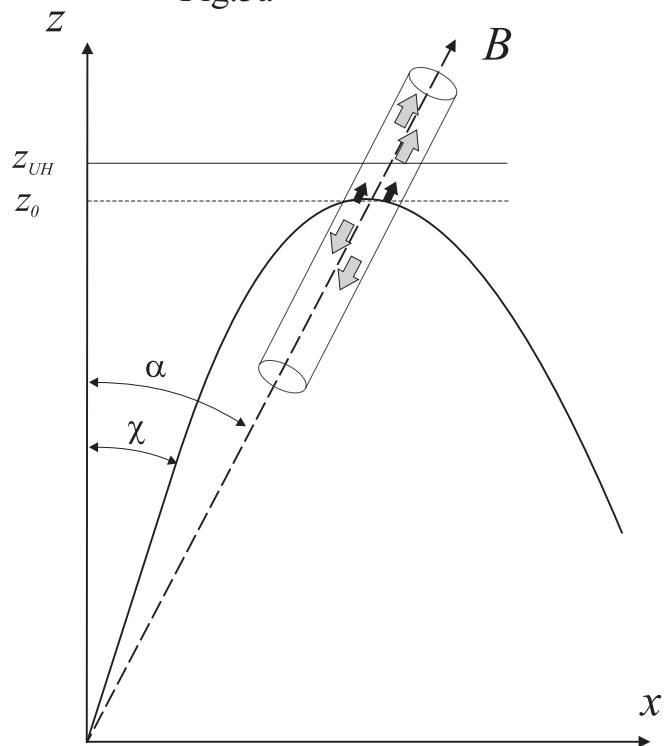b. Beam half width ($\eta(d) = 0$) as a function of s^*.

Fig.3a

Fig.3b

Fig.3c

Fig.3. Magnetic zenith effect at HAARP (a,b) and SURA (c).

a. Power angle distribution of the beam directed to magnetic zenith $\alpha = 14°$, f_0=5.8 MHz, *ERP = 90* MW. Abscise – initial angle (in degrees) to vertical direction. χ_s – spitz angle, χ_t – initial angle for a wave reflected at upper hybrid resonance level. Dashed curve – the amplification of the wave power near z_{duh} (*double resonance*).

b. Scheme of ray tracing. The nonlinearly excited striations and cavity region directed along {\bf B} is shown.

c. Scheme of ray tracing for the case z_0 below z_{uh} is shown. Solid arrows indicate the shift of reflection point above upper hybrid level.
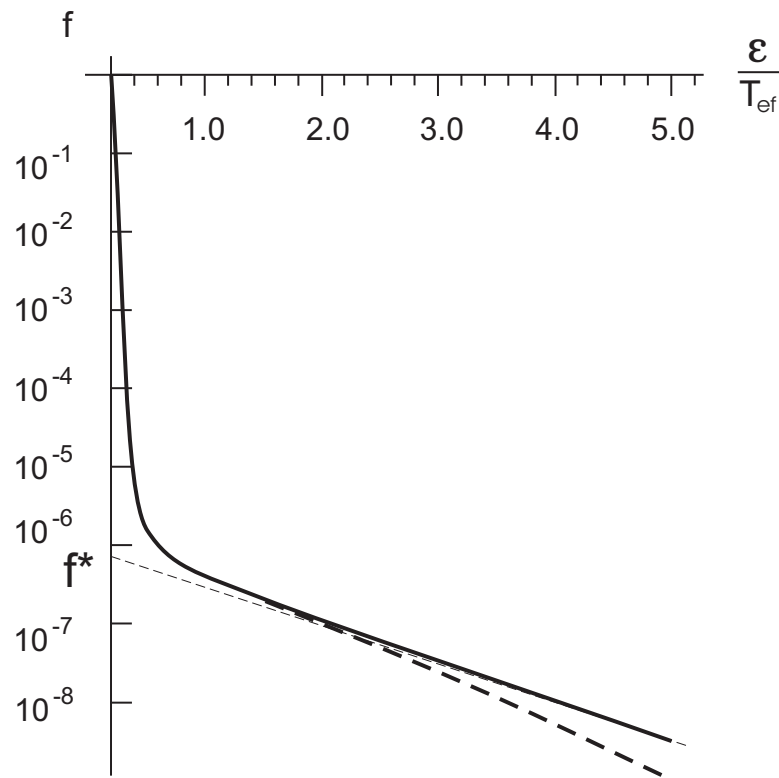
Fig.4

Fig.4. Electron distribution function $f(\varepsilon)$ in the vicinity of acceleration layer at the height $z = 300$ km for $P_0=960$ kW, $f_0=8$MHz (numerical calculations). The temperature of thermal electrons $T_e=0.16$ eV. Effective temperature for the tail of suprathermal electrons $T_{ef} = 10.5$ eV. Effective number density of fast electrons $N_f=(T_{ef}/T_e)^{3/2}f\cdot N_e=2.2 \times 10^{-4}N_e$. Full line for $\delta = const.$, dashed line – taking into account dependence $\delta(\varepsilon)$ according [13].
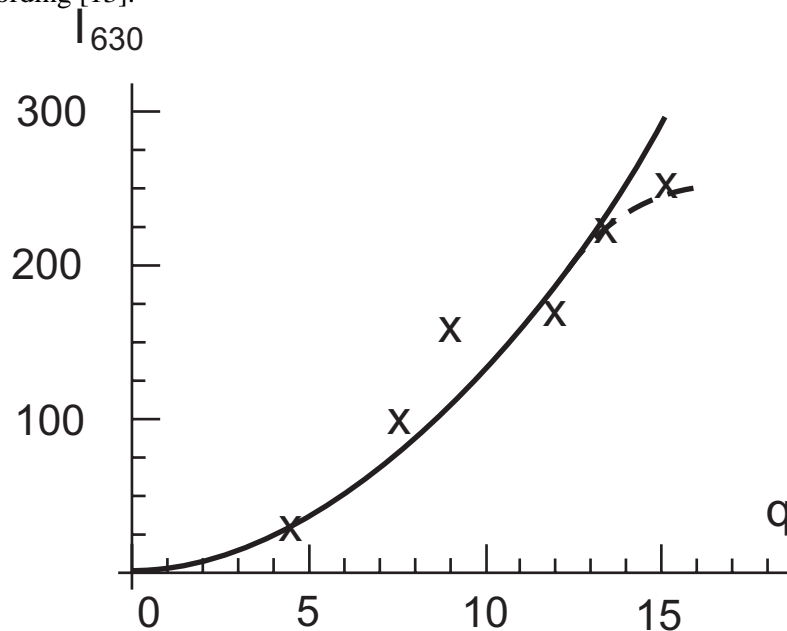

Fig.5

Fig.5. Dependence of the I_{630} intensity in Raileigh on the HAARP transmitter power for $f_0=3.3$ MHz. Curve – the theory, crosses – observations ([1], Fig.5). Dashed line shows the expected saturation of I_{630} due to N_2 vibration losses and electron kinetic effects.

Task 4.   Study of the X-ray emission in different gases due to runaway breakdown phenomena in a laboratory cyclotron installation

Experimental facility

The experimental device consists of the quasi-spherical vacuum chamber of ~45 cm diameter placed between two magnetic coils. The chamber is pumped down by the diffusion pump to pressure $p \leq 10^{-6}$ Torr. The magnetron Samsung OM75P serves as a source of the pulse-periodical ECR field for electron acceleration. The magnetron frequency is 2,45 GHz, its average power is 600, pulse duration 10 ms. A pulse separation rate is 2,5, therefore the pulse magnetron power is ~1,5 KW. The microwave radiation is transmitted through wave guide tract, conic horn antenna and is introduced into the chamber through a quartz window of 0,3 m diameter. The maximum electric field is $E_{0max} \leq 43$ Volts / cm. Radiation passing through the plasma is absorbed by water in a vessel with a glass window. Hyroresonance magnetic field is equal $B_c = 875$ Gauss. The magnetic field in the trap center can vary from 400 up to 900 Gauss in order to control with a position of resonance areas relative to a center of the chamber. In the given experiment the value of a minimum field $B_0 = 580$ Gauss was established, thus a resonance field coordinate on an axes a trap: $z_c = \pm 0,134$ m. There are "slots" about 9 cm between walls of the chamber and coordinates of a resonance field z_c on both sides, where the extraordinary wave can propagate through plasma. The experiments were carried out with various gases (air, argon, helium, hydrogen), which are introduced into the chamber through the needle valve.

The different diagnostic methods were used to study the discharge parameters. This methods include: Gamma - detector of bremsstrahlung radiation excited by accelerated electrons produced by the firm BYCRON model 2,5M2,5/3LP-X ;Gamma - dosimeter (Geyger counter). The range of gamma-quantum energies, measured by the counter is 0,05 -1,5 Mev. Microwave interferometer (λ_i= 0,8 cm) was used for a measurement of average plasma electron density. It represents itself an open confocal cavity, formed by two polished mirrors of 20 cm diameter located on opposite flanges of the chamber. Single Langmuir probe of a diameter $2r = 0,5$ mm and 9 mm length is used for an electron temperature and density measurements. The parameters of plasma in a magnetic field are determined according to Bohm theory using the ion branch of the probe curve . Fenced collector was used for the qualitative analysis of high energy electron velocity distribution.

Experimental results

Thresholds of the *x*-ray generation were measured at wide variation of a microwave power and gases pressure in air and helium. Outcomes of the measurements are presented in Fig.1. The pressure is submitted in relative units; for air the scale is transformed in pressure in terms of Torr by multiplication by a factor 10^{-6}, and for helium by a factor $5,26 \times 10^{-6}$ respectively. The threshold curve looks like Pachin curve for a usual gas breakdown that confirms the defining role of electrons in *x*-rays generation in ECR discharge. The threshold power of *x*-rays generation is about 50 W in pressure range $2 \times 10^{-6} – 3 \times 10^{-5}$ Torr, growing by one order of magnitude outside of this pressure range.

The measurements of plasma parameters were carried out with the single Langmuir probe in dependence of air pressure. The probe measurements were performed jointly with measurements of *x*-ray radiation intensity (Fig.2).

The low pressure area is characterized by a rather low *x*-ray radiation level as well as low plasma density $n_i \sim 10^7$ -10^8 cm^{-3} but high electron temperature $T_e \sim 40$eV. A Debye radius estimation for this concentration and the electron temperature gives magnitude about several centimeters compared to a characteristic size of the magnetic trap ~ 10 cm. As growth of pressure the electron plasma temperature falls down up to $T_e \sim 10$ eV at $p \sim 4 \times 10^{-5}$ Torr. The existence of high electron temperatures, $T_e \sim 40$eV, is confirmed by the results of the spectral measurements. The lines of nitrogen ions radiation with high - up to 4- multiplicity of ionization are registered in a spectrum of the optic radiation of a discharge along with bands of molecular nitrogen. It is considered, that in plasma of low pressure the electron temperature has order of 1/3 -1/2 potentials of ionization of atom i.e. $T_e \sim 30$-50 eV.

At a pressure more than 2×10^{-6} Torr the plasma density sharply increase up to $n_i \sim (1$-$3) \times 10^{10}$ cm^{-3} and it happens substantial growth of a *x*-radiation intensity. Plasma density and intensity of the *x*-ray radiation reaches maximum values at pressure p ~10^{-5} Torr. Then plasma density practically does not vary to the point of pressure ~ 4×10^{-5} Torr, while the intensity of a *x*-ray radiation presents a monotone slope to 0 at pressure growth up to p ~ 6×10^{-5} Torr.

The *x*-ray intensity-pressure dependence in air has a maximum value in pressure range $(1 \div 2) \cdot 10^{-5}$ Torr, in which the maximum value of plasma energy *nT* is reached.

The bursts of a *x*-ray radiation are registered both during pulses of a microwave pump and in intervals between pulses. The results corresponding energy spectra measurements are displayed in Fig. 3. Energy of a main part of accelerated electrons in both cases is about 40 keV. During a microwave pulse along with increase intensity of this group, the formation of high energy "tails" in the distribution function happens. After a microwave pump turning off the *x*-ray radiation is registered during several tens milliseconds, until the fast electrons are kept in a trap. The energy decay constant depending on pressure is given at Fig.4.

Plasma decay after the microwave pulse termination was studied with 8 millimeter microwave resonator in air in the pressure range $p \approx 10^{-6}$-10^{-4} Torr under the average microwave level 600 watts. The decay time rate increases under pressure growth in the range $p \approx 10^{-6}$-10^{-5} Torr up to maximum value $\tau \approx 6$ millisecond at pressure 10^{-5} and then falls down to 500 microsecond at pressure $p \approx 5 \times 10^{-5}$ Torr. It should be note that a behavior of the plasma decay time vs air pressure is qualitatively similar to the x-rays intensity dependence on the pressure that it is shown by Fig.5. Such a dependence may be consequence of residual gas ionization by the runaway electrons, confined in a trap.

As a result of the plasma optical spectra measurements it has been established, that the excitation of linear atom spectra is more effective than the excitation of molecular strips under the conditions of the effective electron acceleration.

The obtained experimental results may be applied to phenomena of runaway electron fluxes interaction with rare air of the upper atmosphere which probably take place in the giant atmosphere discharges related to the lightning activity, well-known as "Red Sprites".
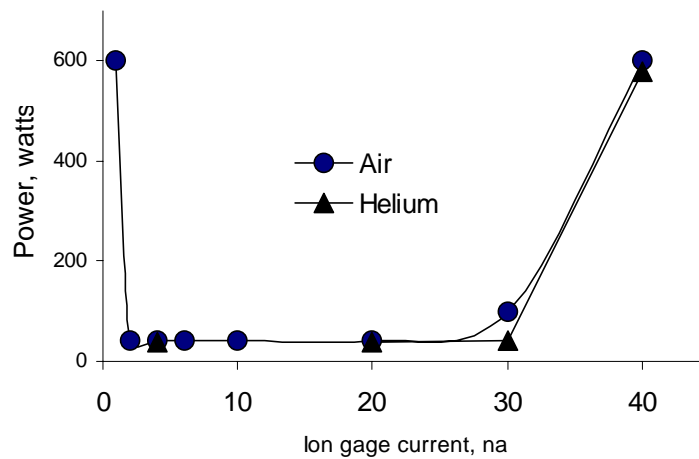

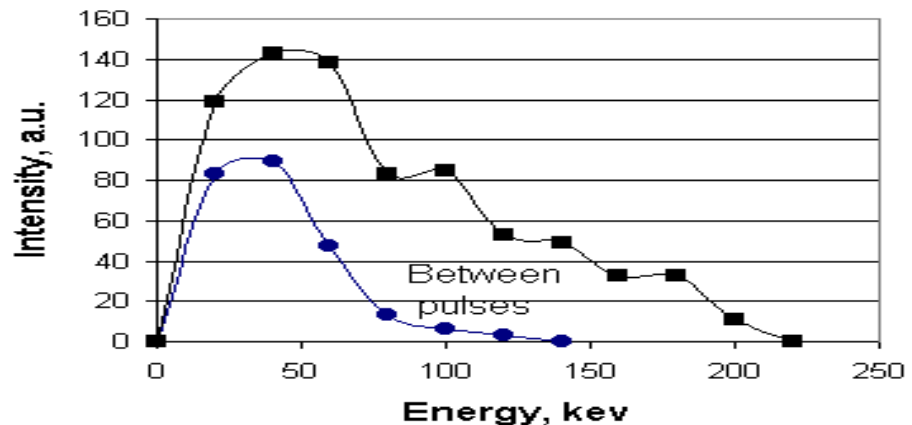Fig.4.1. X-rays generation thresholds in air and helium

Fig.4.2. Plasma density, electron plasma temperature and X-rays intensity dependences on air pressure.
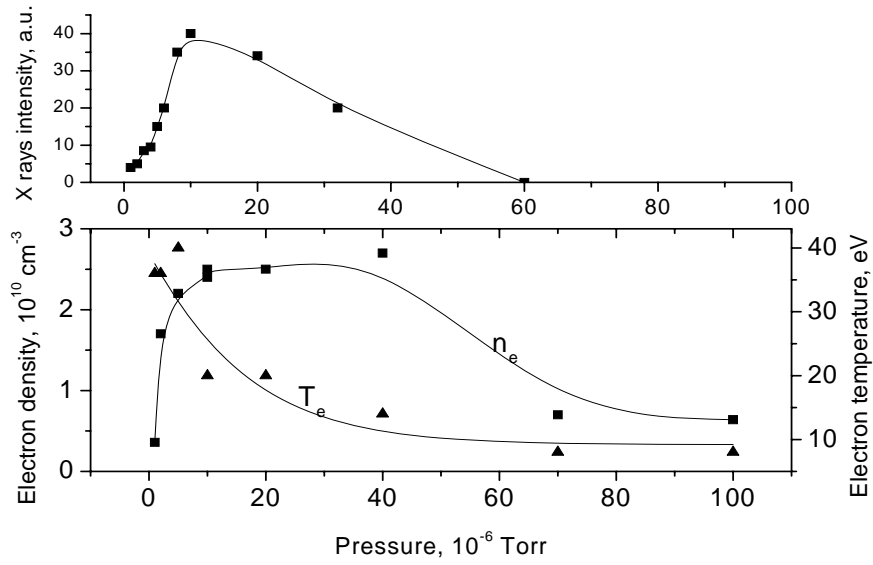
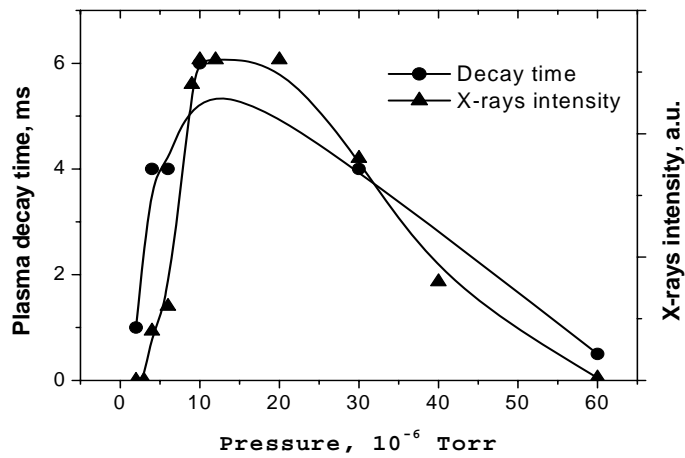Fig.4.3. X-rays energy spectra during the microwave pulse and between the pulses.

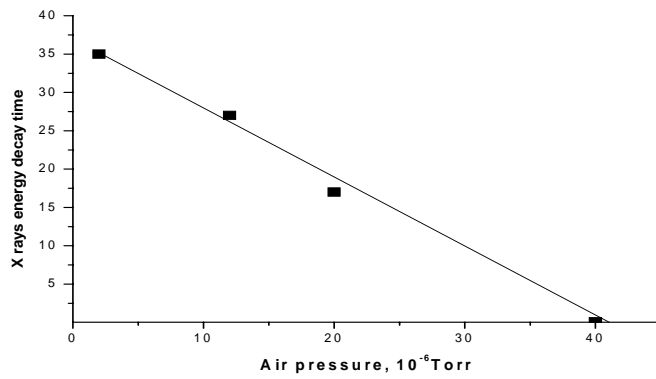Fig.4.4. The energy decay time dependence on pressure.

Fig.4.5. Plasma decay time and X-rays intensity dependences on pressure.

Task 5.   Study of the combined effects of runaway breakdown and cosmic rays on lightning processes in thunderstorm atmosphere

During the Project performance a complex of installations for the registration of extensive atmosphere showers of cosmic rays (EAS) was designed. The complex is situated at the Tien-Shan Mountain Scientific Station and is used together with the radio installations described in Task 6. The following signals are used as triggers of EAS and lightning: a) the signal of the EAS detection b based on Geiger counters; b) the signal of the muon cosmic ray component passing through the muon hodoscopes; c) the signal of the electric field jump.

The shower trigger array has several decade data registration centers connected with each other and with the trigger detector subsystems by the means of cable lines. Topology of the data registration points shown in Fig. 5.1.
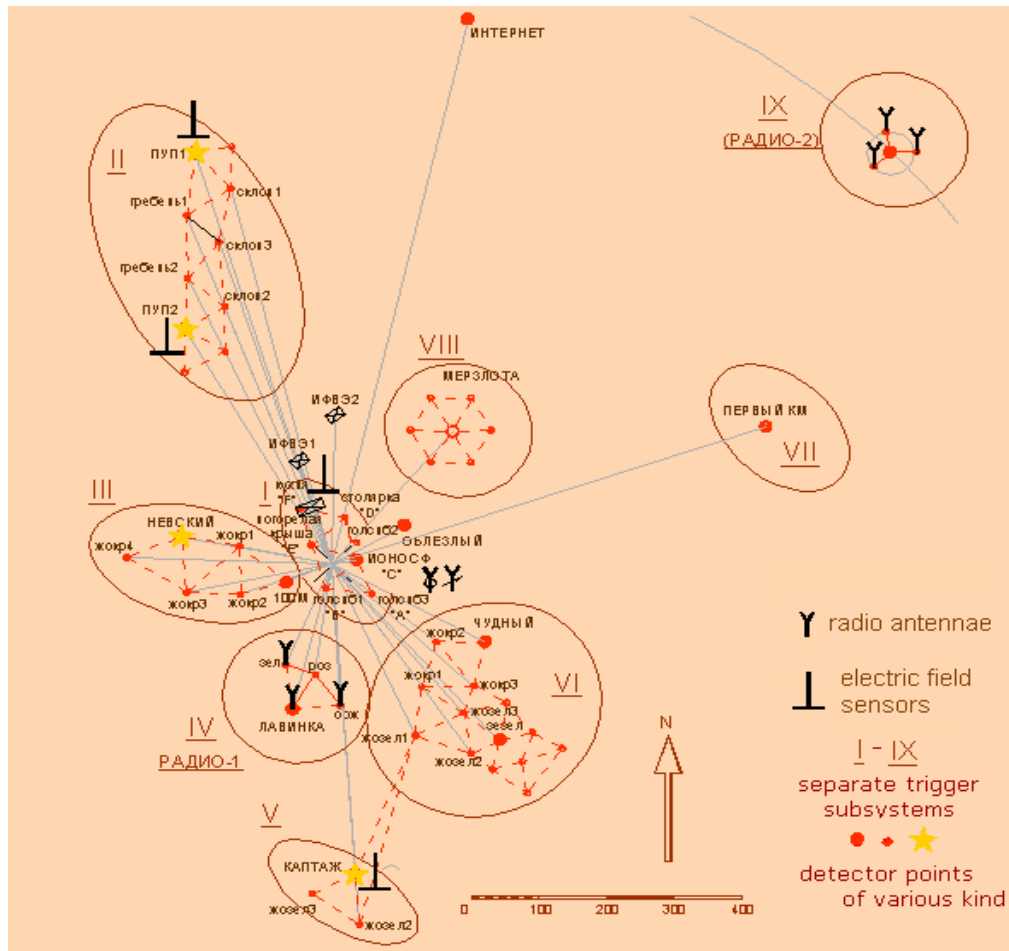

Figure 5.1. Placement scheme of detector points in 2006 measurement season.

One module of the EAS detector consists of 20 counters SI5G. Each counter is a glass cylinder felled with argon, the counter diameter 6 cm and the length is approximately 1 m. The sensitivity area of one detector module is about $0.6 \ m^2$. The power supply units are located inside mini-structures. Signals are transmitted via cable lines from mini-houses to the main registration point were the electronic equipment to create trigger signals is situated.

The main registration point has a cable connection with the system of radio emission registration; it is the same place where the common shower trigger signal is elaborated from coincidence signals of separate elementary triangles (ABC, BCE, CDE, DEF, G, H). The common trigger signal is transmitted to the radio registration system through the special cable; in the moment of its appearance information about the coincidence type, namely identifiers of those detector points who have formed the trigger and those whose pulses were coinciding with the trigger are written to the computer. Later these data could be used to estimate the size of a registered shower. In the main registration center any combination of the ABC, BCE, CDE, DEF, G, H signals is used to generate a common trigger pulse for radio emission reg-

istration system. The trigger signal is formed as a coincidence of signals within 5 μs duration from every three modulus connected in a triangle (ABC for example). That is why the trigger time accuracy of the array is 5 μs. The system of three boxes placed in the vertexes of a 65x65x75 m triangle is capable to select effectively the 1 PeV air showers from the area of 10^4 m^2 (Fig. 5.2). The effective sensitive area of the trigger array is about 0.1 km^2. The trigger system was precisely checked out by comparing the trigger formation on ABC triangle (see Fig. 5.1) with the scintillator (NaI) counter.
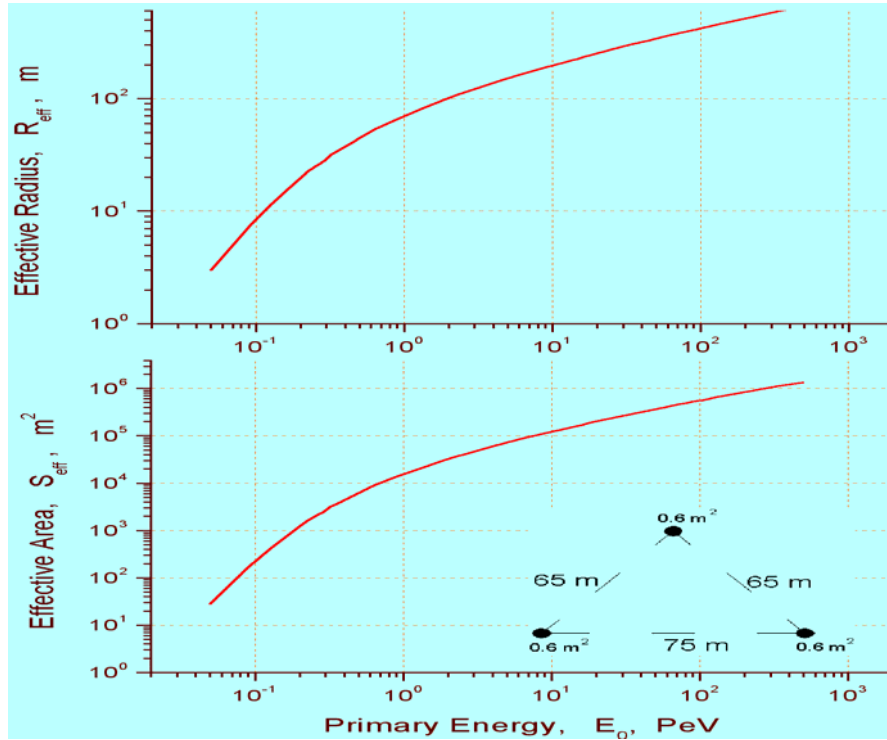

Figure. 5.2. Dependence of the effective shower selection area and radius on the primary EAS energy for the basic trigger triangle.

The signal of the muon cosmic ray component detect in an underground mine (depth 2000 g/cm^2) using large muon hodoscopes with the sensitive area 56 m^2 (Fig. 5.3). Hodoscopes is intend for cosmic ray muon components registration with 5 GeV energy threshold. Hodoscopes is constructed on the basis of 2600 separate gas counters SI-5G (diameter is 60 mm, length of the counter is 600 mm). The counters are grouped on 130 modules. All modules are established on their workplaces in mine, counters are calibrated on working voltage. The installation of signal cables and information gathering programs are made. The muon telescope consisting of 380 counters SI-6G of a smaller diameter (30 mm) is the component part of hodoscopes. The counters are established in eight layers located vertically in such a manner that longitudinal axes of each pair of counters are perpendicular. The installation allows determining a direction of the charged particles crossing and is intended for definition of EAS angle using direction muon component.
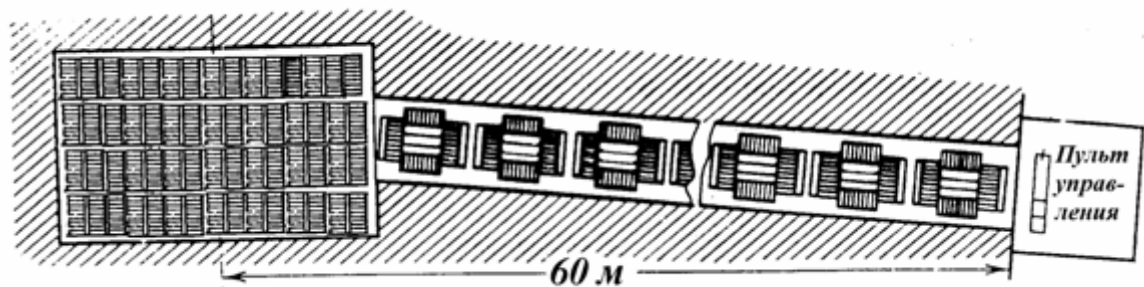
Fig. 5.3. Muon horoscope at the Tian Shan Station complex.

Eighteen NaI scintillation detectors was manufactured to measure the energy spectrum of 20 keV-1.5 MeV gamma rays coming from the thunderclouds. The detectors calibrate on the Tian Shan Station using the sample gamma emission sources (Cs-137, Am-241). Then the counters are placed at the Tian Shan Station complex (Fig. 5.4). It supplied with the specially designed cable line as well as with the electronics provide for the pulse transfer from the counter to the fast eight-cannel analyzer.
Block diagram of fast thunder data registration system is shown in Fig. 5.5.
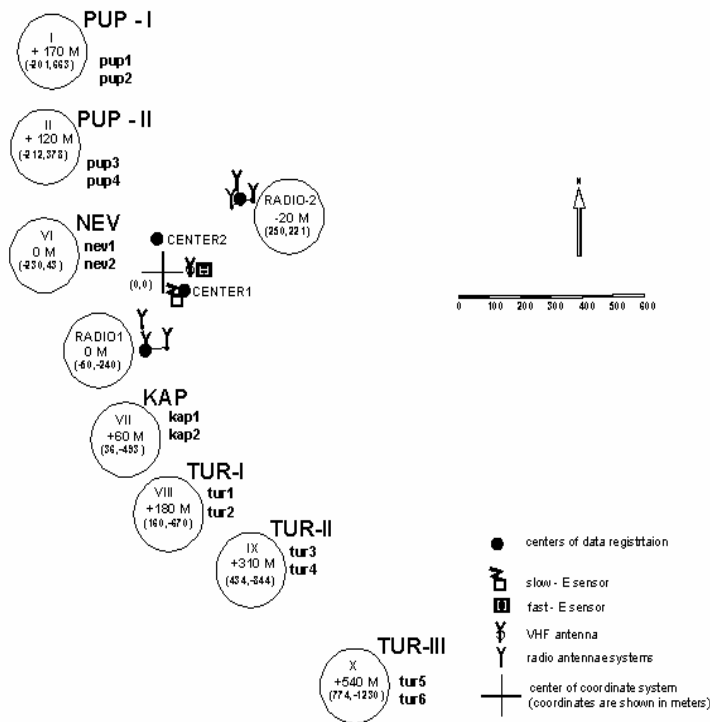
Fig. 5.4. Location of NaI-detectors on the territory of Tien-Shan complex. The heights and horizontal coordinates relative to the Tien-Shan station's geodetic control point are shown near each detector point.
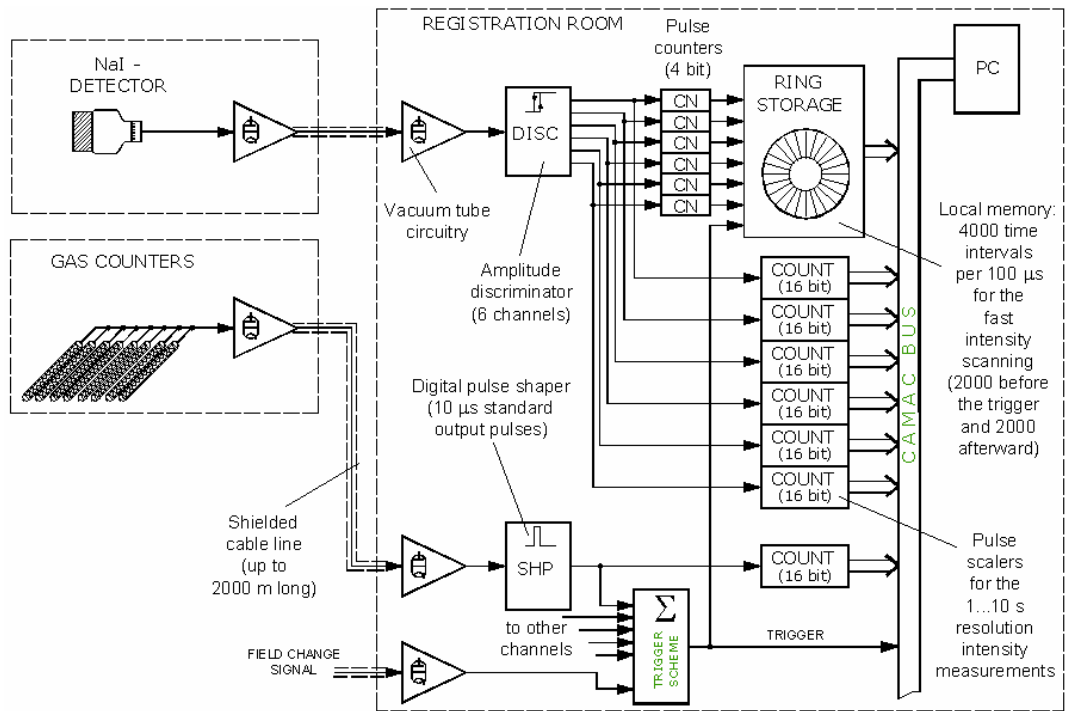
Figure 5.5. Block diagram of fast thunder data registration system.

The process of γ-quanta registration for the NaI scintillation detectors was simulated using of the GEANT code and shown in Fig. 5.6. Results of the mean energy production by a γ-quantum in dependence on quanta energy is shown in Fig. 5.7. It is seen that the efficiency depends noticeably both on the quantum energy and crystal geometry while the energy is nearly equally underestimated by various detectors.
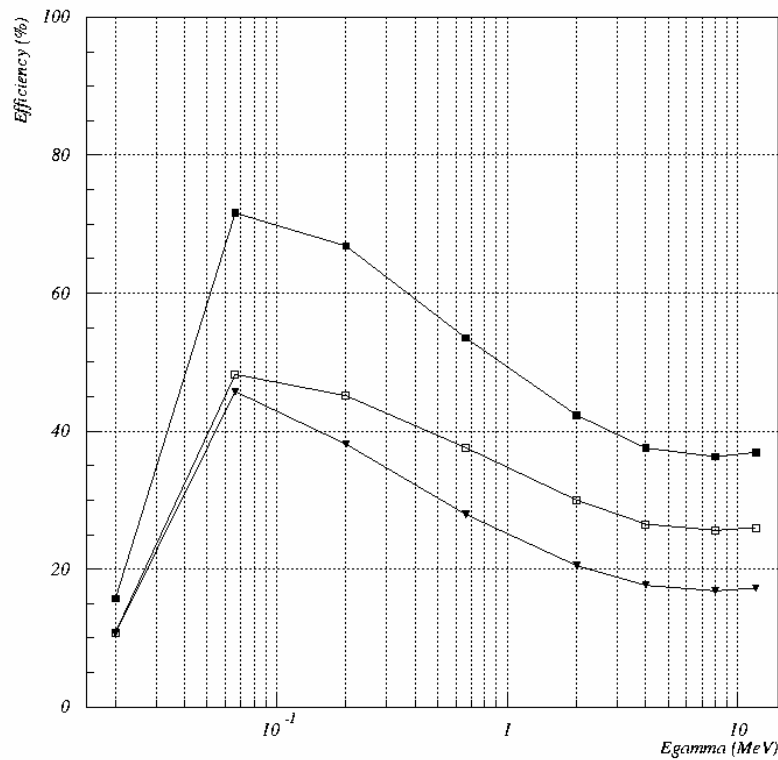
Figure 5.6. Energy dependency of γ–quanta registration efficiency for a set of NaI scintillation detectors: 300×30 mm^2 (filled squares), 110×110 mm^2 (open squares), 63×63 mm^2 (triangles) in a 1 mm thick Al housings.
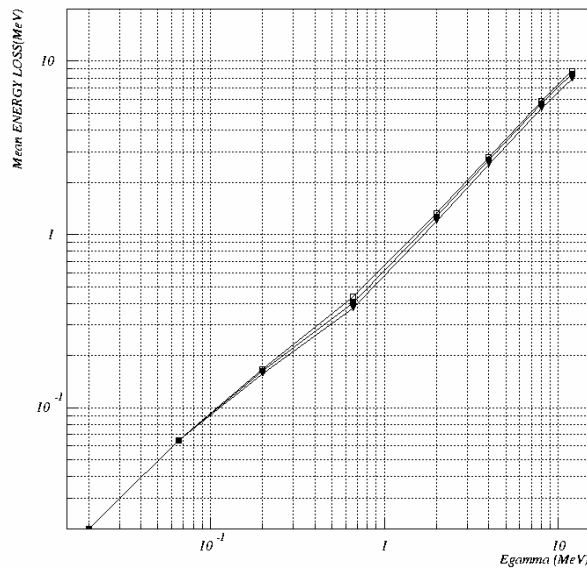
Figure 5.7. Average energy losses of γ–quanta in NaI scintillation detectors in dependence on their primary energy. Scintillators are put into 1 mm thick Al housings and have 300x30 mm^2 (filled squares), 110×110 mm^2 (open squares), 63×63 mm^2 (triangles) sensitive areas.

The typical amplitude spectra for NaI detectors with 63×63 mm^2 crystal sizes are shown in Figure 5.6. The spectra are measured by irradiation with point radioactive sources Am[241] (activity is 1.1×10^5 decay/s) and Cs[137] (activity is 1.09×10^5 decay/s). Relative position of the detector and radioactive sources was changed in various measurements.
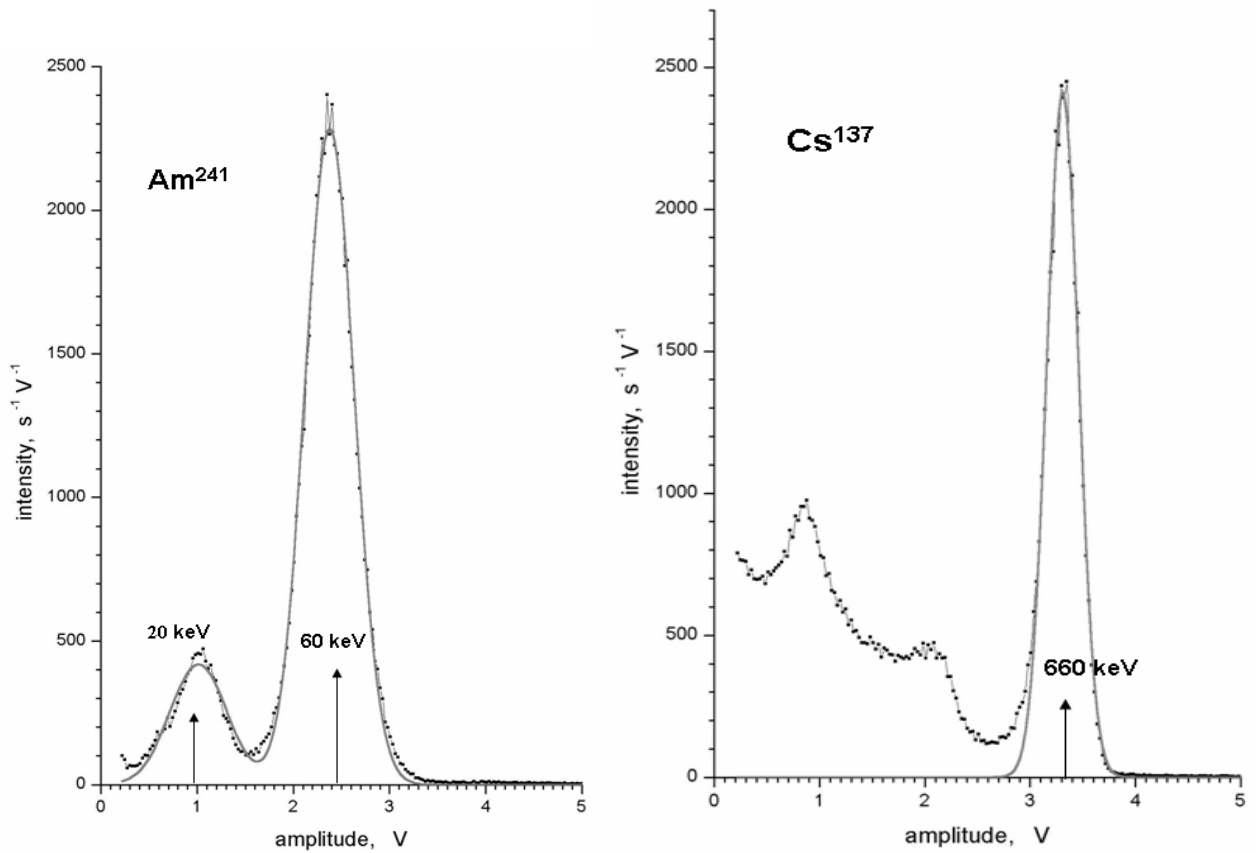
Fig. 5.8. Amplitude spectra of a NaI scintillation detector with a 63×63 mm^2 crystal and a PMT-82 type photo-multiplier tube. The distance between the detector and the source is 6 cm, the PMT feeding voltage is 1650 V in the case of Am[241] source and 1300 V in the case of Cs[137]. The points are the measurement results, the curves − the Gauss approximation.

In the Figure 5.8 are seen distinctly the peaks corresponding to the complete absorption energy of gamma-quanta (marked by arrows). These peaks may be used for determination of gamma-quanta registration efficiency and for estimation of the detector's energy resolution. Hence, two peaks of the Am^{241} spectrum give a 17% and 90% registration efficiency values for the 20 keV and 60 keV gamma-quanta respectively, energy resolution in these peaks being ±26% and ±11%. For the 660 keV peak of Cs^{137} spectrum registration efficiency is 30% with a ±6.5% energy resolution.

The similar analysis was done for the all presently used 18 NaI detectors. Experimental efficiency values of the majority of detectors agree well with the results of calculation for the energies above 60 keV, corrections for low-energy γ-quanta absorption inside the detector walls being necessary in the energy range 20-60 keV.

The data obtained at the Tien-Shan station during 2001-2005 seasons were analyzed. For the first time it is found, that even in the absence of lightnings and thunderstorms, when electrically charged clouds were passing through the station, the flow of secondary electrons and gamma-quanta increases considerably, this increase being in correlation with the change of electrical field in the atmosphere. As a role, the duration of such radiation bursts is about some minutes. The effect is observed in the absence of lightnings, rain and X-ray emission bursts. Also, the long-term (about some hours) changes of gamma-quanta intensity were discovered which are not directly connected with thunderstorm activity.

The intensity of X and gamma ray emissions in thunderstorm condition was measured using eight NaI counters placed in registration points I, II, VI and VII. The record was realized by the trigger signal from the alternating electric field sensor (see Task 6 below). The gamma ray flashes are detected as for screened counters as for unscreened ones. Flashes are seen both in low-energy and high-energy diapasons. One of typical examples of registration of the gamma ray flashes is shown in a Fig. 5.9. The registration of signals by the radio-detector and electrical field detectors are shown in a Fig. 5.10.
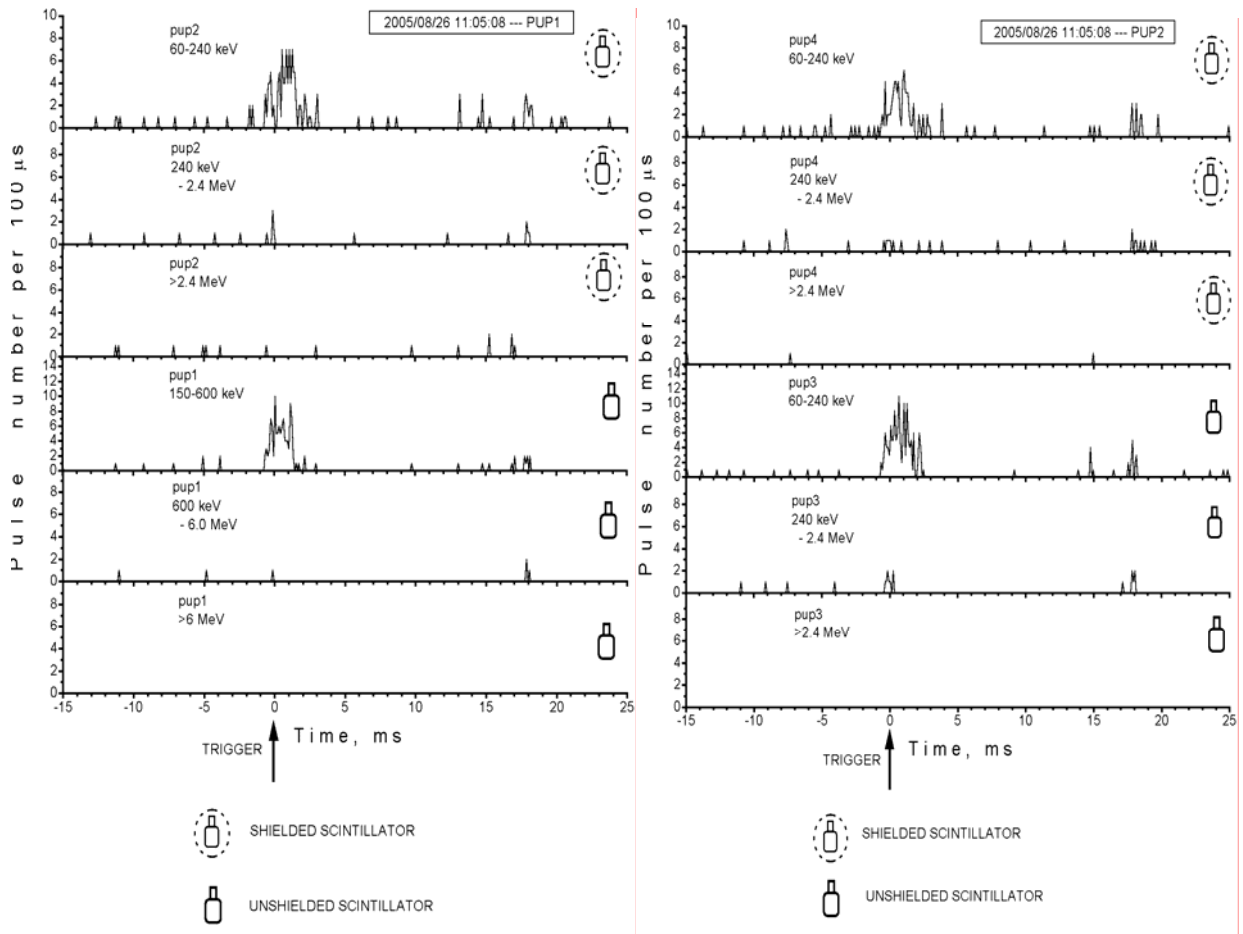
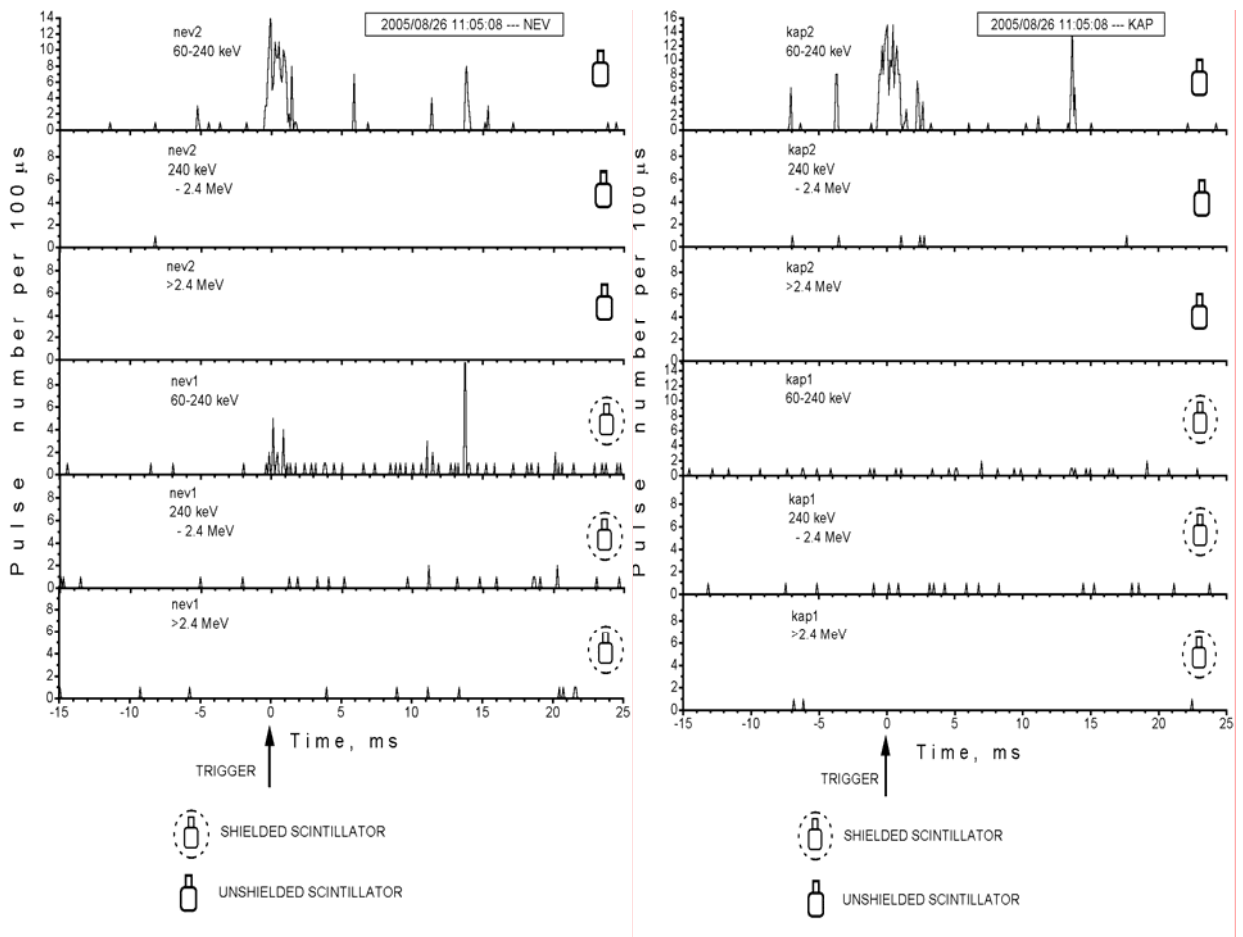Fig. 5.9. The gamma ray flashes records from different NaI detectors (PUP1, PUP2, NEV, KAP) .
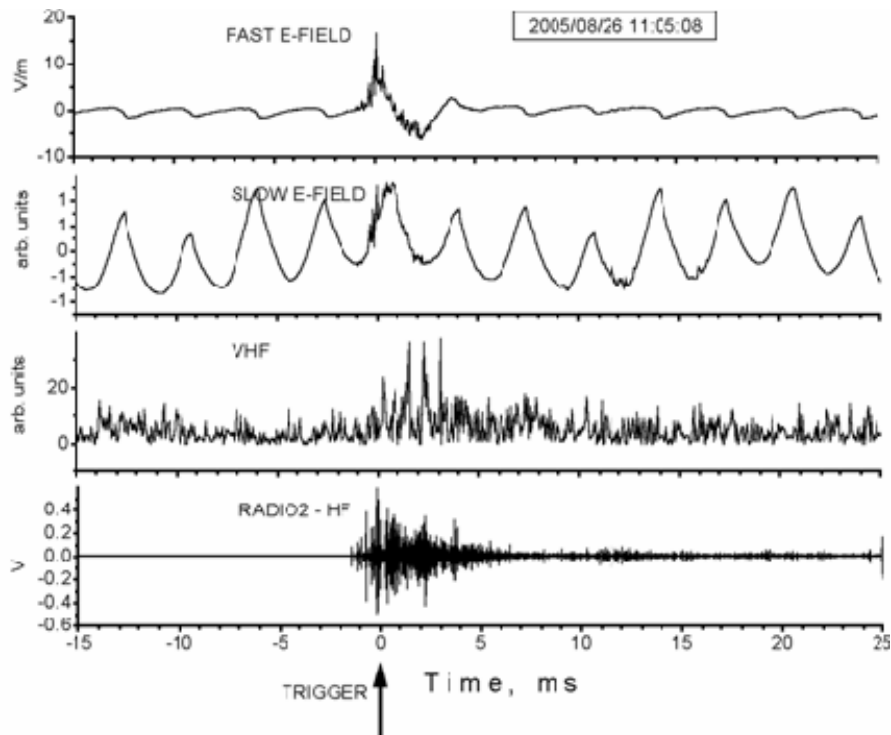

Рис.5.10. An example of the signal records by the radio electrical field detectors according to Fig. 5.6.

The long tail of gamma emission is observed after the return stroke. The similar gamma flashes connected with lightning was observed by Dwyer and coworkers earlier. The spectrum of flashes observed

in our experiments is similar to that of terrestrial gamma flashes (TGF) observed by G.J. Fishman et al from COMPTON satellite and by D. Smith et al from RHESSY.

Conception of the "Foton-Gamma" experiment at ICS

We have studied the possibility to test the hypothesis that the high altitude discharges "Sprites" are concerned with runaway breakdown phenomenon. The theory predicts that runaway breakdown is to be accompanied by the gamma-ray emission with energy 0.1 – 1.0 MeV. This emission should be observed at one time (in millisecond range) with the optical emission from the discharge.

To realize the simultaneous observation of optical and gamma emission of the Atmosphere discharges it is necessary to conduct the space experiment with the instruments sensitive to the optical photons and gamma-quanta. To accumulate the significant statistics of detected events, it is necessary to provide the global survey of the large areas of the upper Atmosphere during a long time. The observations should be carried out on the low-orbital spacecraft with the possibility of detector orientation in the local nadir.

Gamma-quanta should be detected in the energy range 0.1-1.0 MeV. The high density non-organic scintillators (NaI(Tl), CsI(Tl)) of sufficiently large volume are the most effective in this energy range. The wide-field long observations with the detail timing and spectral measurements should be also provided. It requires the storage and regular translation on the Earth of the large data massive.

One of the main technical peculiarities of the elaborated method of measurements is the necessity of the mounting on the spacecraft of the instrument of rather large volume and mass (~30 kg). However, the special requirements to the spacecraft orientation and stabilization are not necessary. The characteristic feature of this experiment is also the necessity of observations of the upper Atmosphere during a long time. In this view one of the most suitable spacecraft is a long-lived orbital space station, in particular, International Space Station (ISS). Because of the station's main orientation mode, which is the "velocity vector – local zenith", it is possible to realize the observations of the upper Atmosphere during the all time of experiment, if the instrument will be directed in the local nadir. The telemetric and energy resources of the ISS are also quite sufficient to provide the proposed experiment. It is also important that the hard magnetic disks, which can be used for data storage in the instrument electronic units, can be taken off and transported after their filling with the help of the ISS personal.

We have formulateded the requirements to the set of "Photon- Gamma" instruments for simultaneous observation of optical and gamma emission of atmospheric high-altitude discharges on the board of the International Space Station (ISS). These instruments should include:

optical emission detectors;

gamma-ray detectors;

electronic power supply units for detectors and preamplifiers;

digital data processing module.

The optical and gamma-ray detectors as well as the electronic power supply units and preamplifiers should be placed in one module, which should be mounted on the outer panel of the Station's module in such a way, that the detector axes should be directed in the local nadir. The digital data processing module should be mounted in the station's pressurized compartment unit. By this, there are no special requirements to fix the instrument coordinate system to the ISS coordinate system, in particular, special requirements to the orientation and stabilization of the instrument axis are not foreseen. The autonomous adjustment system is not necessary.

The optical emission registration system should include three detectors, two of which are sensitive in the red and blue spectral ranges. The red light detector is foreseen for registration of the high-altitude discharge emission and the blue light detector – for registration of the emission of discharges generated at the altitudes less than 50 km, respectively. The third one – the broadband detector should provide the registration of the light from any kinds of discharges.

The gamma-ray registration system should include three co-axial omnidirectional detectors with field of view about 4π sr. The scintillation crystals NaI(Tl) with sizes $\varnothing 12 \times 2.5$ cm should be used as such gamma-ray detectors. As it is well-known, among non-organic scintillators just the NaI(Tl) crystals have the maximal conversion efficiency and as a consequence the best light output for a specified configuration.

Task 6.   Search for the short-time flashes of radio emission during thunderstorm

Theory

A physical concept of an avalanche type increase of a number of energetic electrons in gas under the action of the electric field was proposed by Gurevich, Milikh and Russel - Dupre [1]. The avalanche can grow in electric field $E \geq Ec$. The field E_c is almost an order of magnitude less than the threshold electric field of conventional breakdown E_{th}. The growth of number of electrons with energies $\varepsilon > \varepsilon_c$ 0.1 - 1 MeV is determined by the fact that under the action of electric field E_c fast electrons could become runaway, what means that they are accelerated by electric field E as suggested by Wilson [2]. Due to collisions with gas molecules they can generate not only large number of slow thermal electrons, but the new fast electrons having energies $\varepsilon > \varepsilon_c$ as well. Directly this process - acceleration and collisions lead to the avalanche type growth of the number of runaway and thermal electrons, which was called in [1] "runaway breakdown" RB. The detailed kinetic theory of RB was developed in [3-7].

In atmosphere the critical electric field is

$$E_c \approx 200 (kV/m) \left[\frac{N_m(z)}{N_m(0)} \right]. \tag{1}$$

Here $N_m(z)$ is the neutral molecules density at the height z and $N(0)=2.7 \times 10^{19}$ cm^{-3} - at see level. E_c falls down with z due to exponential diminishing of N_m. At the thundercloud heights z $\approx$ 4 - 6 km, the critical field E_c is 100 - 150 kV/m and exactly these values of electric field are often observed during thunderstorms [8, 9]. When the electric field in thunderstorm cloud reaches the critical value $E \geq E_c$ every cosmic ray secondary electron (its energy $\varepsilon > 1$ MeV) initiates a micro runaway breakdown (MRB). It serves as a source of intensive ionization of air and manifests itself in a strong amplification of X and γ-rays emission and effective growth of conductivity in thundercloud [1, 10]. These effects were observed and compared with RB theory [11-14].

Extensive atmospheric shower (EAS) is accompanied by a strong local growth of cosmic ray secondaries number [17]. A theory of combined effect of RB - EAS was developed in [15]. It was shown that ionization of atmosphere by the shower in RB conditions is growing strong enough to produce local highly conductive plasma and can serve for lightning leader initiation. On the other hand the same effect can stimulate the excitation by thundercloud electric field an intensive local pulse of electric current. This short pulse of electric current can generate radio emission.

As is well known radio emission is generated during thunderstorm in a wide frequency range. It has a high power and was studied in a multiple observations (see monographs [9, 16] and literature cited there). That is why to single out RB - EAS radio pulses in observations is impossible without knowledge of their special features described by the theory. On the other hand the detection and detailed study of this emission has a significant interest either for understanding of lightning generation mechanism or investigation of the fluxes of high energy cosmic ray particles.

Electric current is generated by simultaneous effect of RB and EAS. According to the theory and observations, the seed electrons in EAS are distributed nonuniformly [17]. The typical EAS scale along the direction of motion of relativistic particle $z \approx 5 - 10$ m and in perpendicular direction $R_\perp \approx 100$ m [15, 17]. It means that current pulse structure in z direction is mostly significant what allows us to develop the theory in one dimensional approximation. In RB process high energy electrons effectively generate large number of slow thermal electrons [6, 7]. One can estimate that namely thermal electrons define the current pulse under the action of electric field. The equations describing this process have a form:

$$\frac{\partial N_e}{\partial t} + \frac{\partial(N_e V_e)}{\partial z} = -\frac{N_e}{\tau_{att}} + q, \quad \frac{\partial N_-}{\partial t} = \frac{N_e}{\tau_{att}}, \quad \frac{\partial N_+}{\partial t} = q, \quad \frac{\partial E}{\partial z} = 4\pi e (N_+ - N_- - N_-). \tag{2}$$

We supposed here that electric field is directed along the vertical z. The first equation of system (2) describes the changes of slow electron density N_e induced by drift of electrons in electric field V_e, their birth q due to RB process and death due to attachment. The second and third equations describe the appearance of negative ions N_- resulting from electron attachment and generation of positive ions N_+ due to RB. The fourth equation defines the appearance of polarization electric field.

In equation (2) V_e is the drift velocity under the action of electric field $E_z = E$:

$$V_e = eE/m\nu \tag{3}$$

where ν is electron collision frequency with air molecules. We suppose here that the inclination angle to the vertical of a high energy particle (generating EAS) is small enough, what allows to consider z - component of electric field only. The life-time due to attachment of slow electrons in the air τ_{att} is determined by three - body collisions [18], and the source of secondary electrons q:

$$q = cN_0 \delta(z - ct) F(z, E/E_c).$$ (4)

Here $c \cdot N_0(\varepsilon, r_\perp)$ is a flux of newborn slow electrons generated by EAS in the atmosphere in absence of electric field. The number density of secondary electrons N_0 in the plane orthogonal to z axis is approximately proportional to the energy of cosmic ray particle ε and falls down with the distance $r_\perp$ from the center of EAS [17]. According to well-known Nishimura, Ksimata, Greizen formulae simplified for thundercloud heights [15]

$$N_0(\varepsilon, r_\perp) = n_0 \sqrt{\varepsilon/\beta} \left(\frac{R}{r_\perp}\right) \times \left(1 + \frac{r_\perp}{R}\right)^{-3.5}, \quad \beta = 72\,\text{MeV}, \quad n_0 \approx 1.2 \times 10^{-9}\,\text{cm}^{-2}$$ (5)

Function $F(z, E/E_c)$ determines the slow electron production and their exponential multiplication under the action of electric field E.

The electric current generated due to RB process is determined by slow (thermal) electrons. To determine this current the detailed kinetic theory, taking into account full complex of ionization, recombination and emission processes, was developed in the project. The electric current has the form:

$$j_z = eV_e N\theta(ct - z)\exp(-(ct - z)/l_a)$$ (6)

Here N is the number of thermal electrons, $l_a = c\tau_{att}$.

To solve the kinetic problem on the distribution function f of slow electrons the following processes should be taken into account. The full inelastic collision integral of electrons with molecules $S(f)$ consists of ionization term S_{ion}, excitation of optical S_{op}, vibration S_v and rotational S_r levels, attachment in pair S_{at} and triple S_{at1} collisions [18, 19].

$$\frac{\partial f}{\partial t} = e\mathbf{E}\frac{\partial f}{\partial \mathbf{p}} + S(f) = 0, \quad S(f) = \frac{2N_m}{m\nu}\left[S_{ion}(f) + S_{op}(f) + S_v(f) + S_{at}(f) + S_{at1}(f)\right],$$ (7)

$$S_{ion}(f) = \varepsilon f(\varepsilon)\sigma_{ion}(\varepsilon) - (\varepsilon + \varepsilon_{ion})f(\varepsilon + \varepsilon_{ion})\sigma(\varepsilon + \varepsilon_{ion}),$$ (8)

$$S_{op}(f) = \varepsilon f(\varepsilon)\sum_{i=1}^{N_{op}}\sigma_i^{op}(\varepsilon) - \sum_{i=1}^{N_{op}}(\varepsilon + \varepsilon_i^{op})\sigma(\varepsilon + \varepsilon_i^{op}),$$ (9)

$$S_v(f) = \varepsilon f(\varepsilon)\sum_{i=1}^{N_v}\sigma_i^v(\varepsilon) - \sum_{i=1}^{Nv}(\varepsilon + \varepsilon_i^v)\sigma(\varepsilon + \varepsilon_i^v).$$ (10)

Here we took into account, that ionization optical and vibration energy quanta are large enough: $\varepsilon_{ion} = 12.1$ eV, $\varepsilon_v = 0.29 – 0.44$ eV, $\varepsilon_{op} = 1.9 – 8.1$ eV what allows to consider all air molecules in atmosphere to be at ground state. Cross sections of all these processes are known [18 - 20].

On the contrary, rotational quanta are small: $\varepsilon_{rO2} = 1.79 \times 10^{-4}$ eV, $\varepsilon_{rN2} = 2.48 \times 10^{-4}$ eV and a large number of molecular rotational levels are excited. Due to this rotational collision integral $S_r(f)$ could be presented in differential form

$$S_r(f) = -\frac{1}{2v^2}\frac{\partial}{\partial v}\left[v^3 R_r(v)f(v)\right], \quad R_r(v) = \frac{64\pi a_0^2}{15mv}(0.2\varepsilon_{rO2} + 0.8\varepsilon_{rN2})N_m\sigma_O, \quad a_0 = \frac{\hbar^2}{me^2}.$$ (11)

Dissociative attachment to O_2 molecules is

$$S_{at} = \frac{2N_m}{mv}\varepsilon\sigma_{at}(\varepsilon)f(\varepsilon),$$ (12)

where cross section σ_{at} has a sharp pike near $\varepsilon = 6.7$ eV [16*]. Attachment to oxygen molecules at triple collisions is significant at thermal electron energies only ($\varepsilon \leq 1 \div 2$ eV). Approximately this term could be presented in "tau approximation" [18]

$$S_{at1} \approx \frac{1}{\tau_{at}}, \quad \tau_{at} \approx 2\times10^{-8}\left(\frac{2.7\times10^{19}\ \text{cm}^{-3}}{N_m}\right)\ \text{s.} \tag{13}$$

We note that thermal electron lifetime τ_{at} is inverse proportional to N_m^2. Thus in atmosphere at the height $z=0$, $\tau_{at} = 20$ ns; at $z = 4$ km $\tau_{at} = 50$ ns; at $z = 6$ km $\tau_{at} = 90$ ns. The described kinetic model was studied numerically. The model electric field was supposed to be distributed at $-L_0 \leq z \leq L_0$ as $E(z) = E_m\left(1 - a^2 z^2\right)$, were distance z was measured in ionization length l_i, and parameter $a = l_i/L_0$.

The results are presented in Figs. 6.1–6.4.

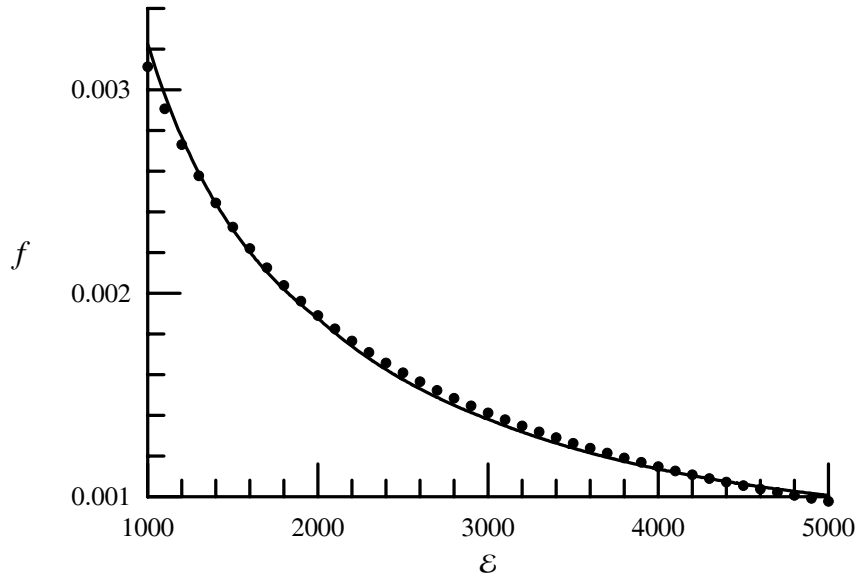Fig. 6.1. Calculated distribution function (points) and analytic asymptotic (line).
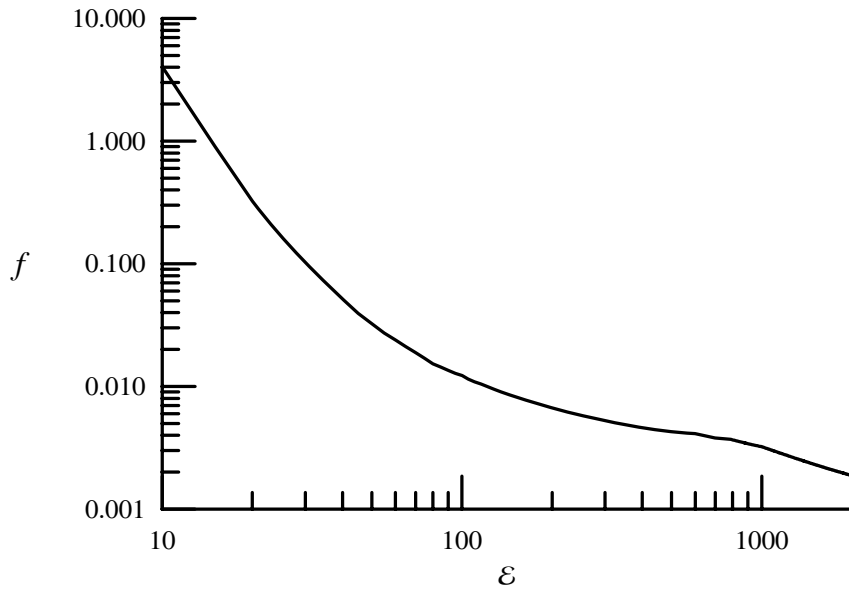

Fig.6.2. Distribution function of fast electrons generated by runaway breakdown process in intermediate energy range.
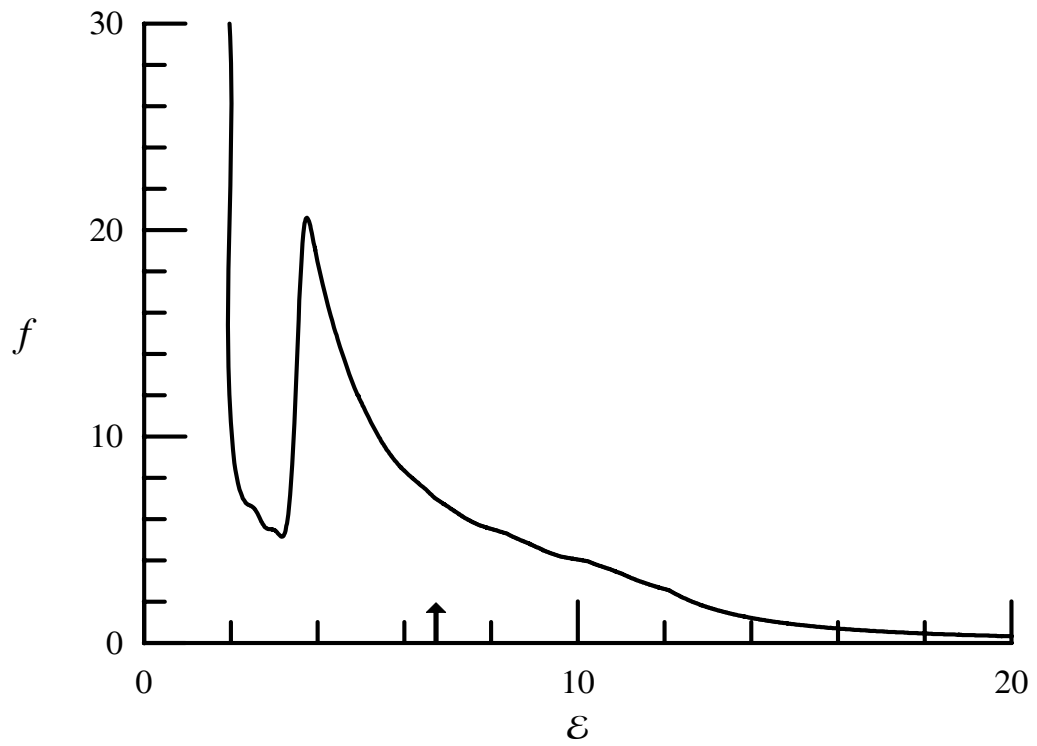
Fig. 6.3. Electron distribution function in low energy range 2 - 20 eV. The maximum of dissociative attachement is shown by the arrow. Strong growth below 2 eV is defined by weak tripple attachement losses.
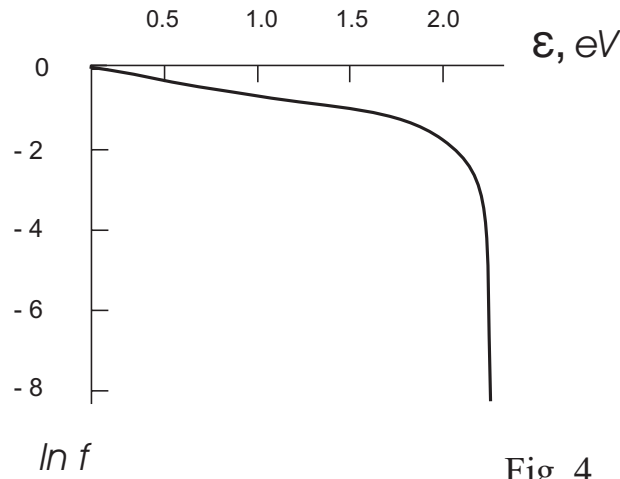
Fig. 4

Fig.6.4. Distribution function of electrons in thermal region. Abrupt fall down near 2 eV is determined by vibration losses. Matching solution given at Fig.6.1 – 6.3, is determined by relations (15), (16).

According to kinetic equation (7) – (13) in RB conditions the following conservation law should be fulfilled

$$\lambda \frac{N}{N_m} + \int\limits_{0}^{2\,eV} \sigma_{at} f(\varepsilon)\varepsilon d\varepsilon + \int\limits_{11.6\,eV}^{10\,keV} \sigma_i f(\varepsilon)\varepsilon d\varepsilon = 0. \tag{14}$$

Equation (14) means conservation of exponentially growing electron number density. As the ionization is mostly effective process and recombination due to the triple attachment is going only in thermal region, the relation (13) could be used to determine the number of thermal electrons N

$$\frac{N}{N_m} = \frac{\tau_{at}}{\lambda \tau_{at} + 1} J_{ion}, \qquad J_{ion} = \int\limits_{11.6\,eV}^{10\,eV} \sigma_i f(\varepsilon)\varepsilon d\varepsilon, \qquad N = \int\limits_{0}^{2\,eV} \sqrt{\varepsilon} f(\varepsilon) d\varepsilon, \tag{15}$$

Where J_{ion} is a full ionization integral and τ_{at} is the life time of thermal electrons due to triple collisions with air molecules (14). The generation coefficient could be determined from (15) as:

$$K_{1\,MeV} = \frac{N}{N_{RB}} \approx 1.5 \times 10^6 \left(\frac{2 \times 10^{19}\ cm^{-3}}{N_m} \right), \tag{16}$$

which means that in RB conditions every seed 1 MeV electron generates in thunderstorm atmosphere K_1 $_{MeV} \sim 1.5 \times 10^6$ thermal electrons. In (16) we took into account, that according to RB solution [6, 7] the density of electrons from 1 MeV to 10 KeV is growing in $ln^2(\varepsilon_{1MeV}/\varepsilon_{10KeV})$ times.

Basing on relation for the current (6) and formulae (16) the radio emission generated by RB-EAS discharge was calculated numerically. The results are presented in Figs. 6.5. Characteristic value of RB – EAS radio pulse amplitude (Fig.6.6.) could be approximated as

$$E \approx 20 \left(\frac{\varepsilon}{10^{17}\ eV} \right) \left(\frac{100\,km}{R_0} \right) \times \exp\left[15 \left(\frac{E_m}{E_c} - 1 \right) \right]\ \frac{mV}{m}. \tag{17}$$

Here ε is the energy of cosmic ray particle, R_0 – is the distance from current region to the receiver, E_m – is the maximal value of electric field, E_c – RB critical field, exponential factor is the result of numerical calculations.
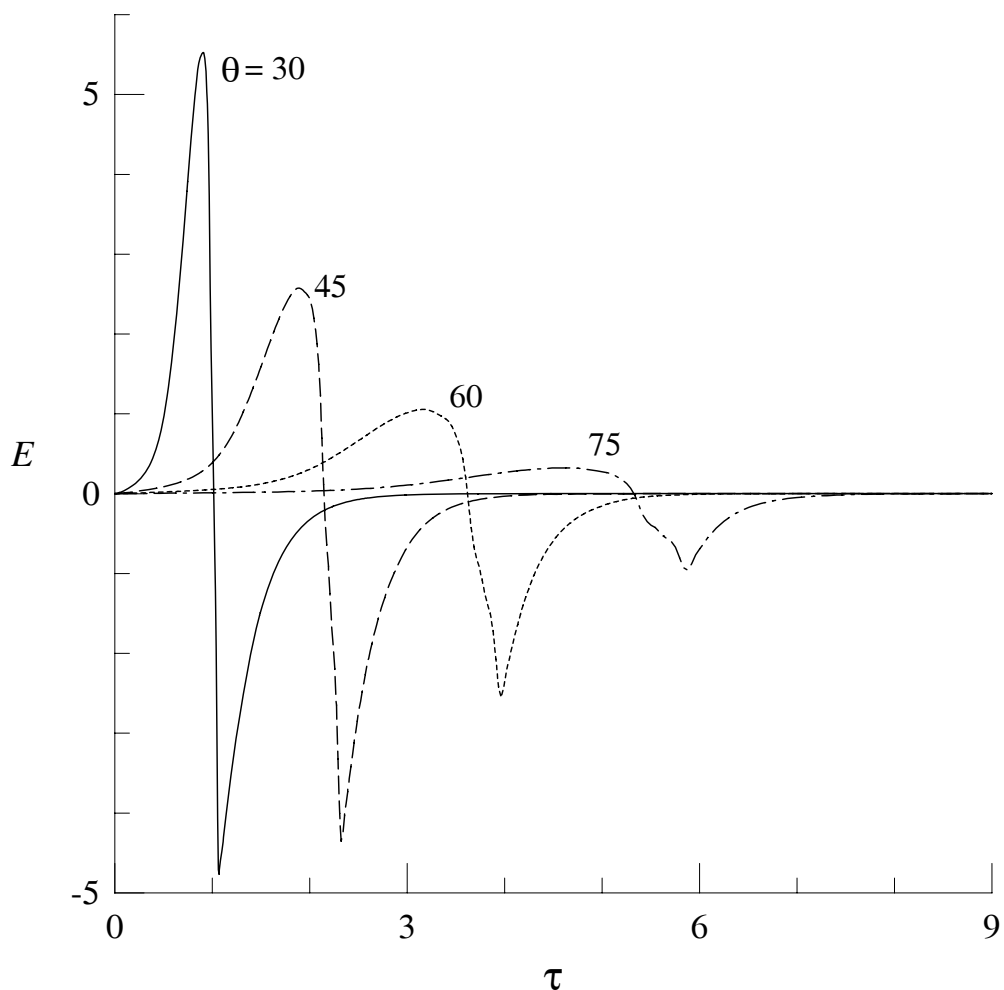
Fig.6.5. The wave form of vertical component of electric field as function of normalized time $\tau = (ct-R_i)/l_i$. θ – the between the direction to the current and the horizon. In atmospheric conditions at the heights 5 – 6 km the ionization length $l_i \approx 100$ m.

Conclusion

The theory of radio emission generated in thundercloud due to RB - EAS interaction was developed. It was shown that the emission has the form of microsecond radio pulses with characteristic frequency around 1 - 10 MHz.

References

[1] A.V.Gurevich, G.M.Milikh, R.Roussel-Dupre Phys. Lett. A 165, 463, 1992

[2] C.T.R.Wilson Proc. Cambridge Philos.Soc. 22, 34 (1924)

[3] R.Roussel-Dupre et al Phys.Rev. E 49, 2257 (1994)

[4] N.G.Lehtinen et al. Geophys. Res. Lett. 24, 2639 (1997)

[5] L.P.Babich et al. Phys.Lett.A 245, 460 (1998)

[6] A.V.Gurevich, et al. Phys. Lett. A 275, 101, (2001)

[7] A.V.Gurevich, K.P.Zybin Physics Uspekhi 44, 11,1119 (2001)

[8] T.Marshall et al. J. Geophys. Res. 100, 7097, (1996)

[9] D. MacGorman, W.D.Rust The electrical nature of the storms, New York, Oxford Univ. Press (1998)

[10] A.V.Gurevich, et al. Phys. Lett. A 282, 180, (2001)

[11] Mc Carthy, G.Parks Geophys.Res.Lett 12, 393 (1985)

[12] K.B.Eack et al. J.Gophys.Res. 101, 29637, (1996)

[13] A.P.Chubenko et al. Phys.Lett.A. 275, 90, (2000)

[14] A.V.Gurevich, G.M.Milikh Phys. Lett. A 262, 457, (1999)

[15] A.V.Gurevich, et al. Phys. Lett. A 254, 79, (1999)

[16] M.A.Uman The Lightning Discharges Orlando, Acad.Press (1987)

[17] S.Z.Belenkij Cosmic Ray Showers (EAS) Atomizdat, Moscow (1987)

[18] A.V.Gurevich Nonlinear Phenomena in the Ionosphere, Springer, NY 1978

[19] A.V.Gurevich, N.D.Borisov, G.M.Milikh, Physics of Microwave Discharges, Gordon and Breach, Amsterdam, 1997

[20] G.Herzberg, Spectra of Diatomic Molecules, Princeton, 1950

Experiments

Description of installations

In frame of this project there were designed and constructed two installations to measure radio emission of lightning discharges in different frequency bands to verify theory predictions.

One of the installations - "Radio-HF" - is designed for the detecting and recording of shot radio pulses with length above 30 ns and for these pulses sources direction finding. Three "Radio-HF" installations were made. One of them is placed at the out-of town laboratory "Vasil'sursk" (SURA facility) of Radiophysical Research Institute, and two others - at the Tien-Shan Mountain Scientific Station (TSMSS) of Lebedev Physical Institute. The use of two spaced installations at TSMSS allows determining of radio emission source position in space using directions to it from two spaced points.

Another installation - "Radio-E" - is designed for recording of the electric field and its variations. VHF receiver operated at about 250 MHz is also a part of this installation. This installation can serve as a source of pulses to trigger other installations that are generated when electric field variations exceeds given threshold. Besides, this installation is able to record trigger pulses both internal and external that are used for time synchronizing of installations. Two "Radio-E" installations were made to place at SURA facility and TSMSS.

"Radio-HF" installation

Block diagram of the "Radio-HF" installation is shown in Fig. 6.6, and its main parameters - in table 1.

This installation consists of three antenna assemblies for spaced receiving, central unit connected to antenna assemblies by cables of equal length, and recording system based on personal computer. Whole system is powered from the uninterruptible power supply.

Each antenna assembly consists of three individual antennas – two crossed by 90 degrees loops to measure horizontal magnetic component and one End-Fed antenna to measure vertical electric component of electromagnetic field. All three antennas are active and contain transistor amplifiers that permitted to diminish antenna size essentially and to obtain more even amplitude-frequency characteristic in the wide frequency range.

Magnetic antenna is a screened rectangular vertically located loop. Loop and pre-amplifier screening is needed to make antenna sensitive only to magnetic component of the field. Otherwise, its directional pattern becomes asymmetric and dependent on frequency. The loop should be loaded with small resistance to even its amplitude-frequency characteristic, and it is connected to pre-amplifier input through step-up transformer acted as a current transformer.
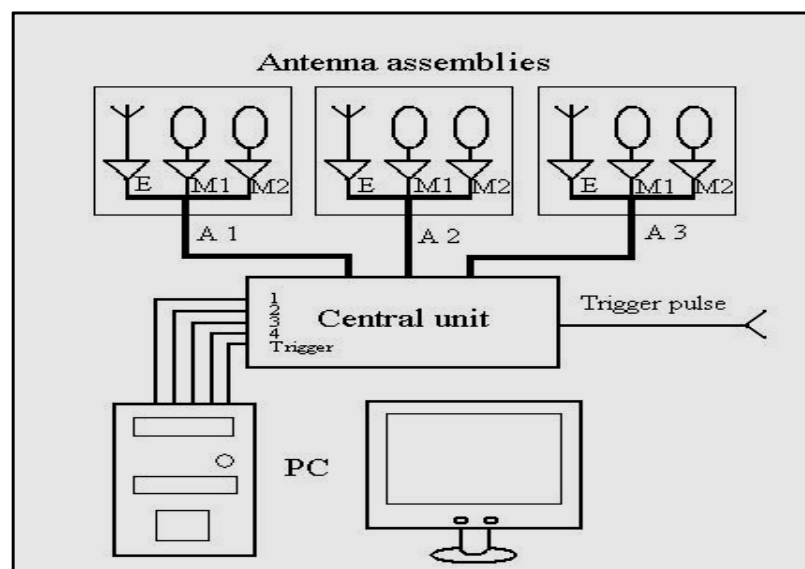

Fig.6.6. Block diagram of the "Radio-HF" installation.

Table. 1. Main parameters of the "Radio-HF" installation.

Frequency range	0.1 – 30 MHz
Amplification	5 – 40 dB
Number of channels	1 - 4
ADC capacity	14 bits
Sampling rate	up to 60 MHz
Record length	up to 1 s
Trigger	internal/external

Electric (End-Fed) antenna is an electrically short rod with disc nozzle at the end placed to enhance antenna capacity. Frequency range expansion of active electric antenna is connected with principally capacity character of the electrically short rod impedance as well as of transistor input impedance at the operating frequencies. Due to this fact, antenna-amplifier connection is a frequency independent divider with a ratio of antenna capacity to amplifier capacity as a transfer coefficient. Antenna capacity enhancement by the disc nozzle broadens the low boundary of its frequency range, which is determined by the product of antenna capacity and input resistance of the pre-amplifier. At the same time high input resistance of the pre-amplifier along with diminishing of low frequency boundary leads to enhancement of low-frequency noise received by antenna, and increase a risk of transistor disruption in strong electric fields. Based on this, pre-amplifier input resistance was chosen as 1 megohm that provide acceptable value of low boundary of antenna frequency range at about 100 kHz level. There are high-voltage feed-through capacitor, gas-filled discharger, and two opposite-parallel diode protection circuit at the pre-amplifier input to protect it from disruption during lightning discharges.

Antenna assemblies are spaced by several ten meters apart (from 50 to 90 m at different locations) and from recording system.

Each of three antenna amplifiers of each antenna assembly is connected to central unit by cables of equal length. Central unit serves for preliminary analog processing of the signals from antenna assemblies aimed to reduction of the dynamic range of received signals to analog-to-digital converter (ADC) input range to prevent loss of information. Both high-pass and low-pass filtering is also performed to decrease low-frequency noise and to prevent spectrum aliasing during data sampling. Antenna assemblies are fed by separate coaxial cables from the power supply that is also a part of the central unit

Commutation of individual antennas with recording system is another role of the central unit. Signals from 9 antennas (3 from each antenna assembly) arrive to the central unit while recording system has only 4 channels. Thus simultaneous recording of signals from all antennas is impossible. Fabric allows to connect any recording channel to any antenna, connections are chosen according to specific goals of experimental investigations.

Recording system is a four-channel receiver based on personal computer and two two-channel ADC boards AMBPCM (base module) with ADM214x60M sub-modules operated in synchronous mode. ADM214x60M sub-module is a two-channel 14-bits ADC with 60 MHz maximum sampling rate. Each AMBPCM base module contains onboard 256 MB memory for intermediate ADC data recording. The use of onboard memory is needed due to high temporal resolution that leads to high rate of data flow (above 200 MB per second at maximum sampling rate) that exceeds PCI bus capabilities of personal computer. Synchronous operation of ADC boards is provided by the use of master-slave mode when one of the boards is a leader and operates another board.

Recording system is operated as follows. Data are continuously recorded to the ring buffer in the base module onboard memory. Trigger pulse forces data recording cessation after a period that is determined by the size of the ring buffer and given pre-history duration (data recording duration before trigger pulse arrival). After that the whole ring buffer is transferred to computer RAM and then to the hard disk. Data recording is interrupted for a time of data transfer and storing. Trigger pulse is generated by base

module comparator either on the external synchronizing pulse arrival (external trigger) or when an input signal of one of the recording channels exceeds given threshold, that is defined programmatically.

Data acquisition software is designed using regular ADC driver and provides several operational modes of the installation differed by record and pre-history duration as well as a source of trigger pulses.

"Radio-E" installation

Block diagram of the "Radio-E" installation is shown in Fig. 6.7, and its main parameters - in table 2.

Permanent ("slow") electric field is measured by electrostatic fluxmeter ("field mill"), designed for atmospheric electric fields measurement under thunderstorm conditions. Electric field measurement uses principle of periodic screening of measuring electrode by rotating grounded disc with notches. Electric circuit of the fluxmeter consists of input repeater with high input resistance, synchronous detector with reference channel connected to photosensor of disc position, low pass filter, output buffer amplifier, and protection circuits from overvoltage and disruption of active elements. Signal from the buffer amplifier is fed to the recording system through a cable. Fluxmeter is placed into a waterproof case designed for setting "plates downward" to diminish precipitation influence on the sensor operation.

Variations of electric field ("fast" field) are measured using capacitor type sensor, which is a rectangular box of 500 x 500 x 150 mm size. Sidewalls of the box are made from an insulating material while top and bottom covers are conducting metallic plates, i. e. capacitor plates (we used fiberglass with copper layer outside). A screened repeater with 50 Hz eliminator and buffer amplifier to feed a long cable is placed inside the box. The bottom capacitor plate is connected to global bus of the amplifier while the top is a sense one. There are a protector tube, high voltage capacitor, and diode limiter at the input of the repeater as well as adjustable attenuator from 0 to 35 dB in 5 dB steps. Power supply of the amplifier is done through screened twisted pair (mic cable). The sensor box is placed into the ordinary plywood box usual for EAS counters installing to protect against precipitations.

Pre-amplifier output is connected through a cable to the analog processing unit designed for signal filtering and generation of pulses under given conditions to switch operational mode of this installation and starting of other installation (trigger pulses). Filter unit consists of plugging high pass filter with 500 Hz cut-off and two switchable low pass filters with 10 kHz and 50 kHz cut-offs. Filtered signal is fed to the recording system.
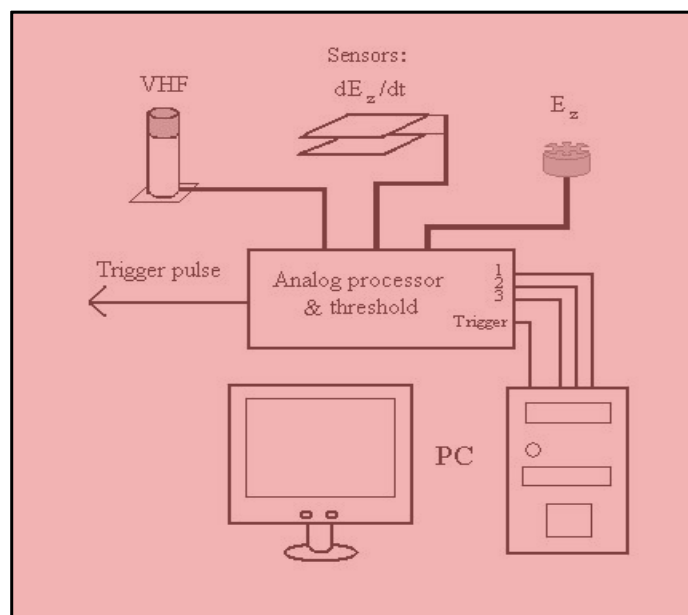

Fig. 6.7. Block diagram of the "Radio-E" installation.

Table. 2. Main parameters of the "Radio-E" installation.

	"slow" E	*"fast" E*
Measurement range	+/- 50 kV/m	+/- 600 V/m
Sensitivity	20 V/m	0.5 V/m
Temporal resolution	0.1 s	50 ms/50mks
ADC capacity	14 bits	
Sampling rate	20 Hz/20 kHz	

Comparator that compares magnitude of the electric field variations with threshold given in advance carries out generation of trigger pulses. A pulse of 100 mks length (trigger pulse) that can be used by other installations is generated when variation of electric field exceeds threshold as well as another pulse of about 1 s length that arrives to digital port of recording equipment. The last pulse is used also to forbid trigger pulse generation during its presence that exceeds characteristic lightning duration. This prevents generation of multiple trigger pulses during given lightning. Threshold is chosen at a level exceeded interference level but low enough to guarantee comparator event from electric field variations of stepped leader of close lightning (at several kilometers).

Recording system is based on the personal computer and L-780M ADC board with maximum sampling rate of 400 kHz and commutator on 16 differential channels. Four channels to record "slow" and "fast" electric field, VHF receiver output, and comparator trigger pulses are used in the considered equipment. Trigger pulses from other installations can also be recorded if necessary.

Recording system (and the whole installation) is operated continuously in automatic mode. Under quiet conditions without thunderstorm activity "slow" mode of data acquisition with sampling rate of 20 Hz in each channel is used. At the same time digital port of ADC board is sampled ones in 0.5 s, and recording system is switched into "fast" mode of data acquisition with sampling rate of 20 kHz in each channel if a pulse (of about 1 s length) arrives. "Fast" mode lasted about 75 minutes that usually exceeds duration of local thunderstorm, and after that recording system is switched back to the "slow" mode. Another pulses arrived to the digital port of the ADC board during "fast" mode do not affect mode of data acquisition.

Experimental results

Experimental investigations were carried out at two points: at Tien-Shan Mountain Scientific Station of Lebedev Physical Institute situated at about 20 km to the south from Almaty (Kazakhstan) at the mountainous place about 3300 m above see level, and at the SURA facility of Radiophysical Research Institute situated at about 120 km to the east from Nizhny Novgorod at the plain place about 300 m above see level. They were aimed to study predicted by theory radio emission of lightning discharges in the wide frequency range with high temporal resolution, its relation to extensive atmospheric showers created by cosmic rays, and generation of gamma emission by lightning discharges.

SURA facility

Checkout and testing of both installations were carried out at SURA facility as well as an investigation of short wave radio emission of lightning discharges. Primary attention was paid to initial stage of lightning radio emission in accordance to theoretical prediction on the lightning initiation by cosmic rays. In 2004 "Radio-HF" installation was operated from internal trigger with record length from 0.1 to 1 s and pre-history from 80 to 500 ms. In 2005 "Radio-HF" was triggered by pulses generated by "Radio-E" installation. Record length was 0.5 s, and pre-history length was 0.1 s. Sampling rate was 60 MHz in all cases. Radio emission from about one and half thousand lightning discharges in more than 10 thunderstorms was recorded during two years of observations. Initial stage of lightning radio emission was recorded in more than 70% events. Analysis of obtained data showed that:

- Short wave radio emission of the lightning is a succession of short pulses (with lengths from less than 100 nanoseconds to few microseconds).

- Background level of radio emission between lightning discharges in thunderstorm does not differ from background level under quiet conditions (at given sensitivity). Usually it is the same between lightning pulses also, at least at the initial stage of lightning evolution.

- Radio emission of each lightning starts with very short bi-polar pulse with initial peak length less than 100 nanoseconds. There is no radio emission differed from background at least 500 milliseconds before the first pulse. Waveform, width, and magnitude of the first pulse are consistent with predicted by the theory of combined action of runaway breakdown and extensive atmospheric shower for primary particle energy of about 10^{16} eV. Hence, we can suppose that lightning discharge is initiated by appropriated cosmic particle if thundercloud electric field exceeds runaway breakdown threshold.

- The first pulse is followed by a series of several similar to it bi-polar pulses with gaps from few ten to few hundred microseconds. Positive and negative polarity of initial pulses (in electric field) occurred about equally in different lightning discharges but is the same in each individual lightning.

An example of short wave radio emission of lightning is shown in different time scales in Fig. 6.8 for the case when initial stage of was observed. All panels show record parts that include initial stage of radio emission. The data was obtained at SURA facility on July 24, 2004 at 21:00:32 local summer time (UT+4) using magnetic antennas. First and third tracks (red and blue) correspond to the same antenna assembly but orthogonal antennas. Two other tracks, second and forth (green and cyan) correspond to two other antenna assemblies. Polarity difference of received signal in the forth channel from other channels most distinctly seen in the bottom, most detailed in time, panel is due to casual connection of appropriate antenna (loop) to the antenna amplifier in opposite polarity

Bottom panel of the Fig. 6.8 shows an initial pulse of lightning discharge radio emission. It is short bi-polar pulse with full length of about 200 ns and first peak length of about 60 ns. Pulse waveform and length are consistent with predicted by the theory of combined action of extensive atmospheric shower and runaway breakdown. These observations provide only circumstantial evidence for the theory while observations of EAS initiated lightning could be direct one. However, such observations are possible only as a result of rare lack because it is impossible to have EAS facility with thundercloud scale (hundreds of square kilometers), and place of lightning initiation and EAS direction are not known in advance. It should be noted that temporal resolution of the installation (about 16 ns) allows us to assert that pulses more short than about 50 nanoseconds are absent in the radio emission of lightning discharge. Second panel from below in Fig. 6.8 shows that radio emission of the lightning starts with a series of pulses similar to the first one with gaps from 5 to 300 mks that essentially exceed pulses lengths. Third panel from below in the Fig. 6.8 shows that later on lightning radio emission is usually a succession of pulses with much exceed their lengths gaps. Top panel of Fig. 6.8 shows that there was no radio emission differed from background during more than 380 ms before the initial pulse.

Fig. 6.9 shows typical spectra of intensity of background radio emission (top panel) and radio emission of lightning discharge (bottom panel) obtained at SURA facility in the evening time and averaged at about 100 ms. The cut of discharge emission spectrum below about 200 kHz is due to frequency characteristic of used sensors (active antennas). Spectrum of lightning discharge radio emission shown in Fig. 6.9 has a maximum at about 5 MHz and characteristic modulation. These features are not common for all discharges. Spectra without maximum are also common when monotonic character of spectrum remains at low frequencies down to sensor cut-off. The same can be said on the spectrum modulation. Broadcasting frequency bands with enhanced interference from radio stations are clearly seen at both spectra shown in Fig. 6.9.

The difference in pulse arrival time at spaced antenna assemblies allows to determine direction to the source of emission using correlation technique. An example of direction finding is shown in Fig. 6.10. Directions to the sources of several pulses received in a few millisecond range are shown in azimuth-zenith angle coordinates.
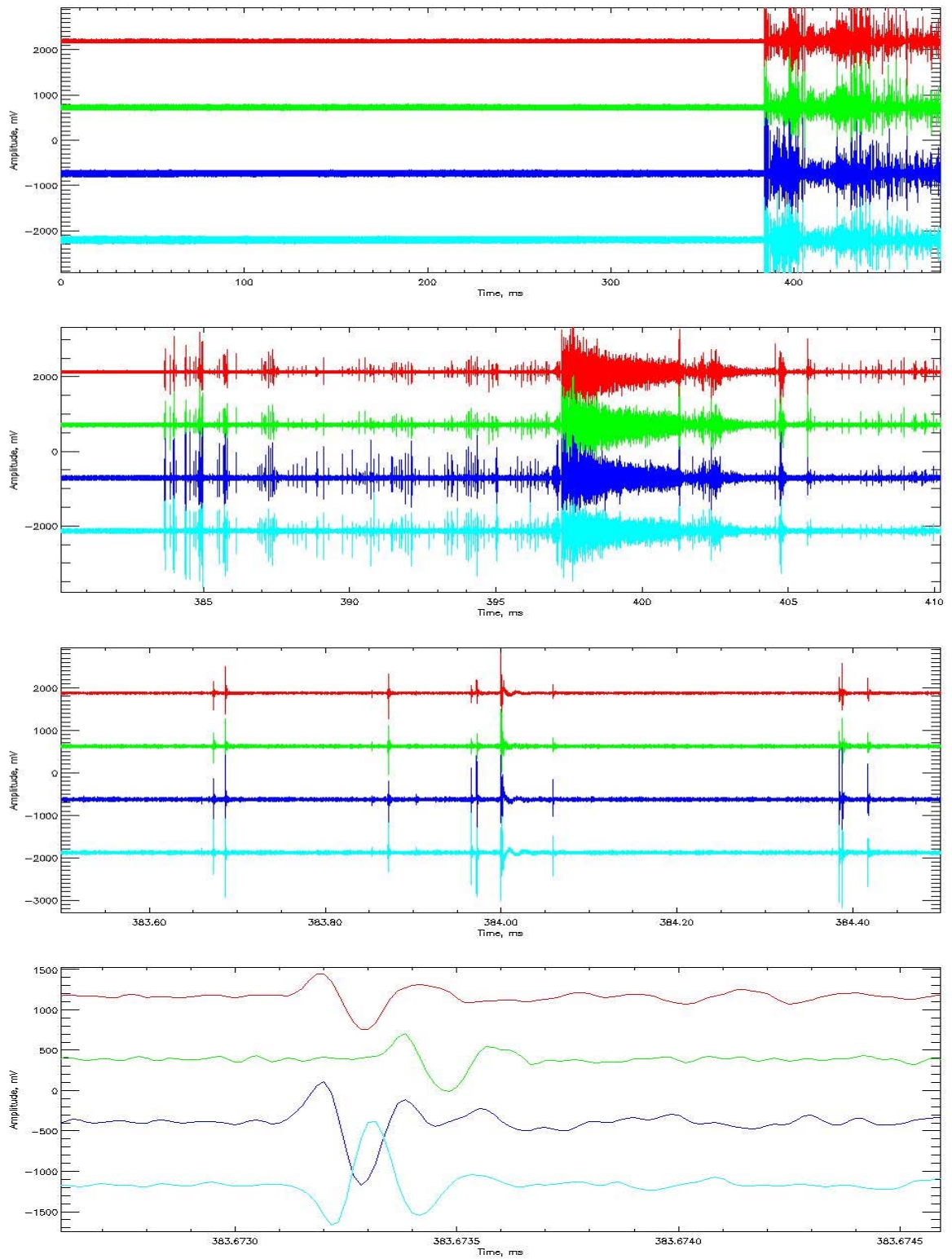
Fig. 6.8. Record of lightning radio emission at different time scales obtained using "Radio-HF" installation at SURA facility on July 24, 2004 at 21:00:32 LT.
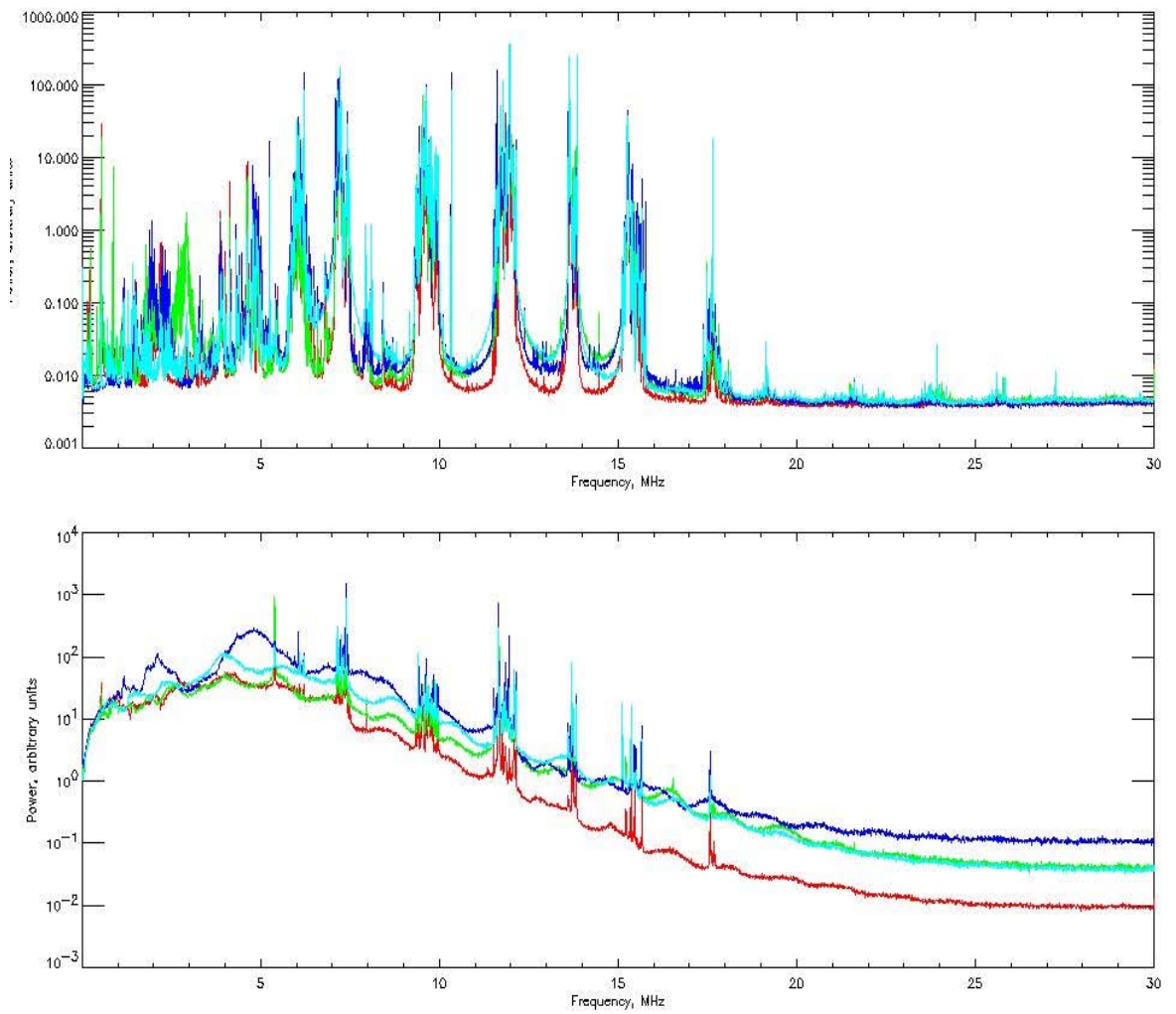
Fig. 6.9. Spectrum of lightning radio emission (bottom) and background spectrum obtained in the absence of thunderstorm activity (top) in the evening time from the data of "Radio-HF" installation at SURA facility.
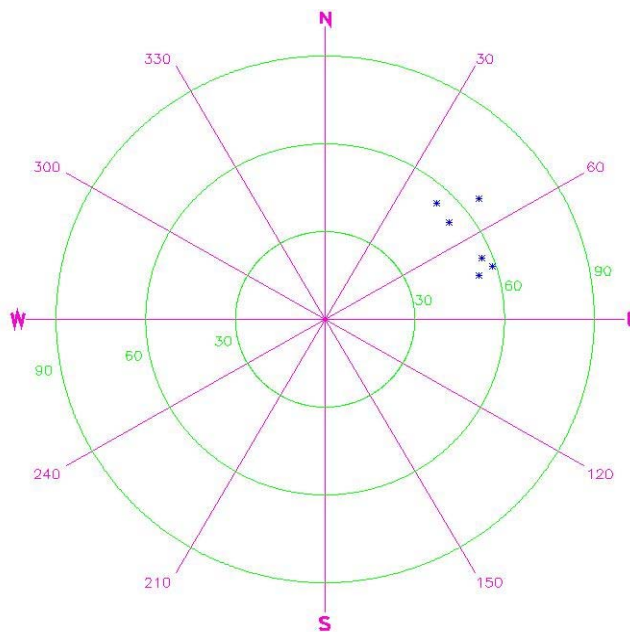

Fig. 6.10. Example of lightning radio emission source direction finding.

TSMSS

Combined investigations of electric field, HF and VHF radio emission, and energetic particle flows and gamma emission under thunderstorm conditions including lightning discharges were carried out at TSMSS. A possibility of generation of rather strong radio emission under thunderstorm conditions due to runaway breakdown when seed high energy particles are delivered by extensive atmospheric showers (EAS) was investigated in 2003 and 2004. Gamma emission of lightning discharge was studied along with radio emission in 2005.

Current tasks required external triggering of "Radio-HF" installations by trigger pulses generated by EAS detecting installation in the first case, and generated by "Radio-E" installation in the second one when the same trigger pulses were used to start gamma emission recording installation.

EAS detecting installation has overall area of about 0.1 sq. km and is able to detect cosmic ray particles with $2 \cdot 10^{14}$ - 10^{15} eV energy. Trigger pulses from this installation were used for radio emission recording by "Radio-HF" installations during 100 mks with 83.2 mks pre-history. Averaged interval between trigger pulses was 2.5 s. Installations were operated continuously from the middle of July to October 2003 and from May to October 2004.

Obtained data contain observations of more than 20 thunderstorms occurred at the station or in immediate vicinity from it. The results of data processing are as follows:

- In the absence of thunderstorm conditions extensive atmospheric showers were not accompanied by radio emission with intensity above used receiver sensitivity.

- About 2% of detected EAS were accompanied by radio emission in form of short bi-polar pulses with few hundred of nanoseconds full length and first peak length of about 100 ns under thunderstorm conditions. First peak polarity of the electric field can be either positive or negative.

- Characteristics of obtained radio emission are consistent with predicted by the theory of combined action of runaway breakdown and extensive atmospheric shower for the primary particle energy of $2 \cdot 10^{14}$ - 10^{15} eV. Probability of radio emission generation by extensive atmospheric shower is stipulated by the probability for atmospheric electric field to reach runaway breakdown threshold at the EAS path.

- Series of pulses usually with essentially larger amplitude presumably concerned with lightning discharges were observed besides of single pulses accompanied EAS. It was determined that attitude position (direction to source of emission) of such series does not coincide with attitude of pulses accompanying EAS. Observed radio pulse series are presumably concerned with stepped leader evolution and return stroke of lightning.

Radio emission records obtained by "Radio-HF" installation *in the absence of thunderstorm conditions* for 20 consecutive trigger pulses from EAS detecting installation on September 9, 2003 at about 4:35 UT (local time is UT+5) are shown in the Fig. 6.11 as an example. Only trigger pulse interference at 85-90 mks from the beginning of records are seen above background level (trigger pulse itself begins at 83.2 mks from the record beginning according to given pre-history duration). Several ten thousand such records were analyzed, and no sign of radio emission accompanying EAS was found.

At the same time *during thunderstorm* short sub-microsecond were observed in individual records as it is seen from Fig. 6.12 analogous to Fig. 6.11 where data obtained during thunderstorm on September 11, 2003 at about 4:40 UT are shown. Radio emission pulses were observed at 4:39:54, 4:39:58, and 4:40:39 UT in advance of trigger pulse arrival few tens mks before it.
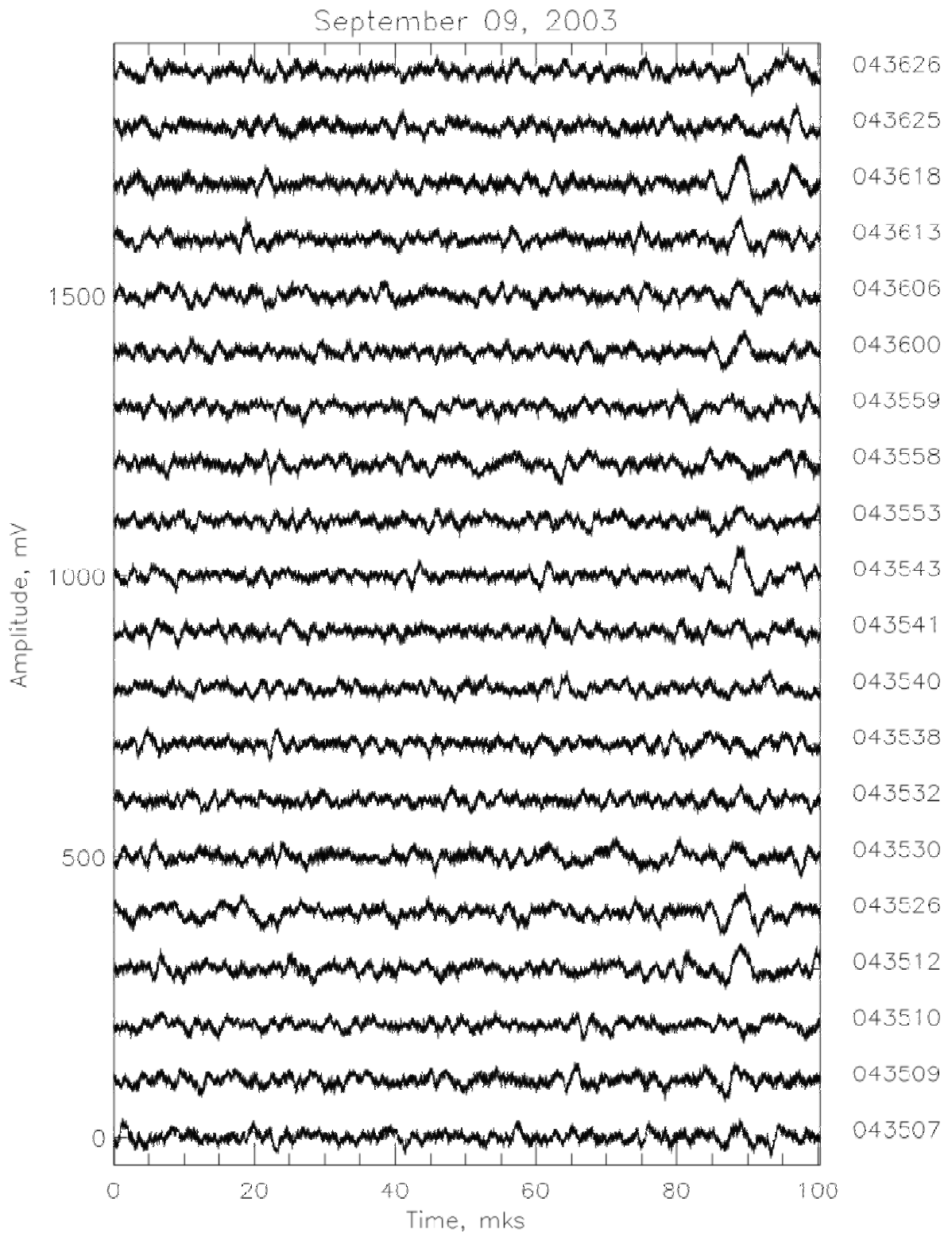
Fig. 6.11. Example of radio emission records triggered by EAS detecting installation in the absence of thunderstorm conditions. Records are shifted one against other by 100 mV. Time of the record is shown at the right in hhmmss UT format.
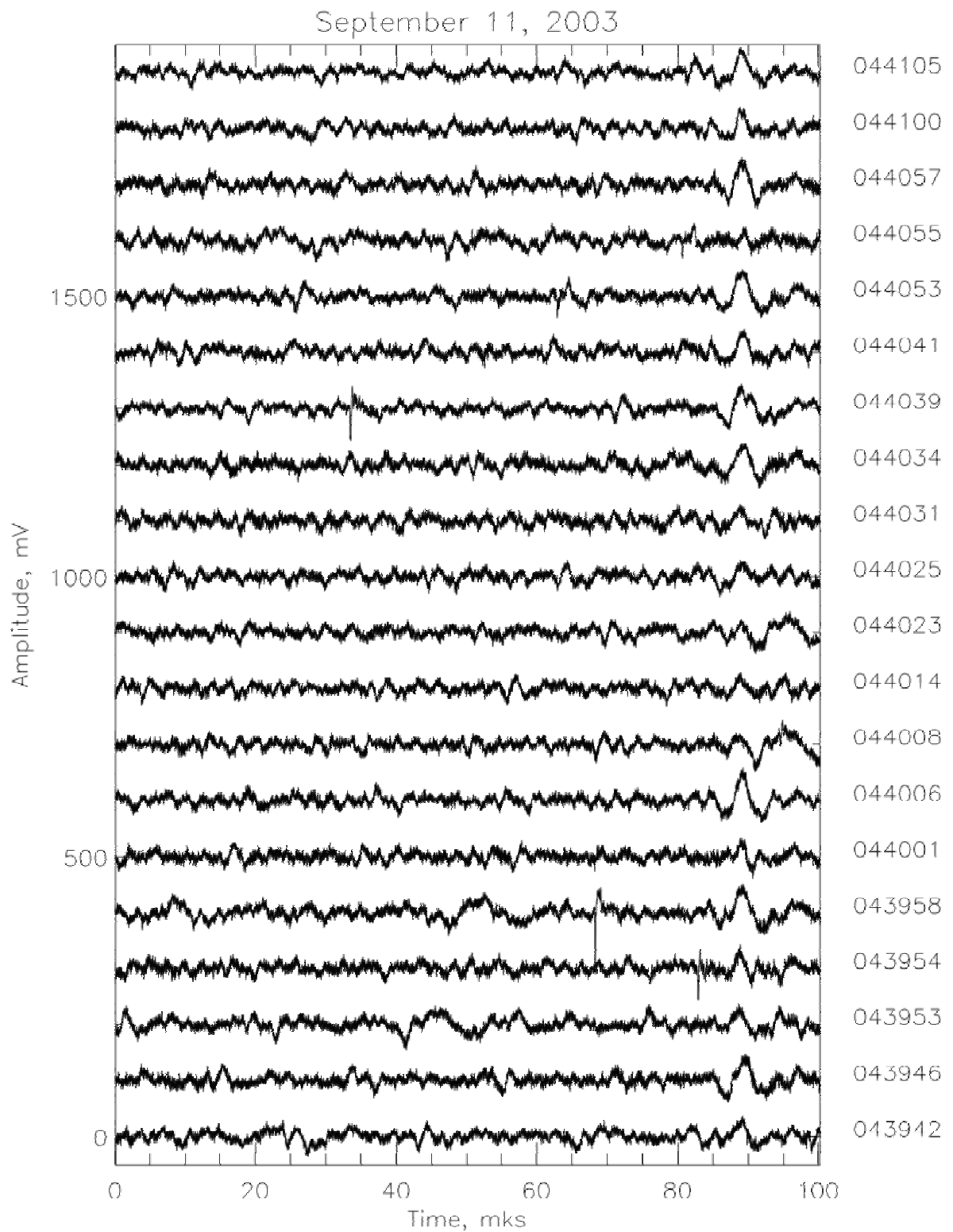
Fig. 6.12. The same as in the Fig. 6.11 but under thunderstorm conditions. Short radio pulses are seen in the records at 043958, 044039, and 043954.

Detailed waveform of radio pulses accompanying EAS is shown in the bottom panels of Fig. 6.13 based on the data obtained on July 25, 2004 during thunderstorm observed at TSMSS about 06 UT. Pulses of both polarities obtained from electric antennas of one of the "Radio-HF" installations are shown. Second and third channels (green and blue) duplicate data from the same antenna assembly. Whole 100 mks records are shown in the top panels, it is seen that radio pulse arrived 10-12 mks before trigger pulse (noise at 83 μs. Such position of radio pulse is stipulated for a delay of trigger pulse relative to EAS arrival due to necessity of its forming and transfer to "Radio-HF" installation and, possibly, by relative position of EAS detecting installation and "Radio-HF". Pulses lengths can be determined from the bottom panels.

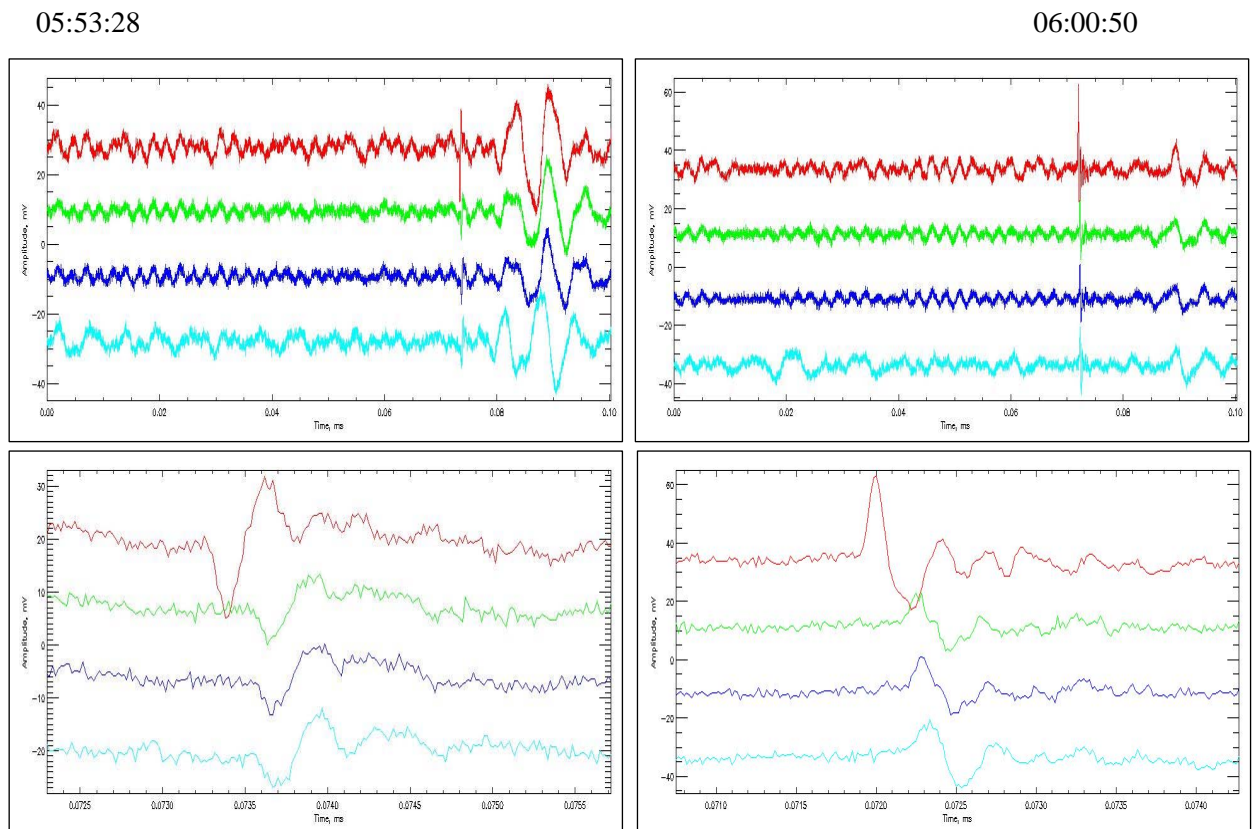05:53:28   06:00:50

Fig. 6.13. Examples of records of short bi-polar pulses accompanying EAS under thunderstorm conditions. Data were obtained at TSMSS on July 25, 2004, time (UT) is indicated above each record. Top panels show whole 100 mks records, bottom – pulses waveforms.
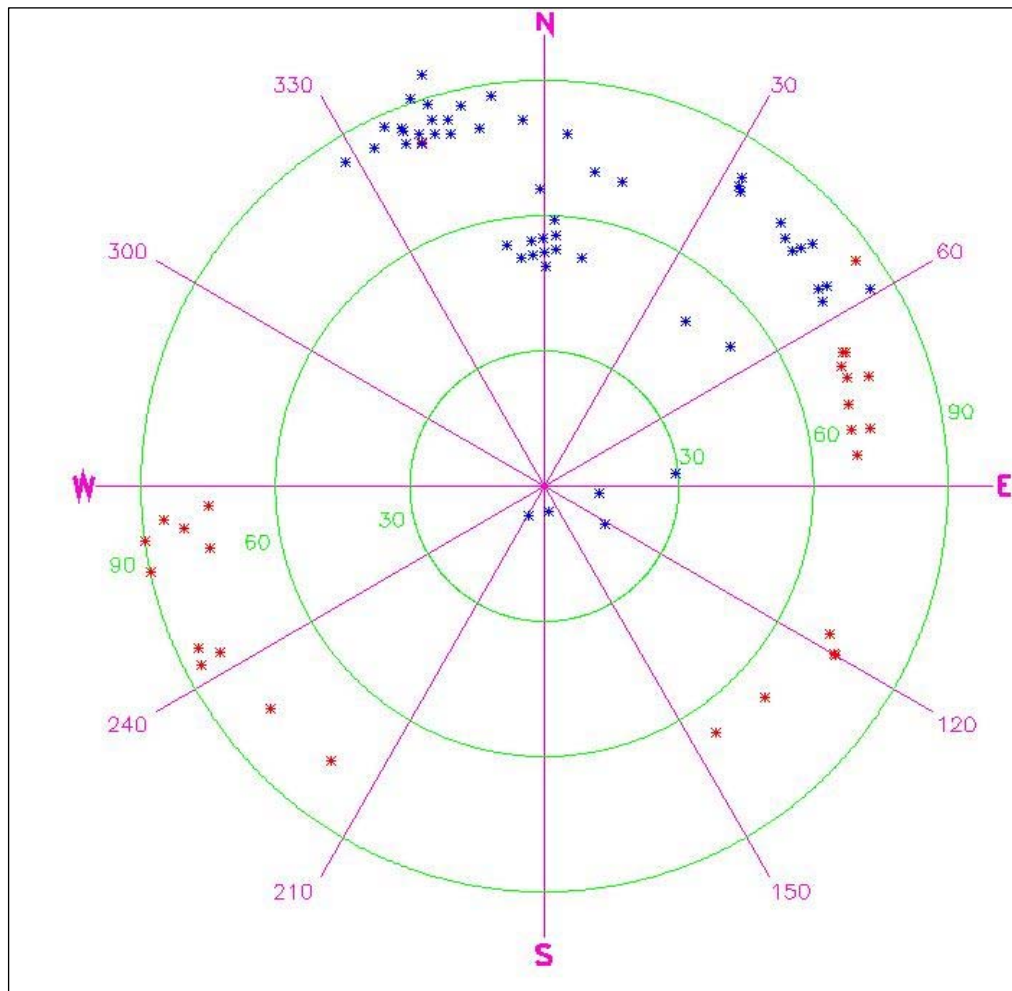
Fig. 6.14. Direction to the sources of bi-polar pulses accompanying EAS (blue crosses) and to the sources of series of pulses concerned with lightning discharges (red crosses) for the thunderstorm on July 25, 2004. Data were obtained at TSMSS.

Results of radio source direction finding at thunderstorm on July 25, 2004 are shown in Fig. 6.14. Blue crosses show directions to the sources of short bi-polar pulses accompanying EAS while red ones show directions to the sources of series of intense pulses presumably concerned with lightning discharges. It is clearly seen that directions to these sources does not coincide: bi-polar accompanying EAS pulses form a group around north and north-east directions with moderate angles to horizon, few pulses also arrived from near zenith direction. At the same time series of pulses concerned with lightning discharges arrived from east and west directions close to horizon.

The use of two spaced "Radio-HF" installations at TSMSS allows to determine an attitude position of radio emission source by directions to it from two installations. An example of such determination is shown in Fig. 6.15 for one of thunderstorms in 2004 along with spacing of installations in 2004 when the distance between them was about 1.5 km. In shown example a pair of short pulses was observed form the direction along the horizon. Most likely, stepped leader near the ground surface caused this emission.
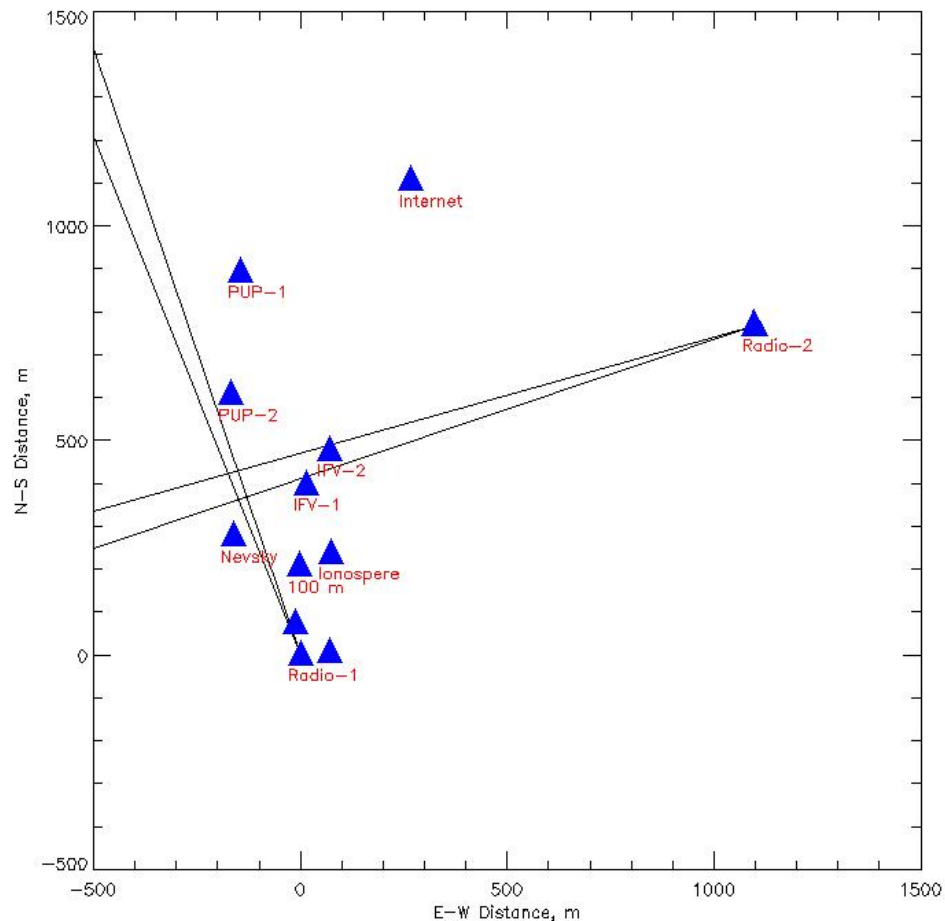
Fig. 6.15. An example of attitude position determination of the radio emission source at TSMSS in one of the thunderstorms in 2004 using data from two "Radio-HF" installations (Radio-1 and Radio-2), spaced by about 1400 m.

Trigger pulses generated by "Radio-E" installation interpreting as return strokes of close lightning discharges were used in the investigations of lightning gamma emission as starting pulses. Trigger pulses were given to both "Radio-HF" installations as well as to installation for gamma emission detection base on NaI sensors. "Radio-HF" installations were operated in external trigger mode with record length of 0.5 s with 0.1 s pre-history, and record length at gamma emission detection installation was 0.4 s with 0.2 s pre-history.

Unfortunately, during experiments in 2005 power supply for two from three antenna assemblies of one of the "Radio-HF" installations was lost, and determination of attitude position of radio emission sources became impossible. In addition, electrostatic field sensor ("field mill") was ill moved in the beginning of August, and its data became spurious. Besides, not all events were recorded by "Radio-HF" installations due to rather high data level and relatively low write speed to the hard disk. A part of events was recorded by only one of the "Radio-HF" installations due to a difference in writing speed at different computers.

At the same time, there were recorded more than 3000 events (at least at one of the installations) during the 2005 campaign lasted from May to September. Most of them were concerned with thunderstorm activity. NaI sensor system recorded more than 1000 events for most of which there were recorded variations of electric field and VHF emission. "Radio-HF" installations recorded 388 from these events including 194 recorded by both.

An example of steady electric field record from fluxmeter (top panel) and from variation electric field sensor (bottom panel) is shown in Fig. 6.16 for the thunderstorm occurred on May 26, 2005 between 06 and 07 UT.
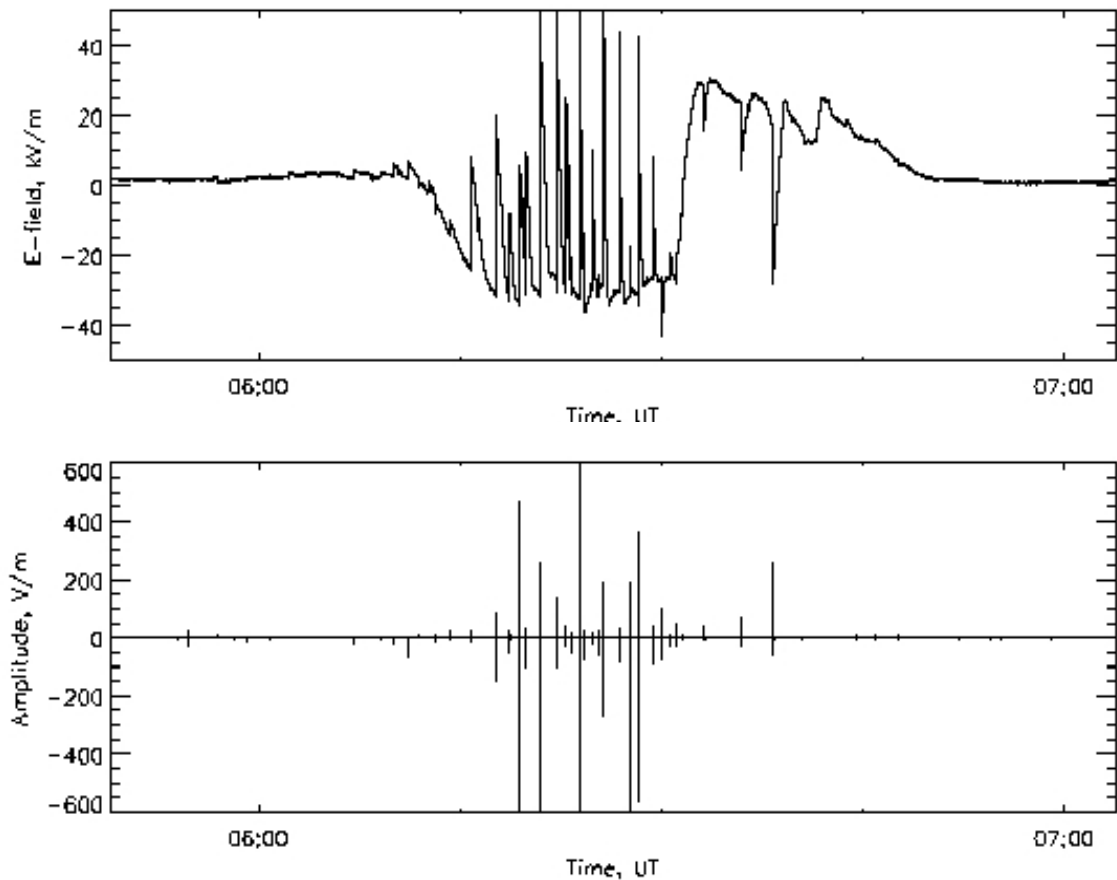
Fig. 6.16. An example of electric field record at TSMSS for the thunderstorm on May 26, 2005. Top panel – "slow" field (fluxmeter), bottom panel – "fast" field (variation sensor).

The record in "fast" mode was started at 05:49 UT with small variations of electric field caused by distant discharges possibly intracloud. The thunderstorm began to cover the station at about 06:10, and steady electric field (top panel) rose to about –40 kV/m in about 5 minutes. After that there was a series of negative discharges during about 15 minutes. The polarity of electric field was rapidly changed at about 06:30, the field reached magnitude +30 kV/m, and there were several positive discharges after that. The rest of the record corresponds to (former) thundercloud out of station. Series of pulses were recorded from electric field variations sensor for all lightning discharges (bottom panel).
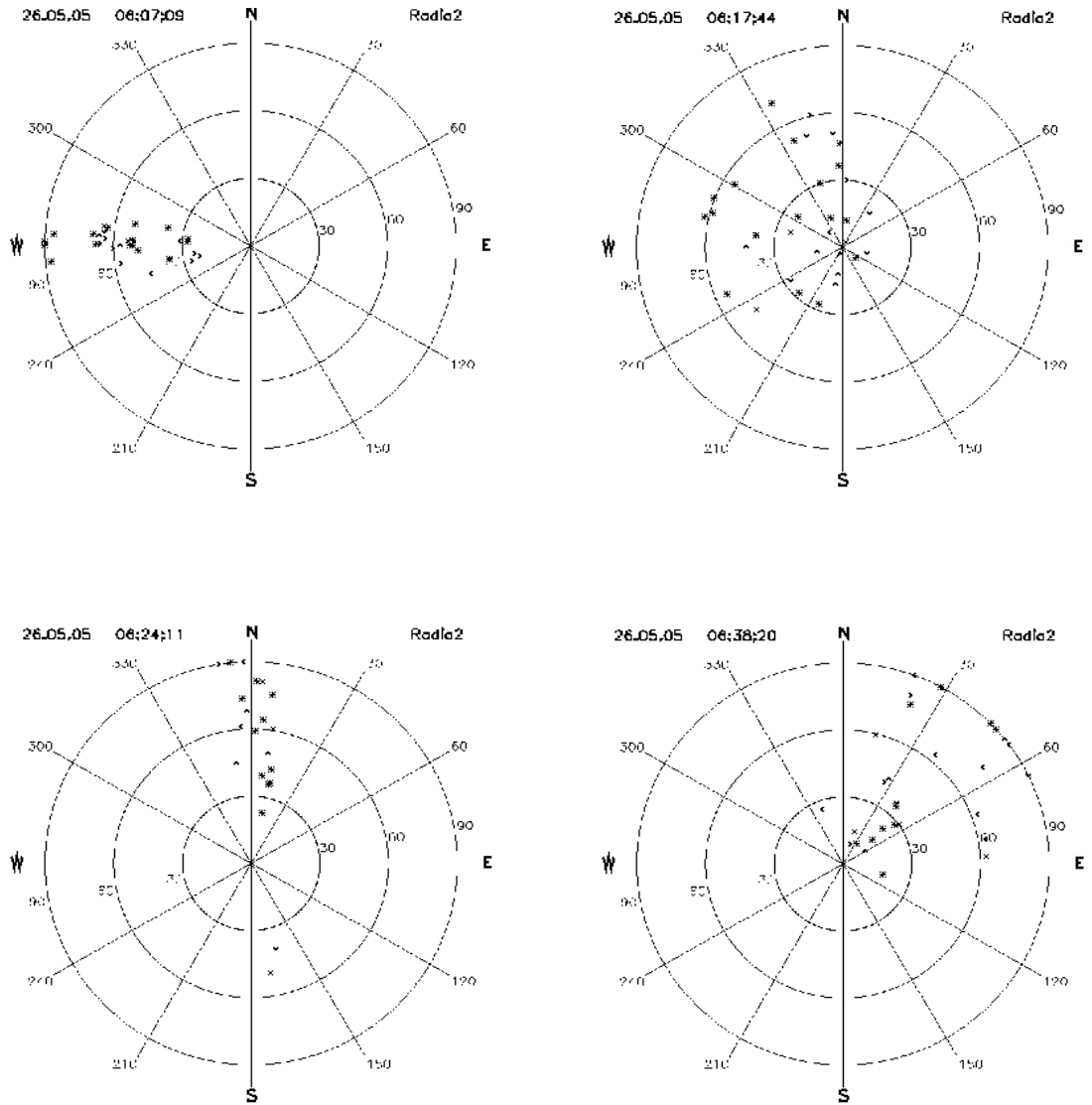
Fig. 6.17. Directions to the radio emission sources for the thunderstorm on May 26, 2005 at different points of time from the data of "Radio-2" installation.

The passing of the thunderstorm above the station is seen from the determination of directions to radio sources at "Radio-2" installation. The change of the directions to radio sources with time from west to east is shown in Fig. 6.17.

An example of simultaneous data records at different installations is shown in Fig. 6.18. Data on the time interval started 100 ms before trigger pulse and lasted 200 ms after it are shown in the left. More detailed data around trigger pulse (from –5 ms to 30 ms relative to it) are shown in the right.
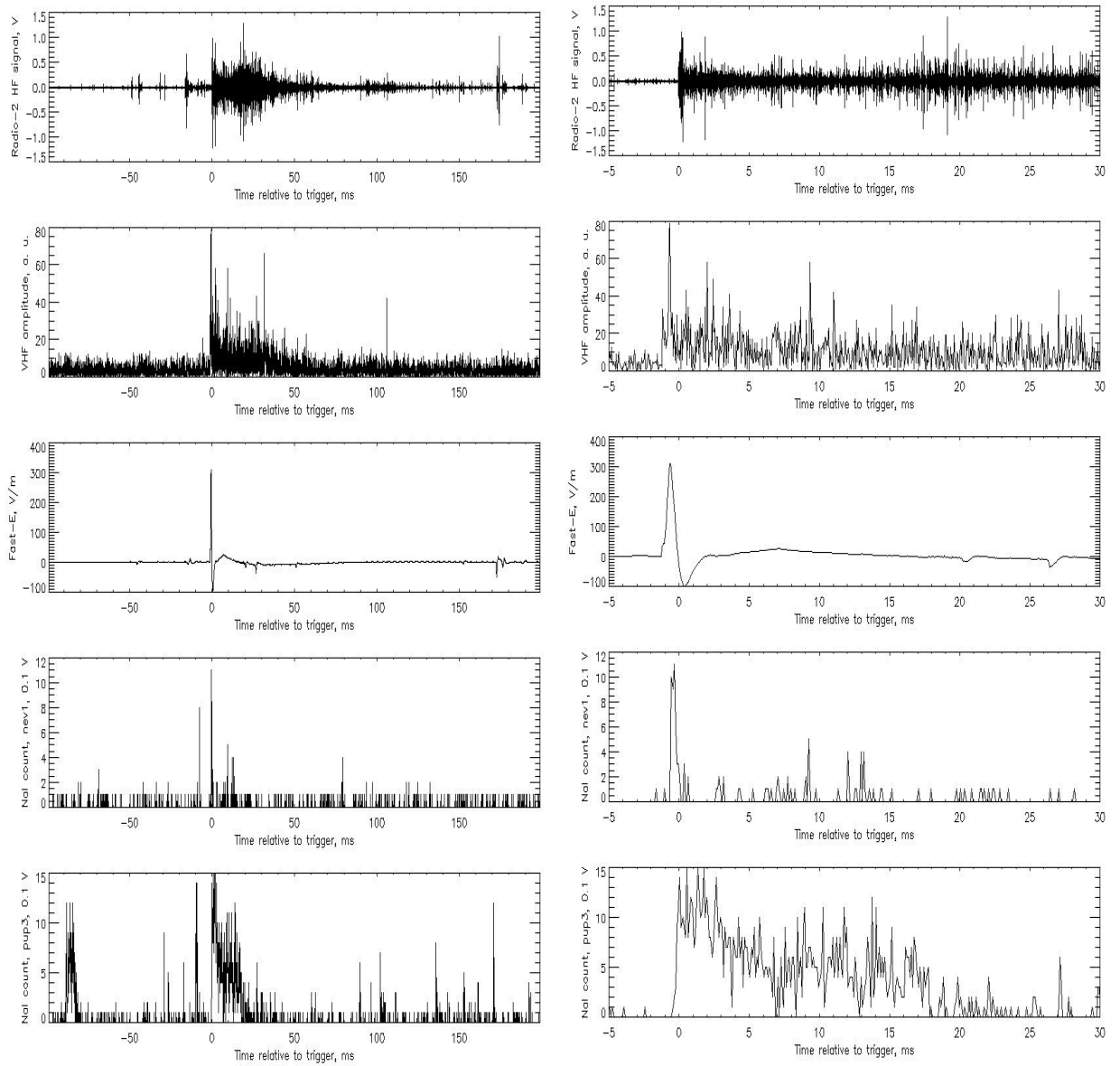
Fig. 6.18. An example of simultaneous recording of (from top to bottom) HF and VHF radio emission, electric field variations, and gamma emission from two NaI sensors (nev1 and pup3).

Runaway breakdown at troposphere heights

A distinct class of radio pulses generated in thunderstorms was effectively studied during recent years in observations of Smith et al. [1-3]. These studies allowed establishing that the radio pulses having enormous peak power up to 100 GW are emitted in the wide frequency range by the intracloud discharges in the tropopause (10 – 20 km). The pulses are short time (≤ 10 μs) and have a definite bipolar form. That is why they were called narrow bipolar pulses (NBP). The observations show that these strong radio pulses are isolated -- not accompanied by usual lightning leader and return stroke. Their optic emission is very weak. A detailed analysis of the whole complex of observational data allowed Jacobson (2003) to state that NBP is a new type of thunderstorm discharge quite different from usual lightning [4]. He speculated that it could have relevance to runaway breakdown effect.

The kinetic theory of this phenomenon based on runaway breakdown was elaborated in the Project. The main idea of the theoretical approach is that at such high heights the EAS become well developed only if the energetic cosmic ray particle momentum is directed close to the horizon. For these conditions the RB - EAS discharge is strongly amplified what lead to the effective diminishing of thundercloud electric field and results in nonlinear saturation of the discharge current. The analytical and numerical analysis of the developed kinetic equation was done under the assumption of the parabolic form of the thunder electric field with the maximum value of the electric field E_m. The RB amplification parameter depends on the energy of the primary cosmic ray particle ε_0, the ratio of the length of the electric field region L to effective avalanche length l_{aeff} and on the ratio of the E_m to the RB critical field E_c. The results are presented in the Table 6.3.

Table 6.3. RB amplification parameter for $L / l_{aeff} = 25$

E_m/ E_c	$\varepsilon_0/10^{16}$ eV						
	0.2	0.6	1.0	2.0	6.0	10.0	100.0
1.4	3.8×10^8	2.9×10^8	2.4×10^8	1.7×10^8	7.5×10^7	5.0×10^7	6.0×10^6
1.6	1.4×10^9	1.03×10^9	7.3×10^8	3.8×10^8	1.3×10^8	6×10^7	5×10^6
1.8	0.4×10^{10}	1.4×10^9	8×10^8	2.0×10^8	2×10^7	6.5×10^6	7.9×10^5

As seen from the Table 6.3 the dependence of the amplification parameter on ε_0 demonstrates the nonlinear feedback effect. Namely, the EAS produced by a high-energy primary cosmic-ray particle generates during the RB-EAS discharge the electric current strong enough to decrease the initial electric field and thus to diminish the current.

Some other results of the calculations are shown in Figures 6.19 and 6.20. All of them are in a reasonable agreement with the observation data. It indicates definitely that NBP are generated by RB-EAS discharge at tropopause heights.

The results of the work are published in [13], see the list of published papers.
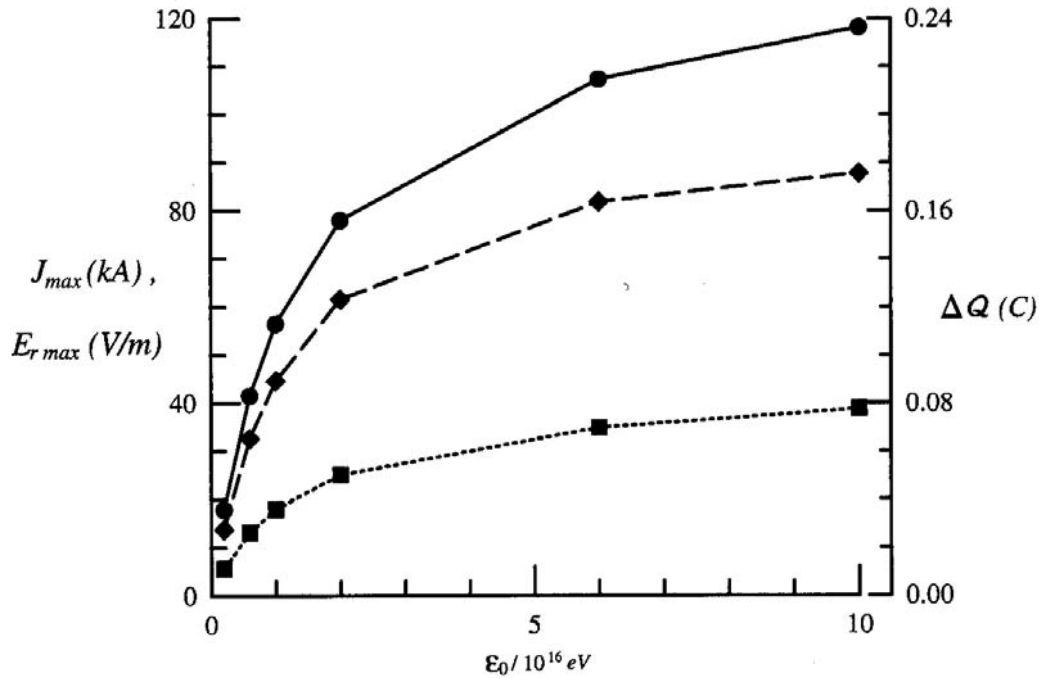
Fig.6.19. The dependence of maximal current J_{max} (solid line), maximal radio wave electric field amplitude at the distance $R = 100$ km (dashed line), and the changing of the thundercloud charge ΔQ (dotted line) on the parameter $\varepsilon_0/10^{16}$ eV.

Fig.6.20. The full energy dissipated in gas heating W_T (dotted line right scale) and radio emission W_{em} (solid line left scale) as a function of parameter $\varepsilon_0/10^{16}$ eV.
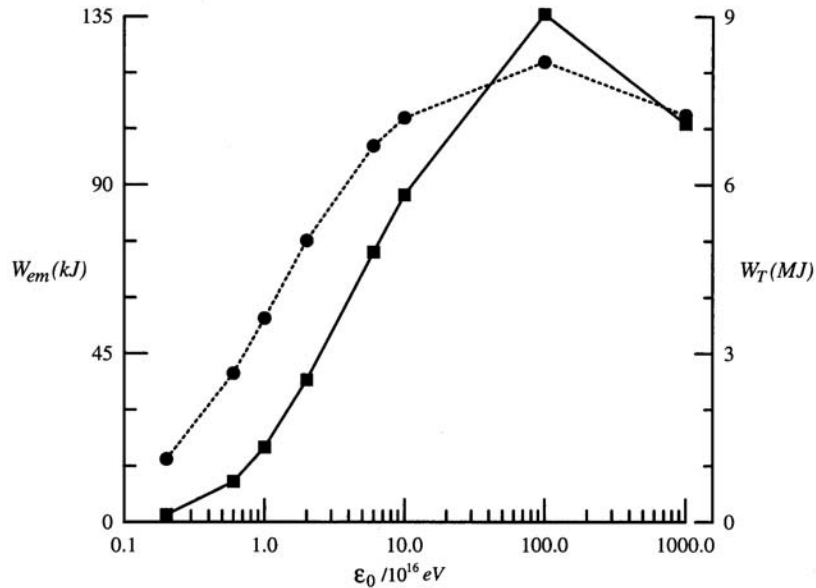
References

[1] D.A.Smith, X.M.Shao D.N.Holden, C.T. Rhodes, M Brook, P.R.Krehbiel, M.Stanley, W.Rison, R.J.Thomas {\it J. Geophys. Res. 104, 4189 (1999),

[2] D.A.Smith K.B.Eack J.Harlin, M.J.Heavner, A.R.Jacobson, R.S.Massey, X.M.Shao, K.C.Wiens {\it J.Geophys.Res 107 D134183 (2002),

[3] D.A.Smith, M.J.Heavner, A.R.Jacobson, X.M.Shao, R.S.Massey, R.J.Sheldon, K.C.Wiens {\it Radio Sci. 39, N1, RS1010, (2004)

[4] A.R.Jacobson {\it J.Geophys.Res 108 D244778 (2003)

Conclusion

Main results on subject "Plasma Instabilities Excited by Ground-based High Power HF ("Heating") Facilities"

- The kinetic theory of Langmuir turbulence developing evolved in ionosphere under the action of powerful radio wave was evolved. Turbulence develops in the thin layer at the resonance height were the plasma frequency is equal to the frequency of the incident wave.
- The numerical algorithm for the investigation of the kinetic model was designed. Algorithm takes into account the electron collisions and the movement of both ion and electron plasma components under the action of both the external and self-consistent electric field.
- It was shown that due to the height heterogeneity of ionosphere the originating flows of fast electrons undergo the multiple acceleration passing through the turbulence layer were the strong oscillations of the electric field are excited. The multiple passing throw the layer takes place due to the electron scattering outside the Langmuir turbulence layer
- It was shown that plasma density depletions (cavitons) are formed in the turbulence layer. The process takes place due to the resonance action of the electric field of the powerful radio wave on the plasma. Exactly in cavitons the acceleration of electrons take place. It was shown that the all the energy transferred from the powerful wave to cavitons is spend for the electron acceleration. This process is the reason of caviton stabilization.
- The plasma luminescence in red and green lines was calculated. It is produced by the pump exciting of the air molecules by the 2 – 20 eV electrons.
- It was shown that the powerful 5 MHz radio emission produce the luminescence in red line due to the direct electron heating. The luminescence in green line is not produced in this case.
- It was shown that the powerful radio emission with frequencies higher than 5 MHZ produce the luminescence in both red and green lines. This luminescence is produced by more energetic electrons, accelerated under the action of Langmuir turbulence.
- The theory of the magnetic zenith effect was developed. It was shown that the effect takes place due to the focusing of the powerful radio wave on the striations elongated along the magnetic field. At that the cannel elongated along the field is arising in plasma. The heating wave is self-acquisitioned in the cannel.
- It was shown that the magnetic zenith effect takes place both in high-latitude ionosphere were the direction of the magnetic field is close to the vertical line and middle-latitude ionosphere were the direction of the magnetic field significantly differs from the vertical one.
- The theory was compared with the observation data obtained on HAARP and SURA facilities. A good enough agreement between the theory and experiment was demonstrated.

Main results on subject "X and Gamma Ray Emission in Runaway Breakdown Processes"

Investigation of the runaway breakdown in conditions of electron-cyclotron resonance conditions using the specially designed installation.

- The formation of the high-energy "tail" of fast electron distribution function as well as the X-ray emission produced by these electrons was studied experimentally in the wide range of gas pressure.
- The optic spectrum of plasma was measured. It was established that in the case of strong electron acceleration the exciting of the line spectrum is more efficient than the exciting of molecular band spectrum.
- The obtained experimental results may be applied to phenomena of runaway electron fluxes interaction with rare air of the upper atmosphere which probably take place in the giant atmosphere discharges related to the lightning activity, well-known as "Red Sprites".

Theoretical and experimental investigation of thunderstorm pulse radio emission and of correlation between the lightning events and the extensive atmosphere showers.

- The theory of radio emission produced by the combined action of runaway breakdown and extensive atmospheric cosmic ray shower (EAS) was elaborated. Emission has the form of short bipolar HF pulse.
- A complex of installations for the registration of extensive atmosphere showers of cosmic rays (EAS) was designed. The complex is situated at the Tien-Shan Mountain Scientific Station and is used together with the radio installations. The following signals are used as triggers of EAS and lightning:
    - a) the signal of the EAS detection b based on Geiger counters;
    - b) the signal of the muon cosmic ray component passing through the muon hodoscopes;
    - c) the signal of the electric field jump.
  The shower trigger array has several decade data registration centers connected with each other and with the trigger detector subsystems by the means of cable lines.
- Scintillate NaI sensors for the registration of X –ray and gamma – ray emissions were designed, calibrated and installed.
- A complex of fast registration for all data array was designed and installed.
- Extensive measurements during thunderstorms were carried out.
- Installations for the measurement of lightning radio emission were designed and produced.
    - Radio-HF for the measurement of the emission in the diapason of 0.1 – 30 MHz
    - Radio-E for the registration of electric field and its variations. It registries the slow variations of electric field (10 Hz), the fast variations (20Hz/20kHz) and VHF (250 MHz) emission.
- Installations were launched at two points: At the Tien-Shan Montain Station (Kazakhstan) and at SURA Station (Nizhniy Novgorod Region, Russia).
- Multiple (greater than 10^3) measurements showed that the radio emission of each lightning starts with very short bipolar pulse having duration about 100 ns. Radio emission different from the background is not observed for at least 500 ms before the first pulse. The form, duration and the amplitude of the pulse are in agreement with those predicted by the theory of the combined action of runaway breakdown and EAS if the energy of the primary cosmic ray particle is about 10^{16} eV.
- Correlations between the short pulses of radio emission and the EAS passing. Namely, during thunderstorm bipolar pulses of HF radio emission were observed correlated within 50 µs interval with the trigger signals from the EAS installation. Such pulses never were observed without thunderstorm.
- Powerful flux of gamma emission was found in the range about 100 µs before the return strokes. The observed emission occupies the wide spatial domain.

List of published papers with abstracts

1. A.P. Chubenko et al. "Effective Growth of a Number of Cosmic Rays Electrons Inside Thundercloud", Phys.Lett A, 309(2003) 90 - 102.
   Significant enhancement of secondary cosmic rays electrons inside electrically charged clouds is established. The effect is observed in a quiet phase of thunderstorm – in the absence of lightning, rainfall and bursts of X-ray emission. The observations are fulfilled in Tien-Shan Mountains at the modernized thunderstorm – cosmic ray (TCR) installation.

2. A.V. Gurevich, L.M .Duncan, Yu.V. Medvedev and K.P. Zybin "Radio emission due to simultaneous effect of runaway breakdown and extensive atmospheric showers" Phys.Lett.A. 301, (2002), 307 – 314.
   The theory of radio emission generated during thunderstorm by cosmic ray particles having high energy ε is developed. The emission is shown to have a form of bipolar radio pulse with characteristic frequency 1-10 MHz. Due to combined action of runaway breakdown and extensive atmosphere shower the emission intensity is high. The radio pulse could be observed for $\varepsilon \geq 10^{17}$ eV up do distances 100–300 km. Thus the runaway breakdown in thunderclouds can play a role of a "spark chamber" for radio detection of high energy particles.

3. A.V. Gurevich, E. Fremouw, J. Secan and K. Zybin "Large scale structuring of plasma density perturbations in ionospheric modifications", Phys.Lett.A. 301, (2002), 320 -326.
   The theory of nonlinear large-scale structuring in ionospheric modifications is developed. THe results of an experiment in the northern ionosphere are presented. The ionospheric modification was produced by HAARP facility (Alaska), and the plasma disturbances were measured using the polar-orbiting satellite Oscar 2. The comparison shows a reasonable agreement between observational data and the theory. For the first time the existence artificially produced plasma depletion structure elongated along magnetic field lines at hundred kilometers is established.

4. A.V. Gurevich, H. Carlson, Yu.V. Medvedev, K.P. Zybin "Langmuir Turbulence in Ionosphere Plasma", Plasma Physics Reports (2004) accepted for publication.
   The kinetic theory of the strong Langmuir turbulence excited nearby the powerful radio wave reflection region is developed. The structure and the number of cavitons arising in the developed turbulence is determined. The electron acceleration is studied. It is shown that that a significant 'tail' of the distribution function is grown. It's effective temperature is 50 - 100 time higher than the plasma temperature. The region occupied by electrons is several hundreds times larger than the Langmuir turbulence layer. The theory results are shown to be in a good agreement with the electron acceleration and the plasma luminosity observed in the experiments.

5. A.V. Gurevich, Yu.V. Medvedev, K.P. Zybin "Thermal electrons and electric current generated by runaway breakdown effect", Phys. Lett. A 321 (2004) 179.
   The kinetic theory of runaway breakdown (RB) for low-energy electrons is developed. The full complex of ionization, emission and recombination (attachment) processes is taken into account. The number of generated in RB process low-energy electrons and electric current is determined.

6. E.D. Tereshchenko, B.Z. Khudukon, A.V. Gurevich, K.P. Zybin, V.L. Frolov, E.N. Myasnikov, N.V. Muravieva, H.C. Carlson "Radio tomography and scintillation studies of ionospheric electron density modification caused by a powerful HF-wave and magnetic zenith effect at midlatitudes", Phys. Lett. A 325 (2004) 381-388.
   Observations of the ionospheric electron density modified by a powerful radio wave of the SURA HF heating facility were carried out in Russia at the middle latitudes in August 2002. Amplitude scintillations and variations of the phase of VHF signals from Russian orbiting satellites passing over the heated region along the chain of three satellite receivers have been recorded. The experimental data were converted to electron density maps using a stochastic inversion. Tomographic measurements conducted during a low magnetic activity revealed that RF powerful waves can produce significant electron density disturbances up to height significantly exceeding altitudes of the F layer peak. Both large-scale plasma enhancements and small-scale density irregularities can be generated by the HF radiation. Wave density structures were also observed within the sector which is much wider than the area covered by the main lobe of the heating antenna. Small-scale density irregularities are mostly field-aligned although large-scale structures can be detected within a much lager area. A distinctive peculiarity of electron density changes occurred during hearing is producing a zone of low density inside the area illuminated

by the antenna beam. The results indicate that satellite radio tomography and scintillation measurements are effective diagnostic techniques giving a valuable information to studies of effects induced by HF modification. The complete system of plasma density disturbances describing by the theory of "magnetic zenith effect" has been for the first time studied in the Letter. A good agreement between the theory and experimental data has been obtained.

7. A.V. Gurevich, A.N. Karashtin, A.P. Chubenko, L.M. Dunkan, V.A. Ryabov, A.L. Shepetov, V.P. Antonova, S.V. Kryukov, V.V. Piskal, M.O. Ptitsyn, L.I. Vildanova, Yu.V. Shlyugaev, K.P. Zybin "Experimental evidence of giant electron-gamma bursts generated by extensive atmospheric showers in thunderclouds", Phys. Lett. A **325** (2004) 389-402.

The 2003 Tian-Shan Mountain Station data was processed. The experiment was devoted to find the correlations between the arrival time of short bipolar pulses of radio emission (SBP) and the moment of the formation of the trigger signal from the spread system of Geiger-Muller counters registering the passage of the widespread flux of the high-energy particles. The 150 events during the two observed thunderstorms was found when SBP came less then 100 μs before the trigger. SBP coming in the absence of thunderstorm conditions was not found. The data obtained are in agreement with the runaway breakdown theory prediction. One of the conditions for runaway breakdown is the existing of seed high-energy (~1 MeV) particles, cosmic ray secondaries, for example.

It was established that the trigger forming delays with respect to the SBP are distributed practically uniform within 100 μs interval. It correspond to the distance of several decades kilometers between the signal sources, ftaking into account the characteristic velocity of comic ray shower about that of light. It was concluded, that the large delay value contradicts the interpretation of the trigger signal as the direct signal of the EAS passage. The proposed interpretation of the data obtained suppose that the trigger array have registered the diffusive gamma ray born by the EAS passage at the distance from the facility but not the direct passage of the EAS. The another runaway breakdown condition, namely the electric field value must exceed the critical value, is supposed to be fulfilled as well.

8. A.V. Gurevich, K.P. Zybin " High energy cosmic ray particles and the most powerful discharges in thunderstorm atmosphere" Phys. Lett. A 329 (2004) 341.

The runaway breakdown — extensive atmospheric shower discharge (RB-EAS) excited in thunderstorm atmosphere by high-energy cosmic ray particles ($\varepsilon_p > 10^{17}$–10^{19} eV) generate very powerful radio pulse. The RB-EAS theory is compared with observations of radio pulses. An agreement between the theory and experiment is established. The existence of nowadays satellite and ground based systems which obtain regularly a large amount of observational radio data could allow to use them in combination with other methods for effective study of high energy cosmic ray particles.

9. A.V. Gurevich, Yu.V. Medvedev, K.P. Zybin "New type discharge generated in thunderclouds by joint action of runaway breakdown and extensive atmospheric shower", Phys. Lett. A 329 (2004) 348.

The kinetic theory of electric discharge in thunderclouds generated by runaway breakdown (RB) and extensive atmospheric shower (EAS) is developed. A giant growth of relativistic and thermal electrons, gamma and radio emission is predicted. The theory is compared with the recent results of EAS-radio experiments at Tien Shan mountains and with observations of lightning initiation process and narrow bipolar radio pulses. A reasonable agreement between the theory and observations is established. A new methods in cosmic ray physics is proposed: *RB detection of extra high-energy particles $\varepsilon_p > 10^{18}$ eV.*

10. A.V. Gurevich, K.P. Zybin, "Runaway breakdown and the mysteries of Lightning", Physics Today, May 2005, 37–42.

The observed electric fields in thunderstorms are generally too weak to initiate the atmosphere's electrical breakdown. But cosmic rays can play a surprising role in the drama of lightning.

11. A. V. Gurevich, K. P. Zybin, H. C. Carlson "Magnetic-Zenith Effect" Radiophysics and Quantum Electronics v. 48 №9 (2005), 686-699.

We develop a theory of the magnetic-zenith effect (MZE) observed upon the ionosphere modification by powerful radio waves. The dependences of MZE on main parameters, such as the magnetic-field inclination angle, pump-wave frequency and power, and angular width of HF beam are obtained. The optimal elevation angle of pump-wave beam is predicted.

12. A.N. Karashtin, Yu.V. Shlyugaev and A.V. Gurevich, "High-Frequency Radio Emission of the Lightning Discharge", Radiophysics and Quantum Electronics v. 48 №9 (2005), 711-719.
A special system created to register short electromagnetic pulses has been used to study high-frequency (0.1–30 MHz) radio emission of lightning discharges. It has been shown that the emission is a sequence of short pulses. The shape, width, and amplitude of the first (bipolar) pulse agree with those predicted by theory with account for the combined action of the effect of the runaway electron breakdown and an extensive atmospheric shower for the energy of the initial particle of the order of 10^{16} eV.

13. A.V. Gurevich, K.P. Zybin and Yu.V. Medvedev, "Amplification and nonlinear modification of runaway breakdown", Phys. Lett. A 349 (2006) 331-339.
The astonishing natural phenomenon of narrow bipolar pulses (NBP) are isolated discharges in thunderstorms at tropopause heights (10 – 20 km) that generates enormously powerful radio emission but lasts only a few microseconds. The theory of this phenomenon based on runaway breakdown is elaborated. At such high heights extensive atmospheric shower (EAS) become well developed only if the energetic cosmic ray particle momentum is directed close to the horizon. For these conditions the runaway breakdown – extensive atmospheric shower (RB - EAS) discharge amplified strongly what lead to the effective diminishing of thundercloud electric field and results in nonlinear saturation of the discharge current. A reasonable agreement of the theory with NBP observations is demonstrated.

14. V.P. Antonova, T.P. Arsov, L.I. Vildanova, S.V. Kryukov, N.M. Nesterova, V.V. Piskal, R.Yu. Polyakov, V.A. Ryabov, T.H. Sadykov, A.P. Chubenko, S.Ya. Shalamova, A.L. Shepetov "Shower trigger installation at Tyan-Shan Mountain Station", (to be published).

List of presentations at conferences and meetings

1. A.V. Gurevich "The spreading of powerful radio waves through the atmosphere", plenary lecture, Proceedings of the XX All-union conference on the radio waves spreading, Nizhnii Novgorod, July 2–4, 2002 г., p. 15–19 (in Russian).

2. A.V. Gurevich "Runaway breakdown phenomena", a lecture at the Conference "Nonlinear Phenomena in Environmental Research", N.Novgorod, September 6 – 12, 2003.

3. A.V. Gurevich, A.N. Karashtin, A.P. Chubenko, L.M. Dunkan, V.A. Ryabov, A.L. Shepetov, V.P. Antonova, S.V. Kryukov, V.V. Piskal, M.O. Ptitsyn, L.I. Vildanova, Yu.V. Shlyugaev, K.P. Zybin "Experimental evidence of giant electron-gamma bursts generated by extensive atmospheric showers in thunderclouds", The 28-th conference on cosmic rays, Moscow, MEPI, June 07–11, 2004 (in Russian).

4. A.V. Gurevich, "Radio emission due to cosmic ray interaction with thunderclouds", RF Ionospheric Interactions Workshop, Santa Fe, New Mexico, 18-21 April 2004, Proc. VI, 698-727.

5. A.V. Gurevich, Yu.V. Medvedev, H.C. Carlson, K.P. Zybin, "Langmiur turbulence in nonuniform ionospheric plasma", RF Ionospheric Interactions Workshop, Santa Fe, New Mexico, 18-21 April 2004, Proc. V.II, 1149-1157.

6. E.D. Tereshenko, B.Z. Khudukon, A.V. Gurevich, K.P. Zybin, V.L. Frolov, E.N. Myasnikov, N.M. Muravieva, H.C. Carlson, "Radio tomography and scintillation studies of ionospheric electron density modification caused by a powerful HF-wave", RF Ionospheric Interactions Workshop, Santa Fe, New Mexico, 18-21 April 2004, Proc. V.II, 1158-1166.

7. A.V. Gurevich, "Cosmic rays and electromagnetic processes in atmosphere", Frontiers of Nonlinear Physics, Nizhny Novgorod, July 5-12, 2004.

8. A.V. Gurevich "Modern state of ionospheric modification problem", "Effects of Artificial Action on the Earth Ionosphere by Powerful Radio Waves", VI International Suzdal URSI Symposium, Moscow, October 18-21, 2004

9. A.V. Gurevich, H.C. Carlson, Yu.V. Medvedev, K.P. Zybin, "Langmiur turbulence in nonuniform ionospheric plasma", "Effects of Artificial Action on the Earth Ionosphere by Powerful Radio Waves", VI International Suzdal URSI Symposium, Moscow, October 18-21, 2004, Book of abstracts, Nizhny Novgorod, 2004, p.23.

10. A.V. Gurevich, H.C. Carlson, K.P. Zybin, "Magnetic zenith effecting ionospheric modifications", "Effects of Artificial Action on the Earth Ionosphere by Powerful Radio Waves", VI In-

ternational Suzdal URSI Symposium, Moscow, October 18-21, 2004, Book of abstracts, Nizhny Novgorod, 2004, p.24.

11. A.V. Gurevich, "Runaway breakdown in thunderstorm electric field", "Effects of Artificial Action on the Earth Ionosphere by Powerful Radio Waves", VI International Suzdal URSI Symposium, Moscow, October 18-21, 2004.

12. A.V. Gurevich, "Runaway breakdown and extra-powerful radio emission", "Effects of Artificial Action on the Earth Ionosphere by Powerful Radio Waves", VI International Suzdal URSI Symposium, Moscow, October 18-21, 2004.

13. A.P. Chubenko, A.V. Gurevich, A.N. Karashtin, I. Amurina, V.P. Antonova, T.P. Arsov, P.A. Chubenko, S.V. Kryukov, K.K. Mukasshov, N.M. Nesterova, V.V. Piskal, R.Yu. Polyakov, M.O. Ptitsyn, V.A. Ryabov, T.Kh. Sadykov, S.A. Shalmanova, A.L. Shepetov, Yu.V. Shlyugaev, L.I. Vildanova, M.I. Vildanova, K.P. Zybin "The modern status of Tien-Shan complex Installation for studying RB-processes in thunderclouds", "Effects of Artificial Action on the Earth Ionosphere by Powerful Radio Waves", VI International Suzdal URSI Symposium, Moscow, October 18-21, 2004, Book of abstracts, Nizhny Novgorod, 2004, p.75.

14. A.V. Gurevich, A.N. Karashtin, A.P. Chubenko, L.M. Dunkan, V.A. Ryabov, A.L. Shepetov, V.P. Antonova, S.V. Kryukov, V.V. Piskal, M.O. Ptitsyn, L.I. Vildanova, Yu.V. Shlyugaev, K.P. Zybin "Experimental evidence of giant electron-gamma bursts generated by extensive atmospheric showers in thunderclouds", "Effects of Artificial Action on the Earth Ionosphere by Powerful Radio Waves", VI International Suzdal URSI Symposium, Moscow, October 18-21, 2004, Book of abstracts, Nizhny Novgorod, 2004, p.76.

15. A.V. Gurevich, Yu.V. Medvedev, K.P. Zybin, " New type discharge generated in thunderclouds by joint action of runaway breakdown and extensive atmospheric shower ", "Effects of Artificial Action on the Earth Ionosphere by Powerful Radio Waves", VI International Suzdal URSI Symposium, Moscow, October 18-21, 2004, Book of abstracts, Nizhny Novgorod, 2004, p.79.

16. A.N. Karashtin, Yu.V. Shlyugaev, A.V. Gurevich, "Radio emission at the initial stage of lightning", "Effects of Artificial Action on the Earth Ionosphere by Powerful Radio Waves", VI International Suzdal URSI Symposium, Moscow, October 18-21, 2004, Book of abstracts, Nizhny Novgorod, 2004, p.80.

17. A.V. Gurevich, "Runaway breakdown and its role in thundercloud discharges", International Symposium "Topical Problems of Nonlinear Wave Physics", 2–9 August 2005, St. Petersburg– N. Novgorod, Russia.

18. A.V. Gurevich, K.P. Zybin "Atmospheric electricity – models and the possibility of spacecraft observations", "Space Science Week", Space Research Institute of RAS, Moscow 2005, October 3 – 6.